University of Cyprus

DEPARTMENT OF PHYSICS

PERTURBATIVE CALCULATION OF FUNDAMENTAL QCD QUANTITIES

DOCTOR OF PHILOSOPHY DISSERTATION

DEMETRIANOS GAVRIEL

2024

University of Cyprus

Department of Physics

Perturbative calculation of fundamental QCD quantities

Demetrianos Gavriel

A dissertation submitted to the University of Cyprus in partial fulfillment of the requirements for the degree of Doctor of Philosophy.

May 2024

Validation page

Doctoral Candidate: Demetrianos Gavriel

Doctoral Thesis Title: Perturbative calculation of fundamental QCD quantities

The present Doctoral Dissertation was submitted in partial fulfillment of the requirements for the Degree of Doctor of Philosophy at the ***Department of Physics*** *and was approved on May 20, 2024 by the members of the* ***Examination Committee****.*

Examination Committee:

Committee Member: Prof. Constantia Alexandrou _____

Committee Member: Prof. Giannis Koutsou _____

Research Supervisor: Prof. Haralambos Panagopoulos _____

Committee Member: Prof. Fotios Ptochos _____

Committee Member: Prof. Ettore Vicari _____

Declaration of doctoral candidate

The present doctoral dissertation was submitted in partial fulfillment of the requirements for the degree of Doctor of Philosophy of the University of Cyprus. It is a product of original work of my own, unless otherwise mentioned through references, notes, or any other statements.

Demetrianos Gavriel

_____

Acknowledgements

Firstly, I express my sincere gratitude to my advisor, Professor Haralambos Panagopoulos, for his invaluable guidance, extensive knowledge, and unwavering encouragement and support throughout my doctoral studies. His mentorship serves as both an inspiration and a guiding light, and I am truly honored to have been his student.

Secondly, I extend my appreciation to Dr. Gregoris Spanoudes and Dr. Marios Costa for their collaborative efforts in many of the calculations presented in this work. I especially want to acknowledge Dr. Gregoris, whose invaluable support has been consistently accessible and reliably precise in his guidance.

I would also like to acknowledge Dr. George Milis and my colleagues at PHOEBE Research and Innovations, where I held a part-time position of Algorithms Developer during my PhD studies. Dr. Milis exemplifies true leadership and understanding, allowing me the flexibility to pursue my PhD without any interference, for which I am deeply grateful.

Furthermore, I wish to express my gratitude to my fellow PhD colleagues, Leonida, Taso, Herodoto, and Andrea, for engaging in insightful discussions on both my dissertation and the field of Physics.

I am endlessly grateful to my family and my fiancée, Anastasia, for her boundless love, unwavering support, personal attention, and care.

Lastly, I extend my gratitude to the University of Cyprus and Professor Panagopoulos for the financial assistance provided, enabling me to attend numerous conferences over the past three years as part of my doctoral journey.

Περίληψη

Η διατριβή αυτή παρουσιάζει μια σειρά από διαταρακτικούς υπολογισμούς σε δυο μελέτες που αφορούν θεμελιώδης μεγέθη στη Κβαντική Χρωμοδυναμική (QCD). Οι περισσότεροι από τους υπολογισμούς πραγματοποιούνται μέσα στο πλαίσιο του φορμαλισμού του πλέγματος, χρησιμοποιώντας μια σειρά από βελτιωμένες δράσεις πλέγματος που χρησιμοποιούνται συχνά σε αριθμητικές προσομοιώσεις.

Αρχικά, υπολογίζονται τα σφάλματα διακριτοποίησης στη θεωρία διαταραχών, οι οποίες είναι ανάλογες της μάζας των φερμιονίων ($\mathcal{O}(am)$), που εμφανίζονται στην σταθεράς σύζευξης της QCD, χρησιμοποιώντας τον φορμαλισμό του πλέγματος. Η ανάλυση περιλαμβάνει τον υπολογισμό του παράγοντα επανακανονικοποίησης Z_g σε τάξη διόρθωσης δυο βρόγχων, χρησιμοποιώντας γκλουόνια Symanzik και φερμιόνια clover σε μια αυθαίρετη αναπαράσταση της ομάδας βαθμίδας $SU(N_c)$ και N_f γεύσεις φερμιόνων με πεπερασμένη μάζα, λαμβάνοντας υπόψη τη βελτίωση πρώτης τάξης της πλεγματικής σταθεράς ($\mathcal{O}(a)$). Για τον υπολογισμό του Z_g χρησιμοποιείται η μέθοδος του πεδίου υποβάθρου (background) υπολογίζοντας τις κβαντικές διορθώσεις τόσο στο διαδότη υποβάθρου όσο και στο κβαντικό διαδότη του γκλουονίου. Αυτό επιτρέπει τον διαταρακτικό υπολογισμό των σφαλμάτων διακριτοποίησης λόγω του πλέγματος $\mathcal{O}(am)$ που προκύπτουν από την πεπερασμένη μάζα του φερμιονίου. Η εξάλειψη των όρων $\mathcal{O}(am)$ αποτελεί κρίσιμη στις μελέτες των μη-διαταρακτικών υπολογισμών για τη βελτίωση των προσδιορισμών ακριβείας της σταθεράς σύζευξης χρησιμοποιώντας τη θεωρία πεδίου στο πλέγμα.

Επιπρόσθετα, εξετάζεται η επανακανονικοποίηση ενός πλήρους σετ από μη τοπικούς τελεστές γκλουονίων αναλλοίωτους κάτω από μετασχηματισμούς βαθμίδας, σε τάξη διόρθωσης ενός βρόγχου στο φορμαλισμό του πλέγματος. Το μοτίβο ανάμειξης των τελεστών αυτών κατά την επανακανονικοποίηση τους προσδιορίζεται χρησιμοποιώντας επιχειρήματα συμμετρίας, τα οποία επεκτείνονται πέρα από τη θεωρία της διαταραχών. Επιπλέον, υπολογίζονται οι παράγοντες επανακανονικοποίησης των τελεστών μέσα στο σχήμα ($\overline{\text{MS}}$) μέχρι τάξη διόρθωσης ενός βρόγχου, Μαζί με τους παράγοντες μετατροπής από το σχήμα κανονικοποίησης RI′ στο σχήμα $\overline{\text{MS}}$. Οι υπολογισμοί πραγματοποιούνται με τη χρήση του διαστατικού ομαλοποιητή αλλά και του πλεγματικού ομαλοποιητή, χρησιμοποιώντας την δράση γκλουονίων Wilson. Οι υπολογισμοί αυτοί αποτελούν σημαντικοί στη μελέτη μη διαταρακτικές μελέτες των συναρτήσεων κατανομής των γκλουονίων (PDFs) στο πλέγμα.

Abstract

This dissertation presents a series of perturbative calculations in two main projects concerning fundamental quantities in Quantum Chromodynamics (QCD). The majority of the calculations are conducted within the framework of lattice field theory, using a range of improved lattice actions commonly used in numerical simulations.

Initially, the perturbative results of the discretization errors, which are proportional to the quark mass ($\mathcal{O}(am)$), are calculated on the QCD running coupling within lattice perturbation theory. The analysis involves the calculation of the 2-loop renormalization factor Z_g using improved lattice actions for an arbitrary representation of the $SU(N_c)$ gauge group and N_f multiplets of fermions with a finite quark mass respecting the $\mathcal{O}(a)$ improvement. The background field method is employed to compute Z_g by evaluating quantum corrections on both the background and quantum gluon propagator. This allows the perturbative evaluation of the $\mathcal{O}(am)$ lattice errors arising from the finite quark mass. The elimination of these $\mathcal{O}(am)$ effects is crucial for the nonperturbative studies of precision determinations of the strong coupling constant using lattice field theory.

Furthermore, the renormalization of a complete set of gauge-invariant gluon nonlocal operators in lattice perturbation theory is investigated. The mixing pattern under renormalization of these operators is determined using symmetry arguments, which extend beyond perturbation theory. Additionally, the renormalization factors of the operators within the modified Minimal Subtraction ($\overline{\text{MS}}$) scheme are derived up to one-loop, along with the conversion factors from the modified regularization invariant RI$'$ scheme to $\overline{\text{MS}}$. The computations are performed by employing both dimensional and lattice regularizations, using the Wilson gluon action. This work is relevant to nonperturbative studies of the gluon parton distribution functions (PDFs) on the lattice.

Contents

List of Figures

List of Tables

Chapter 1

Introduction

The Standard Model of particle physics stands as the cornerstone of our current understanding regarding elementary particles and their interactions, representing the most comprehensive theory to date in physics. Developed over the latter half of the 20th century, the Standard Model elegantly describes, through the framework of quantum fields, three of the four fundamental forces of nature: electromagnetism, weak interactions, and strong interactions. Notably, it omits gravity, which is considered negligible at the atomic and subatomic scales.

At the Standard Model core, there are two main categories of particles: fermions and bosons. Fermions, the building blocks of matter, are divided into two groups, known as quarks and leptons. Quarks come in six flavors: up, down, charm, strange, top, and bottom, each with its corresponding antiquark. Quarks with different flavors have different masses. These particles have fractional electric charges and interact via the strong force mediated by gluons. Quarks combine to form composite particles called hadrons, such as protons and neutrons. Leptons, on the other hand, include the particles electron, muon, tau, and their associated neutrinos. Unlike quarks, leptons do not participate in the strong force and have integer electric charges. They interact via the weak force and electromagnetism. Bosons are force-carrying particles responsible for mediating the fundamental forces of nature. Gauge bosons, including the photon, W and Z bosons, and gluons, transmit the electromagnetic, weak, and strong forces, respectively. The Higgs boson, another crucial boson, is responsible for giving mass to other particles through the Higgs mechanism.

Quantum Chromodynamics (QCD) is a fundamental component of the Standard Model, describing the strong force that binds quarks together within hadrons. Formulated in the 1970s, Quantum Chromodynamics (QCD) introduced the concept of color charge. This is an additional quantum property analogous to electric charge in Quantum Electrodynamics (QED). In QCD, quarks carry three types of color (red, green, and blue), while antiquarks carry their corresponding anticolors. Gluons, the mediators of the strong force, also carry color charge, enabling them to interact with quarks and with each other. There are eight types of gluons corresponding to the eight generators of the non-abelian group $SU(3)$, upon which QCD is based. Its development emerged in response to the need for a consistent theory of strong interactions. This need arose due to the observation of a vast number of new particles in high-energy experiments conducted in the 1950s and 1960s. The theory not only explained the discovered particles but also successfully predicted the existence of new particles.

Two key properties of QCD are confinement and asymptotic freedom. Confinement refers to the phenomenon whereby isolated quarks cannot exist freely but are always bound together within color-neutral combinations, such as mesons and baryons. Mesons are composed of one quark and one antiquark, resulting in integer spin particles, while baryons consist of three quarks or three antiquarks, forming half-integer spin particles. Asymptotic freedom, on the other hand, describes the weakening of the strong force at very short distances, allowing for the use of perturbative techniques in high-energy interactions. Quarks and gluons tend to behave as nearly free particles in high energies. David Gross, Frank Wilczek, and David Politzer, recipients of the 2004 Nobel Prize in Physics, were the first to identify the property of asymptotic freedom.

The formulation of QCD not only provided a coherent explanation for the strong interaction but also led to a deeper understanding of the structure and dynamics of hadrons. Through theoretical calculations and experimental verifications, QCD has successfully provided insights into phenomena such as deep inelastic scattering and hadron spectroscopy. Additionally, it has shed light on the behavior of quark-gluon plasma at extreme temperatures and densities. Furthermore, QCD plays a crucial role in our understanding of the early universe, particularly during the quark-gluon epoch moments after the Big Bang, when the fundamental interactions were governed by high-energy QCD dynamics. As such, the study of QCD continues to be a vibrant field, where theoretical investigations are interconnected with cutting-edge

experimental efforts, pushing the boundaries of our knowledge of the fundamental components of matter and the forces that govern them.

1.1 Lattice QCD

Lattice QCD, pioneered by Kenneth Wilson in 1974 [2], represents a groundbreaking nonperturbative regularization method within theoretical physics. Departing from the limitations of conventional perturbative techniques, lattice QCD offers a robust computational framework for investigating numerous aspects of strong interaction dynamics and the structure of hadrons. In the study of quark and lepton flavor physics, precision lattice QCD input remains indispensable for interpreting experimental findings. Notably, it aids in determining hadronic contributions to the muon's anomalous magnetic moment, form factors in light- and heavy-flavor sectors essential for testing the unitarity of the Cabibbo–Kobayashi–Maskawa (CKM) matrix, and validating potential lepton-universality anomalies. Additionally, lattice QCD provides precision determinations of quark masses, the strong coupling constant, and nucleon parton distribution functions, all crucial for precision Higgs physics and beyond-the-Standard-Model (BSM) searches at the Large Hadron Collider (LHC). Furthermore, lattice QCD makes possible computations related to nucleon/nuclear form factors, associated charges, and various nucleon matrix elements, which are important to investigations into violations of fundamental symmetries and the exploration of new physics. These calculations, alongside numerous others, provide essential inputs for both theoretical phenomenological models and experimental studies in particle physics [3].

Lattice regularization involves discretizing Euclidean spacetime into a four-dimensional hypercubic lattice, where each point is separated by a lattice spacing denoted as a. This approach allows the numerical approximation of the continuum QCD functional integral within a finite lattice framework. Quark fields are positioned at lattice sites, while gauge fields reside on the links connecting these sites. The lattice spacing acts as the ultraviolet regulator, filtering out high frequencies and ensuring the finiteness of the quantum field theory in high-energy regions. More precisely, it sets a cutoff on momentum integration, restricting it to the finite range of the first Brillouin zone ($-\pi/a < p_\mu < \pi/a$) during lattice computations in momentum space. In regions of low energy, the finite lattice size L acts as the infrared regulator. The continuum theory is

attained by extrapolating lattice results to an infinitely large lattice size ($L \to \infty$) and approaching the limit of an infinitesimal lattice spacing ($a \to 0$). This convergence can be achieved by adjusting the bare coupling constant (which characterizes the strength of interactions in the theory) to zero according to the renormalization group.

An essential benefit of lattice QCD is that it harnesses the power of Monte Carlo simulations. These simulations use inputs like bare coupling and quark masses to approximate the path integral inherent to the theory. By employing random sampling techniques, Monte Carlo simulations are essential for two purposes: predicting how hadronic quantities depend on bare parameters and verifying the accuracy of QCD as the theory of strong interactions through experimental comparisons. However, the simulations remain computationally demanding due to the large number of degrees of freedom, requiring the use of approximations. A critical constraint in numerical calculations lies in the range of the lattice spacing. Common algorithms slow down proportionally to a^5 and thus a common approach is to perform simulations with several different lattice spacings, typically spanning a range from around 0.1 fm to 0.01 fm or smaller to extrapolate.

Despite the effectiveness of lattice QCD, it faces challenges when simulating certain physical quantities. Statistical errors, stemming from Monte Carlo importance sampling, are relatively easy to estimate. However, systematic uncertainties present a significant obstacle in lattice QCD calculations. These errors mainly originate from discretization effects. Simulations are performed using finite lattice spacing and sizes, resulting in undesired contributions to nonperturbative estimates, even as the continuum limit is approached. Alongside discretization effects, finite volume effects also contribute to uncertainties. These are related to the spontaneous chiral flavor symmetry breaking, leading to the appearance of pions as light Goldstone bosons. To address these challenges, innovative methodologies and careful error consideration are necessary.

In recent years, significant progress has been made in numerical simulations, driven by advancements in algorithms, the introduction of novel techniques, and the enhancement of computational capabilities. These enhancements have enabled simulations to closely resemble physical values in various parameters. Additionally, the integration of machine-learning applications and the development of quantum computation will further expand these capabilities. With ongoing support and

development, lattice QCD will continue to provide vital inputs to numerous fields within particle physics.

1.2 Perturbative lattice QCD using improved actions

In principle, there is no unique formulation for a continuum action on the lattice. The only restriction when discretizing the QCD Lagrangian of the continuum theory is ensuring its recovery in the continuum limit. Lattice actions typically fail to preserve all symmetries present in continuum actions due to the discretization of spacetime on the lattice. However, constructing gauge-invariant lattice actions is essential because the renormalizability of QCD relies on gauge symmetry. Additionally, there is no universally optimal lattice action applicable to all physical systems. Each variation has its own set of advantages and disadvantages depending on the specific symmetries of the case study. Although every lattice action introduces discretization effects that disappear only in the continuum limit ($a \to 0$), numerical simulations require careful controlling of these errors before extrapolating to this limit. Constructing improved actions, which minimize discretization errors, ensures better behavior across all lattice spacings, consequently improving simulation outcomes. These approaches are widely adopted by leading international research groups in numerical simulations. It is advantageous to control these errors at nonzero lattice spacing for two main reasons: Firstly, for large errors, it is unclear how to reliably extrapolate to $a \to 0$, and secondly, unimproved actions necessitate working with very small lattice spacings, imposing significant computational demands, particularly in full QCD simulations. Consequently, employing improved actions at larger values of a while maintaining quality results proves beneficial. Furthermore, these improved actions are anticipated to preserve more symmetries of the continuum theory.

The naive fermion action, a straightforward discretization of the continuum action, replaces the continuum derivative with a symmetric difference on the lattice. However, this results in the appearance of unwanted fermionic degrees of freedom known as doublers in the continuum limit. This occurs because the naive discretization describes $2^4 = 16$ fermions instead of one, thereby violating the desired one-to-one correspondence with continuum fermions. The fermion propagator

illustrates this fermion doubling problem by having sixteen poles for zero fermion mass within the first Brillouin zone. In particular, the appearance of doublers is related to the challenge of formulating lattice fermions with continuum chiral symmetry, as stated by the Nielsen-Ninomiya theorem [4]. According to the theorem, lattice fermions preserving locality and having an explicit, continuum-like chiral symmetry while avoiding doublers are impossible. The first attempt to address this issue was Wilson's fermion formulation by introducing an extra term in the action, effectively giving mass to the doublers and causing them to decouple in the continuum limit. Despite this improvement, it introduces discretization errors linear in the lattice spacing.

The most common fermion actions with discretization errors of order $\mathcal{O}(a^2)$ include the clover (improved Wilson) [5], staggered [6] , and Ginsparg-Wilson (overlap [7–9] and domain wall [10, 11]) formulations. While these improved actions have addressed the doubling problem, they have sacrificed some features or symmetries of the continuum theory. For instance, the clover action removes doublers but explicitly breaks chiral symmetry. Twisted-mass fermions [12], a variant of clover fermions, offer an alternative strategy by automatically removing errors linear in the lattice spacing (without parameter tuning) under 'maximal twist' [13–15]. However, they introduce isospin-breaking effects, which diminish in the continuum limit. Staggered fermions offer another approach. While this formulation preserves one nonsinglet axial symmetry and reduces discretization errors to $\mathcal{O}(a^2)$, it retains four doublers, referred to as 'tastes', complicating result interpretation. To eliminate this issue, contributions from undesired tastes are eliminated by taking the fourth root of the fermion determinant within the path integral. However, taste-mixing effects arise for nonzero lattice spacing values. Ginsparg-Wilson fermions represent a significant advancement, providing a lattice formulation that maintains a continuum-like chiral symmetry without doublers [16]. This class includes domain-wall and overlap fermions, each with its own advantages and computational costs. Domain-wall fermions use a fictitious fifth dimension, with chiral modes localized on opposite four-dimensional surfaces, while overlap fermions explicitly satisfy the Ginsparg-Wilson relation. Despite their theoretical appeal, these formulations come with increased computational complexity, at least an order of magnitude greater than for other actions.

To enhance computational efficiency and stability, lattice fermion formulations are often combined with link smearing techniques, involving the use of smeared gauge

fields in the covariant derivatives of the fermion action, such as stout [17] (e.g., SLiNC fermions [18]), HYP [19], and HEX links [20]. Smearing techniques can also reduce taste symmetry-breaking errors inherent in staggered fermions (e.g., Asqtad fermions [21], HISQ [22]). However, overly aggressive smearing may distort short-distance physics and exacerbate discretization errors. Ultimately, the choice of fermion formulation in lattice QCD simulations depends on the balance between computational efficiency and the necessity for exact chiral symmetry. While formulations like Ginsparg-Wilson fermions are favored for applications where chiral symmetry plays a critical role, others may be preferred for their computational simplicity and efficiency in less demanding scenarios.

The Symanzik-improvement program [23] has been employed in the gauge part of improved actions, using the concept of 'on-shell improvement' [24] to minimize discretization errors at order $\mathcal{O}(a^2)$. In this context, the Symanzik-improved action is structured into different contributions, each corresponding to a possible independent closed loop (Wilson loop) formed by a combination of links. Each Wilson loop is associated with a single parameter upon which the action depends. Various versions of the Symanzik-improved gauge action are available, differing based on the particular selection of coefficients. Among these, the tree-level Symanzik and Iwasaki [25] actions are two of the most widely used choices.

While the lattice framework is primarily introduced for nonperturbative computations, perturbative calculations on the lattice provide valuable insights and practical benefits. Although incapable of fully describing lattice field theory, perturbation theory offers essential information for various applications, including determining renormalization factors, understanding scaling violations, and studying anomalies.

To ensure meaningful comparisons of lattice results to experimental data, appropriate renormalization of the bare quantities is necessary. This process involves the renormalization of operators, fields, and parameters used in calculations before reaching the continuum limit. However, obtaining nonperturbative estimates of renormalization factors via numerical simulations poses challenges, such as potential mixing with other operators under renormalization, which can make signals difficult to disentangle. In such instances, the use of perturbation theory becomes invaluable, as it provides a more transparent pathway for revealing mixing patterns compared to nonperturbative methods.

One of the key advantages of lattice perturbation theory lies in its role in establishing the connection between lattice schemes and the physical continuum theory. This involves determining a conversion factor that transforms renormalized quantities defined in a nonperturbative lattice scheme, such as the modified regularization-independent (RI′) scheme [26, 27], into a continuum scheme, like the modified minimal subtraction scheme ($\overline{\text{MS}}$) scheme. Such calculations rely on perturbation theory since continuum schemes are typically defined in a perturbative framework.

Additionally, lattice perturbation theory contributes to understanding phenomena like anomalies, continuum limit recovery, and scaling violations, which are essential for obtaining precise predictions from lattice simulations. Perturbative calculations provide analytical control over the continuum limit, facilitating the transition from discrete lattice models to continuous physical theory. Practically, lattice perturbation theory complements numerical simulations by providing accurate perturbative coefficients that can be compared with nonperturbative results. This comparison helps validate both perturbative and nonperturbative methods and offers insights into systematic errors arising from numerical simulations.

Performing perturbative calculations on the lattice presents significant challenges due to their high complexity. Algebraic expressions for typical two-loop Feynman diagrams involve hundreds of thousands of terms, making computations overwhelming. Consequently, despite their significant physical importance, many observables have only been partially explored using unimproved lattice actions, often limited to one loop or the lowest order in lattice spacing. This partial exploration constitutes a major source of systematic error, particularly as simulations aim for increased precision. Despite these challenges, recent decades have seen a few higher-loop calculations performed on the lattice, using various improved actions. These advancements contribute to the refinement and validation of lattice QFT simulations.

1.3 Dissertation overview

The dissertation presents a series of results in two main calculations using lattice perturbation theory; the discretization errors on the QCD running coupling

proportional to the quark mass, and the renormalization of gluon nonlocal operators. The structure of this dissertation is outlined as follows.

In Chapter 2, we examine the determination of the strong coupling constant. This chapter discusses methodologies for calculating the world average of the strong coupling constant, focusing on its derivation from lattice QCD, which is considered the most precise method. We also review recent advances in calculating the strong coupling from lattice QCD, such as step-scaling and decoupling methods. These methods show promise in better controlling systematic uncertainties and improving precision.

Chapter 3 reviews the theoretical foundations of the renormalization group, a fundamental concept in quantum field theory. It explores the Callan-Symanzik equation and beta function in detail, with a particular emphasis on their definition and derivation on the lattice.

Moving on to Chapter 4, the dissertation revisits the background field formalism and gauge fixing in both classical continuum and lattice actions. This chapter offers insights into the implementation of background fields in perturbative lattice QCD.

Chapter 5 includes the first main calculation of the dissertation, building upon the theoretical framework established in Chapters 2-4. It presents lattice QCD respecting the $\mathcal{O}(a)$ improvement, outlining the necessary formulation needed for the calculations. This includes improved lattice actions and the process of deriving the discretization errors $\mathcal{O}(am)$ on the running coupling from Green's functions using the background field method. The chapter also presents the calculation results of these discretization errors for both one and two loops.

In Chapter 6, the focus shifts to hadron structure, revisiting various aspects related to Parton Distribution Functions (PDFs). It reviews the experimental derivation of PDFs through global QCD analyses and then explores their computation from lattice QCD, examining their Mellin moments and discussing methods to determine their x-dependence. Moreover, it explores the three-dimensional structure of hadrons, introducing the Generalized Parton Distributions (GPDs) and the Transverse Momentum Dependent (TMD) PDFs. The chapter concludes with a detailed discussion of gluon PDFs and their derivation process.

Chapter 7 defines gluon nonlocal operators and explores their symmetry properties. This includes examining their transformation under charge conjugation, parity, and

time reversal, along with their symmetry properties within the rotational/octahedral point group. Understanding these symmetries is essential for establishing the mixing pattern of the operators under renormalization.

Chapter 8, building on the framework laid in Chapters 6 and 7, presents the second main calculation, which includes the perturbative renormalization of gluon nonlocal operators. This chapter displays the one-loop perturbative results, using both dimensional and lattice regularizations, of the renormalization factors of the operators in the $\overline{\text{MS}}$ scheme. Additionally, it presents the conversion factors between RI' and $\overline{\text{MS}}$ renormalization schemes.

Finally, Chapter 9 concludes the dissertation by summarizing the findings and contributions. It reflects on the implications of the research and suggests potential paths for future study. Additionally, Appendices A and B provide supplementary information, that was omitted from the main body of the dissertation to improve readability.

The results presented here will be published in the following papers:

- Gavriel D., Panagopoulos H., Spanoudes G., *"Renormalization of non-local gluon operators in lattice perturbation theory"*, PoS(LATTICE2023) 301, arXiv:2311.17468 [hep-lat]
- Costa M., Gavriel D., Panagopoulos H., Spanoudes G., *"Mass effects on the QCD β-function"*, PoS(LATTICE2023) 147, arXiv:2311.15796 [hep-lat]
- Gavriel D., Panagopoulos H., Spanoudes G., *"Perturbative renormalization of non-local gluon operators"*
- Costa M., Gavriel D., Panagopoulos H., Spanoudes G., *"Perturbative determination of $\mathcal{O}(a\,m)$ improvement on the QCD running coupling"*

Chapter 2

Strong coupling constant

Quantum Chromodynamics, as already discussed in 1, is the quantum field theory of the strong interaction between quarks and gluons. The strength of the interaction is characterized by a parameter of the theory, namely the strong coupling constant α_s. As we will discuss, this parameter is not a constant, but it depends on the energy scale μ of the interaction process. QCD is a non-abelian gauge theory, with symmetry group $SU(3)$, and exhibits few specific properties. At low energy scales of $\mu \sim 1$GeV, α_s becomes strong, leading to the confinement of quarks and gluons, with the formation of hadrons. On the other hand, quarks interact weakly with increasing energy, and α_s vanishes at asymptotically high energies. This process is known as asymptotic freedom. At these high energy ranges of $\mu \sim 100$GeV, perturbative expansion can be applied where the theory can be formulated as an expansion in powers of the coupling constant [28].

2.1 World average of $\alpha_s(m_Z^2)$

As a reference, α_s is evaluated at the energy scale of the Z-boson pole mass, $\alpha_s(m_Z^2)$. The world average value is obtained by the Particle Data Group (PDG) and amounts to $\alpha_s(m_Z^2) = 0.01180 \pm 0.0009$ [29], with relative uncertainty of $\approx 0.8\%$. The order of relative uncertainty is substantial compared to the other interaction couplings.

For the determination of the strong coupling constant, PDG first group measurements into different categories and calculates their average. These averages are then used to

obtain the value and uncertainty of the world average of $\alpha_s(m_Z^2)$. The observables are classified into the following categories (for details look at Table 2.1 and Figure 2.1):

- Hadronic τ decays and low Q^2 continuum (τ decays and low Q^2): Calculations for τ decays are available at Next to Next to Next to Leading Order (N^3LO). Data are obtained from ALEPH and OPAL collaborations, mainly from the 2-pion and the 4-pion modes (in the V channel).
- Decays and masses of heavy quarkonia ($Q\bar{Q}$ bound states): Results are obtained by studies of the charmonium and they are available at $NNLO$ and N^3LO.
- PDF fits: Taken both from global PDF fits and analyses of singlet and non-singlet structure functions.
- Hadronic final states of e^-e^+ annihilations (e^-e^+ jets and shapes): Measurements were taken at PETRA and LEP. Non-perturbative corrections are important and can be estimated either via Monte Carlo simulation or analytic modeling.
- Observables from hadron-induced collisions (hadron colliders): Calculations of $NNLO$ for $t\bar{t}$ or jet production at both the LHC and HERA, and Z+jet production at the LHC.
- Electroweak precision fit (electroweak): Measurements of W boson decays and Z boson decays, from the Tevatron, LHC, LEP, and the SLC experiments.
- Lattice: An average of different methods is determined by the 'Flavour Lattice Averaging Group' (FLAG).

PDG implies some restrictions at which an individual observable is suitable for use in the determination of the strong coupling constant. They take account of the observable's sensitivity to α_s as compared to the experimental precision. Also, the accuracy of the perturbative prediction has to be at least Next to Next to Leading Order (NNLO). Moreover, they consider the size of non-perturbative effects and the scale at which the measurement is performed.

Decreasing the uncertainty of α_s is extremely important. It will minimize the theoretical "parametric" uncertainties in the calculation of processes that are dependent on the strong coupling constant, as is the case of those measured at the LHC. In particular, α_s uncertainty propagates in total uncertainty of cross sections in

Category	$\alpha_s(m_Z^2)$	relative uncertainty
τ decays and low Q^2	0.1173 ± 0.0017	1.4%
$Q\bar{Q}$ bound states	0.1181 ± 0.0037	3.1%
PDF fits	0.1161 ± 0.0022	1.9%
e^+e^- jets & shapes	0.1189 ± 0.0037	3.1%
electroweak	0.1203 ± 0.0028	2.3%
hadron colliders	0.1168 ± 0.0027	2.3%
lattice	0.1184 ± 0.0008	0.7%
world average(without lattice)	0.1175 ± 0.0010	0.9%
world average(with lattice)	0.1180 ± 0.0009	0.8%

TABLE 2.1: PDG average of the categories of observables [1]. These are the final input to the world average of $\alpha_s(m_Z^2)$.

key processes of the Higgs production at $\sim 2-4\%$ [30],[31]. In addition, computations of total and partial hadronic Z boson widths are heavily affected by the input of $\alpha_s(m_Z^2)$ value. Furthermore, the strong coupling constant is crucial in top-quark physics, such as the top mass, width, and its Yukawa coupling [32]. Finally, the energy evolution of the QCD coupling has implications in physics beyond the Standard Model (e.g. physics in Planck scales).

Looking at determinations of $\alpha_s(m_Z^2)$ in Figure 2.1, one can notice the overall consistency of each category and their high precision. This undoubtedly leads to a validation of the asymptotic freedom as a prediction of QCD. In the next 10 years, the relative uncertainty of the $\alpha_s(m_Z^2)$ world average is expected to be reduced to one-half (from 0.8% to $\approx 0.4\%$), through experimental and theoretical advances.

2.2 Strong coupling constant from Lattice QCD

The lattice contribution to the world average of $\alpha_s(m_Z^2)$ is the most precise among those seven PDG groups as can be seen from Table 2.1. Its value, $\alpha_s(m_Z^2) = 0.01184 \pm 0.0008$, is given by the 'Flavour Lattice Averaging Group' (FLAG) [33]. FLAG is a lattice QCD community and they are responsible for collecting and bringing information on lattice results for specific physical quantities, including α_s, to the whole particle physics community.

Aside from perturbative calculations at high energies, low energy scale computations are crucial for the determination of α_s. In recent years, exponential development in

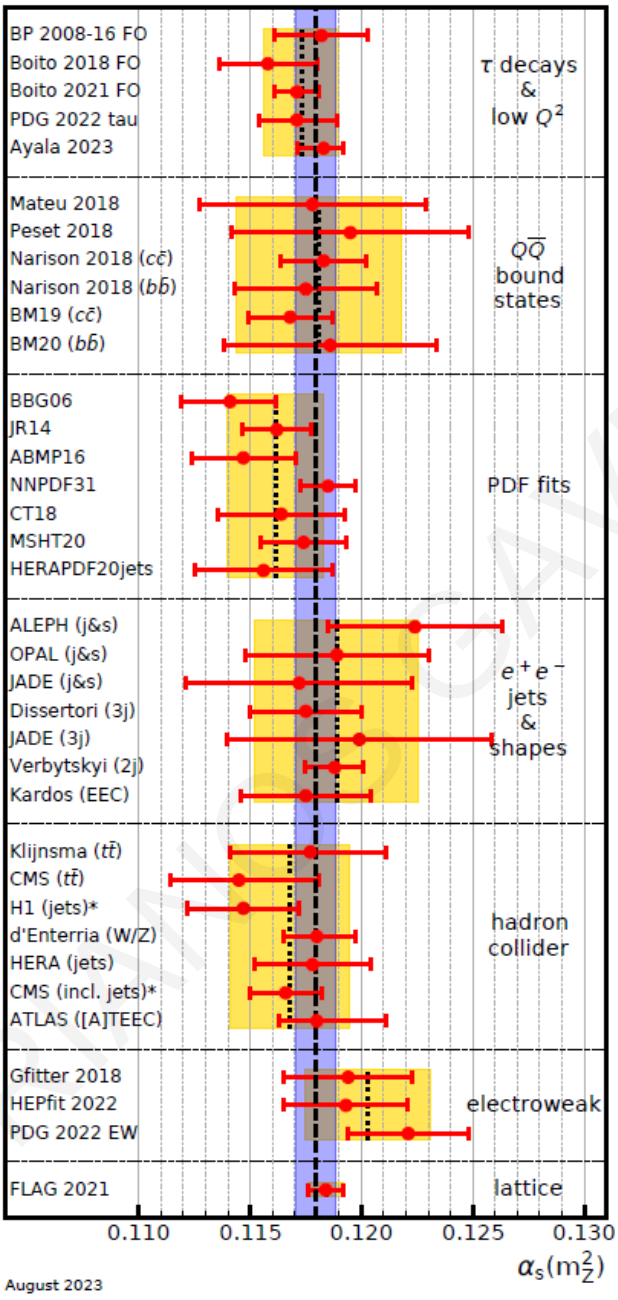

FIGURE 2.1: Summary of determinations of $\alpha_s(m_Z^2)$ from seven categories. The yellow shaded area and dotted lines indicate the pre-average values of each group. The dashed line and blue shaded area represent the final $\alpha_s(m_Z^2)$ world average. This figure has been taken from [1]

numerical techniques allowed the formulation of QCD on a discrete lattice of space-time points and thus the study of the non-perturbative regime. However, employing lattice QCD introduces systematic uncertainties in the precise determination of α_s. These uncertainties are associated with perturbative truncation, discretization errors in continuum limit extrapolations, and finite volume effects.

Overcoming the limitations of simulations is challenging without employing a specific strategy to control systematic uncertainties. One proposed approach for addressing these challenges in lattice QCD simulations is the step-scaling method which utilizes a finite-volume renormalization scheme [34]. This strategy enables the nonperturbative scale evolution up to very high energies within the regime of QCD, where perturbation theory can be safely applied. Thus, it effectively eliminates systematic errors in a controlled way, as opposed to most "large volume" approaches, enabling the precise determination of α_s across various energy scales. The subsequent section offers an in-depth review of this strategy.

Various methods have also been studied by lattice QCD groups to determine the strong coupling constant. This includes using the static quark-antiquark energy [35], the moments of quarkonium correlators [36], the small Wilson loops [37], hadronic vacuum polarization [38], QCD vertices [39], and eigenvalues of the Dirac operator [40]. Each approach presents distinct challenges and benefits; for a comprehensive overview, see Ref. [41].

Within the next ~ 10 years, the current relative uncertainty of the lattice contribution to $\alpha_s(m_Z^2)$ ($\pm 0.7\%$), is expected to be reduced in half. For example, this can be achieved by improving the step-scaling method or using it in combination with the decoupling strategy (e.g. decoupling of heavy quarks [34]). Also, perturbative calculations of N^{3}LO and N^{4}LO contributions can further improve the determination of $\alpha_s(m_Z^2)$.

2.3 Step-scaling and decoupling method

The precision determination of the strong coupling through lattice QCD involves a nonperturbative definition of the quantity $O(\mu)$, which relies on a short distance scale of $1/\mu$. This quantity can be expressed as a perturbative series:

$$O(\mu) \overset{q\to\infty}{\sim} \alpha_s(\mu) + \sum_{n=2}^{N} c_n \alpha_s^n(\mu) + \mathcal{O}\left(\alpha_s^{N+1}(\mu)\right) + \mathcal{O}\left(\frac{\Lambda}{q}\right)^p + \dots \tag{2.1}$$

where N is the number of known coefficients of the perturbative series. Using Eq.2.1 it becomes possible to approximate the value of $\alpha_s(\mu)$. On the lattice, in addition to determining the value of $O(\mu)$, it is necessary to establish the scale μ in terms of units

of a well-measured hadronic quantity, such as the ratio μ/m_p, where m_p denotes the proton mass.

Equation (2.1) encompasses two types of corrections; the nonperturbative ("power") corrections, appearing as $(\Lambda/q)^p$, and perturbative corrections arising from the truncation of the perturbative series to a finite order N, represented as $\alpha_s^{(N+1)}(\mu)$. Generally, both types of uncertainties decrease as μ approaches infinity.

As discussed in previous sections, lattice QCD simulations use an infrared cutoff, denoted by $\Lambda_{\mathrm{IR}} = L^{-1}$ (where L denotes the size of the finite space-time volume of the simulation), and an ultraviolet cutoff, denoted by $\Lambda_{\mathrm{UV}} = a^{-1}$ (where a represents the lattice spacing). To avoid finite volume effects, the spatial volume of the lattice (denoted as L^3) must be large enough. On the other hand, to match the lattice results to perturbative QCD calculations reliably, one needs to reach a high energy scale μ while still staying significantly below the cutoff scale of the lattice $(1/a)$. This ensures that perturbative expansions remain valid and keep lattice discretization effects due to the finite lattice spacing sufficiently small. These requirements can be summarized by the conditions:

$$\frac{1}{L} \ll m_\pi \ll \mu \ll \frac{1}{a} \tag{2.2}$$

where m_π is the pion mass. The above relation indicates that a single lattice simulation is confined to a limited range of energy scales and this is referred to as the "window problem". This constraint implies that the ratio of lattice size to lattice spacing (L/a) needs to be on the order of thousands. Furthermore, reaching the continuum limit $(a \to 0)$ requires using a range of lattice sizes that satisfy the above constraint. Additionally, it's desirable to have a range of energy scales μ to verify that the perturbative regime has been reached.

These conflicting requirements force compromises in lattice determinations. Typically, the energy scales reached for perturbative matching tend to be low. Even under optimal circumstances, systematic errors stemming from truncation of the perturbative series and/or contributions from nonperturbative effects often overshadow the analysis. Hence, if the objective is to determine both the hadronic scale (e.g., m_p) and the value of the observable $O(\mu)$ within a single lattice simulation, a large lattice volume is necessary, with L approximately greater than or equal to $1/m_\pi$. This approach is termed 'large volume'. As a result, the attainable

energy scales μ are typically confined to a few GeV at most. Although power corrections decrease rapidly with the energy scale μ, the logarithmic dependence of the strong coupling on the energy scale results in perturbative uncertainties diminishing very gradually:

$$\alpha_s(\mu) \overset{q\to\infty}{\sim} \frac{1}{\log\left(\mu/\Lambda_{\mathrm{QCD}}\right)} \tag{2.3}$$

As a consequence, in many cases, lattice QCD determinations of the strong coupling are primarily influenced by the truncation uncertainties of the perturbative series. Most "large volume" approaches, exhibit perturbative uncertainties between approximately 1% and 3% in $\alpha_s(m_Z^2)$. Therefore, a significant reduction in the uncertainty of the strong coupling can only come from other approaches that address the multiscale problem discussed above.

The most effective approach for nonperturbatively determining the coupling $\alpha_O(\mu)$ at high energy involves employing a finite-volume renormalization scheme [42]. These schemes are constructed based on observables O defined within a finite space-time volume. The renormalization scale of the coupling μ is then equated with the inverse spatial size of the finite volume ($\mu = L^{-1}$). In essence, a running coupling is established through the variation of certain correlation function(s) as the system's volume changes. Consequently, finite volume effects are integrated into the definition of the coupling, rather than being viewed as a systematic uncertainty in its determination. This presents a clear advantage, as lattice systematics are managed once a single condition is fulfilled: $L^{-1} = \mu \approx a^{-1}$, resulting in $L/a \gg 1$. This scenario is considerably simpler than needing to satisfy Eq. 2.2. In theory, there is considerable flexibility in selecting a finite-volume scheme. However, practical applications entail careful consideration of various technical aspects [43]. Typically, Schrödinger functional (SF) boundary conditions are used to define finite volume couplings. This involves imposing Dirichlet boundary conditions in Euclidean time at $x_0 \in \{0, T\}$, along with periodic boundary conditions having a period L in the spatial directions.

A specific implementation of the finite-volume renormalization scheme can be achieved through the step-scaling approach. In the step-scaling method, the energy scale is stepped up recursively by a fixed scale factor, typically 2. By utilizing multiple lattices with different sizes, a wide range of physical scales can be covered without representing all hadronic scales simultaneously. This bypasses the window problem, as the method

allows for the representation of physical scales in a step-wise manner. At each step, the lattice size effectively decreases, allowing for higher energy scales to be probed while avoiding significant finite volume effects.

The application of the step-scaling method has shown promising results, notably in determining the strong coupling constant. By matching the scale μ_{had} to a hadronic quantity at the lowest scale reached and recursively stepping up the energy scale, perturbation theory can be safely applied at high energy scales, enabling accurate determinations of α_s.

In the short to medium term, progress may still be achievable by employing the step-scaling method with smaller scale factors in larger volumes. This would require dedicated efforts to control and eliminate finite volume effects at each step, possibly focusing on observables less affected by such effects.

However, the computational resources required for the full step-scaling method are substantial. Alternative strategies, such as the decoupling strategy that has been recently proposed [44], offer a more efficient approach to scale evolution with comparable precision. This strategy involves tracing scale evolution in a pure gauge theory and combining it with nonperturbative computations for dynamical quarks. The decoupling strategy relies, to some extent, on QCD computations with $N_f \geq 3$ degenerate heavy quarks at a low energy scale requiring the introduction of massive finite volume couplings. When linking observables at different quark masses, it is important to keep a constant lattice spacing up to order $\mathcal{O}(a^2)$, and hence there is a need to study a lattice theory that respects $\mathcal{O}(a)$ improvements.

Chapter 3

Renormalization group and beta function

The fundamental property of a quantum field theory is locality. Fields are independent degrees of freedom with independent quantum fluctuations defined at different spacetime points. Quantum fluctuations at very short distances emerge as loop Feynman diagrams of virtual particles with high momentum. Loop integrals over the virtual particles yield ultraviolet divergences that appear only in the values of a few parameters such as the bare masses and coupling constants. Thus, quantum fluctuations at short distances barely affect a theory, only through the values of a few of its parameters.

3.1 Renormalization group

A physical picture by K. Wilson[45] suggests that any quantum field theory is defined fundamentally with a cutoff $\tilde{\Lambda}$ that has some physical significance.

In Wilson's treatment, parameters of a renormalizable field theory are determined by a set of renormalization conditions applied at a certain momentum scale, called the renormalization scale (μ). These conditions define the values of the Green's functions at a certain point and remove all ultraviolet divergences.

Rescaling the theory and integrating out high-momentum degrees of freedom over a shell of momentum space can be thought of as a transformation of the Lagrangian [46].

Continuous iterations of this method over infinitesimally thin shells of momentum space will result in a continuous transformation of the Lagrangian. Integrating over high momentum degrees of freedom can be illustrated by a trajectory in the space of all possible Lagrangians. These transformations are often referred to as renormalization group [1].

To better understand the concept of renormalization group let us see the following example. Consider a correlation function of fields at momentum p_i, where $p_i << \tilde{\Lambda}$. A way of calculating this correlation function perturbatively is to use the original Lagrangian L, so the effects of quantum fluctuations at small distances are exposed in loop diagrams. Alternatively, one can first integrate over all momentum shells down to the scale of momenta p_i constructing an effective Lagrangian L_{eff}, and then compute the correlation function. In this way, the high momentum effects have already been absorbed in new coupling constants (g', m') and their effects show up directly in the Lagrangian. Therefore, divergences can be described as contributions from all momentum scales in a Feynman diagram.

Nevertheless, the parameters of the Lagrangian may vary drastically under renormalization group transformations, since we have to iterate the transformations repeatedly. So, we can define a fixed point where scale transformations leave the theory invariant and the coupling does not vary under them. Typically the free field Lagrangian, where all perturbations vanish ($m^2 = g = 0$), is considered a fixed point.

In conclusion, all parameters of a renormalizable field theory can be thought of as scale-dependent quantities. This scale dependence is described by the renormalization group equations. The solution of these equations will lead to finite correlation functions with certain scaling laws.

3.2 Callan-Symanzik equation

Assume we have a renormalized massless quantum field theory with specific renormalization conditions at a renormalization scale μ. We can also define the theory at a different scale $\mu^{'}$, as the renormalization scale is arbitrary. The two

[1] They do not form a group set of group theory, because their inverse operation cannot be defined.

theories coincide if their bare Green's functions,

$$\langle\Omega|\mathcal{T}\phi_0(x_1)\phi_0(x_2)\dots\phi_0(x_n)|\Omega\rangle \tag{3.1}$$

are described by the same functions of the bare parameters (bare coupling constant g_0, the cut-off $\tilde{\Lambda}$, etc.). Note that these functions do not have any dependency on μ.

The renormalized Green's function is given in terms of the bare one and the field strength renormalization Z:

$$\langle\Omega|\mathcal{T}\phi(x_1)\phi(x_2)\dots\phi(x_n)|\Omega\rangle = Z^{-n/2}\,\langle\Omega|\mathcal{T}\phi_0(x_1)\phi_0(x_2)\dots\phi_0(x_n)|\Omega\rangle \tag{3.2}$$

Now, let us look at an infinitesimal change of μ to $\mu+\delta\mu$ in the connected n-point renormalized function $G^{(n)}(x_1, x_2\dots x_n)$. To keep the bare Green's functions fixed, we have to make appropriate shifts in the field strength and the coupling constant as well:

$$\begin{aligned}\mu &\to \mu+\delta\mu \\ g &\to g+\delta g \\ \phi &\to (1+\delta\eta)\phi\end{aligned} \tag{3.3}$$

However, the shift in any renormalized Green's function is only caused by the field rescaling,

$$G^{(n)} \to (1+n\,\delta\eta)G^{(n)} \tag{3.4}$$

Considering that $G^{(n)}$ is a function of μ and g, we can express the transformation by:

$$dG^{(n)} = \frac{\partial G^{(n)}}{\partial\mu}\delta\mu + \frac{\partial G^{(n)}}{\partial g}\delta g = n\,\delta\eta\,G^{(n)} \tag{3.5}$$

It is a standard to define the following dimensionless parameters:

$$\beta \equiv \frac{\mu}{\delta\mu}\delta g \tag{3.6}$$

$$\gamma \equiv -\frac{\mu}{\delta\mu}\delta\eta \tag{3.7}$$

and substituting back in Equation 3.5. Thus, multiplying through by $\mu/\delta\mu$, we derive the Callan-Symanzik equation [47], [48]:

$$\left[\mu\frac{\partial}{\partial\mu} + \beta(g)\frac{\partial}{\partial g} + n\,\gamma(g)\right] G^{(n)}(\{x_i\};\mu,g) = 0 \tag{3.8}$$

The parameters β and γ do not depend on x_i and must be the same for every n. In addition, β and γ are independent of the cut-off $\tilde{\Lambda}$, because the Green's function $G^{(n)}$ is renormalized, and as a consequence, by dimensional analysis, they cannot depend on μ as well. Thus, they are only dependent on the dimensionless variable g.

Trivially, the same arguments can be generalized to other massless theories with multiple fields and coupling constants, provided that there is a γ function for each field and a β function for each coupling.

The computation of the β and γ functions can be established easily by first calculating explicit perturbative expressions of smartly chosen Green's functions. The resulting counterterms that cancel divergences of these expressions, will be dependent on scale μ. Now, because Green's functions expressions satisfy the Callan-Symanzik equation, we can solve for β and γ functions. In fact, β and γ functions will be related to counterterms and their exact formulas will depend on the specific renormalization procedure.

In conclusion, the Callan–Symanzik equation is a differential equation that describes the evolution of the n-point correlation functions under variation of the energy scale at which the theory is defined.

3.3 Beta and gamma functions

Callan–Symanzik equation introduces two functions, $\beta(g)$ and $\gamma(g)$. These functions are related to the shifts in the renormalized coupling and the renormalized field strength, needed to preserve the values of the bare Green's functions for an infinitesimal shift in the renormalization scale μ.

In this section, we express β and γ functions in terms of the parameters of bare perturbation theory (Z, g_0 and $\tilde{\Lambda}$) to get a deep understanding of these functions. Again, for simplicity, we consider a massless theory with a cut-off regulator.

The renormalized coupling g is related to the bare coupling constant g_0 by a renormalization function $Z_g(\mu)$,

$$g = Z_g(\mu) g_0 \tag{3.9}$$

where $Z_g(\mu)$ explicitly manifest the dependence of coupling on μ. A shift of $\mu \to \mu + \delta\mu$, increases the renormalized coupling constant by:

$$\delta g = \left[Z_g(\mu + \delta\mu) - Z_g(\mu) \right] g_0 = \left(\frac{\partial Z_g}{\partial \mu} \delta\mu \right) g_0 \tag{3.10}$$

Therefore, we can express the original definition of β (3.6) as:

$$\beta(g) = \mu \frac{\partial}{\partial \mu} g|_{g_0, \tilde{\Lambda}} \tag{3.11}$$

Furthermore, we can rewrite the original expression for γ with regard to the parameters of bare perturbation theory. Using the fact that the bare and renormalized fields are related by:

$$\phi = \left[Z(\mu) \right]^{-1/2} \phi_0 \tag{3.12}$$

, γ function is given as:

$$\gamma(g) = \frac{1}{2} \frac{\mu}{Z} \frac{\partial}{\partial \mu} Z \tag{3.13}$$

The relation in 3.11 is exact, but the fact that β does not depend on the cutoff $\tilde{\Lambda}$ is not obvious. Nevertheless, one needs to remember the original definition of β in which the cut-off independence comes after the renormalized Green's functions.

According to the definition of $\beta(g)$ in 3.11, the beta function is the rate of change of the renormalized coupling at the scale μ corresponding to a fixed bare coupling. Or otherwise stated as the rate of the renormalization group flow of the coupling constant g.

If $\beta(g) > 0$, the renormalized coupling increases with increasing energy scale. In the case of zero β function, the coupling is independent of the scale and the theory is scale-invariant (or conformally invariant). On the contrary, a negative sign for the β function, as it happens in QCD, indicates a renormalized coupling that decreases at high energies leading to an asymptotically free theory.

Studying the asymptotic high energy limit for QCD ($g \to 0$), one can write the expansion of the β function in powers of g (see [49]):

$$\beta(g) = -b_0 g^3 - b_1 g^5 - b_2 g^7 + \mathcal{O}({g_0}^9) \tag{3.14}$$

So far, we have adopted a massless gauge theory with a general renormalization scheme. Different schemes will vary as the definition of g, m, and the scale of fields, and therefore produce different β and γ functions. The parameters of one renormalization scheme can be determined in terms of another scheme.

Explicitly, two renormalization couplings g_A and g_B of two different renormalization schemes, are related to each other as a function of odd polynomial [49]:

$$g_B = G(g_A) = g_A + G(1)\, g_A^3 + \mathcal{O}(g_B^5) \tag{3.15}$$

The function $G(g_A)$ is equal to g_A up to order g_A^3 since both g_A and g_B are equal to g_0 at leading order. Furthermore, we assume that $G(g_A)$ is invertible.

The two β functions can be related using the definition in 3.11:

$$\beta_A(g_A) = \mu \frac{dg_A}{d\mu} = \mu \frac{\partial g_B}{\partial \mu} \frac{\partial g_A}{\partial g_B} = \beta_B(g_B) \frac{\partial g_A}{\partial g_B} \tag{3.16}$$

where

$$\frac{\partial g_A}{\partial g_B} = 1 - 3G(1)\, g_A^2 + \mathcal{O}(g_B^4) \tag{3.17}$$

On the other hand, an analogous equation can be written for $\beta_B(g_B)$ in terms of g_A using the perturbative expansion in 3.14:

$$\begin{aligned} \beta_B(g_B) &= -b_0^B {g_B}^3 - b_1^B {g_B}^5 + \mathcal{O}({g_B}^7) \\ &= -b_0^B\, {g_A}^3 - (b_0^B\, 3G(1) + b_1^B)\, {g_A}^5 + \mathcal{O}({g_A}^7) \end{aligned} \tag{3.18}$$

Substituting the above equation back to 3.16, one finds

$$\begin{aligned} \beta_A(g_A) &= \left[-b_0^B\, {g_A}^3 - (b_0^B\, 3G(1) + b_1^B)\, {g_A}^5\right] \left(1 - 3G(1)\, g_A^2\right) + \mathcal{O}({g_A}^7) \\ &= -b_0^B {g_A}^3 - b_1^B {g_A}^5 + \mathcal{O}({g_A}^7) \end{aligned} \tag{3.19}$$

proving that $b_0^A = b_0^B$ and $b_1^A = b_1^B$. Therefore, the first two coefficients b_0, b_1 are universal for massless gauge theories, in the sense that they do not depend on the regularization nor the renormalization scheme. However, coefficients $b_i (i \geq 2)$ depend on the renormalization scheme and must be determined perturbatively.

By integrating the definition of β function in 3.11, we obtain an integration constant Λ. Λ is a renormalization group invariant parameter and is given as:

$$\Lambda = \mu \exp\left[\int_{g(\mu)}^{g(\Lambda)} \frac{d\tilde{g}}{\beta(\tilde{g})}\right] \tag{3.20}$$

where the asymptotic behavior of $1/\beta(\tilde{g})$ in a gauge theory, using the power series expansion of β 3.14 can be written as:

$$\frac{1}{\beta(\tilde{g})} = -\frac{1}{b_0\tilde{g}^3}\left(1 - \frac{b_1}{b_0}\tilde{g}^2 + \frac{b_1^2 - b_0 b_2}{b_0^2}\tilde{g}^4 + \mathcal{O}(\tilde{g}^6)\right) \tag{3.21}$$

So, the integral takes the form of:

$$\int_{g(\mu)}^{g(\Lambda)} \frac{d\tilde{g}}{\beta(\tilde{g})} = \left[\frac{1}{2b_0 g^2} + \frac{b_1}{2b_0}\ln(g^2)\right] + \int_{g(\mu)}^{g(\Lambda)} d\tilde{g}\left[\frac{1}{\beta(\tilde{g})} + \frac{1}{b_0\tilde{g}^3} - \frac{b_1}{b_0^2\tilde{g}}\right] \tag{3.22}$$

Thus, substituting back in 3.20 we obtain the Λ parameter of a gauge theory:

$$\Lambda = \mu[b_0 g^2(\mu)]^{-b_1/(2b_0^2)} e^{\left(-\frac{1}{2b_0 g^2(\mu)}\right)} \exp\left\{-\int_0^{g(\mu)} d\tilde{g}\left[\frac{1}{\beta(\tilde{g})} + \frac{1}{b_0\tilde{g}^3} - \frac{b_1}{b_0^2\tilde{g}}\right]\right\} \tag{3.23}$$

This expression is exact and hence is valid beyond perturbation theory. Dimensionful quantities and parameters of a gauge theory can be expressed in units of Λ. Moreover, the Λ parameter can be used for perturbative predictions of jet cross sections and hence provide a way to compare high energy theory with experiments. We can think of the Λ parameter as an intrinsic scale of the theory. Therefore, renormalization conditions of the theory can be specified by the value of the renormalized coupling at a given scale, or equivalently by the value of the Λ parameter.

At high energy regime, i.e. $\Lambda/\mu << 1$, the running of the coupling is given by,

$$\alpha(\mu^2) \simeq \frac{1}{b_0 t}\left(1 - \frac{b_1}{b_0^2}\frac{l}{t} + \frac{b_1^2(l^2 - l - 1) + b_0 b_2}{b_0^4 t^2}\right) \tag{3.24}$$

where $t \equiv \ln(\mu^2/\Lambda^2)$, $l = \ln t$ and $\alpha = g^2/4\pi$.

The running coupling α of one renormalization scheme can be expressed in terms of another scheme, according to 3.15:

$$\alpha_A(\mu^2) = \alpha_B(\mu^2) + d_1^A(\mu^2)\alpha_B^2(\mu^2) + d_2^A(\mu^2)\alpha_B^3(\mu^2) + \dots \tag{3.25}$$

where d_1^A and d_2^A are 1- and 2-loop coefficients relating to the running coupling in these schemes. By taking only the leading term of 3.24, we can derive an expression that relates the Λ parameters of two schemes at the same energy scale:

$$\frac{\Lambda_A}{\Lambda_B} = \exp\left(\frac{d_1^A}{2b_0}\right) \tag{3.26}$$

3.4 Beta function on lattice regularization

Employing lattice as a regulator in quantum field theory, introduces a new parameter, namely as the lattice spacing, which determines the distance between neighboring lattice points. Henceforth, we will assume a theory on a 4-dimensional lattice with lattice spacing a.

In general, measurable quantities in lattice theories depend on lattice spacing. In particular, they are defined in such a way that they redeem their continuum value at the limit of $a \to 0$. Therefore, a variation of a should not affect physical observables. Such a fluctuation must be compensated only by a change of a on the bare parameters involved in the Lagrangian.

We now assume a measurable quantity O with dimensions of mass (or inverse length) dO. We also define its lattice form $\hat{O}$. On lattice, $\hat{O}$ is dimensionless and it depends on the bare parameters of the theory. Its continuum limit suggests that:

$$O(g_0, a) = \frac{\hat{O}}{a^{dO}} \tag{3.27}$$

implying simultaneously that:

$$O(g_0(a), a) = O_{\text{physical}} \tag{3.28}$$

Equations 3.27 and 3.28 are equal in the limit of small a, so $\hat{O} = a^{dO} O_{\text{physical}}$. Therefore we can determine g_0 in terms of a and O_{physical}, assuming $\hat{O}$ is known. Thus, the coupling constant is always related to a measurable quantity.

For sufficiently small lattice spacing, there is a universal $g_0(a)$ applicable to all quantities. In this manner, we can use any convenient observable to define the bare coupling $g_0(a)$. For example, let us choose the quark-antiquark static potential [50]. Suppose that R is the distance between the quark-antiquark pair measured in physical units, and its lattice version is given by,

$$V(R, g_0(a), a) = \frac{1}{a}\hat{V}(\frac{R}{a}, g_0(a)) \tag{3.29}$$

where R/a is their separation distance in lattice units. However, the observable $V(R, g_0(a), a)$ must be invariant under variations of the lattice spacing. This is ensured by

$$a\frac{d}{da}V(R, g_0(a), a) = \left[a\frac{\partial}{\partial a} - \left(-a\frac{\partial g_0}{\partial a}\right)\frac{\partial}{\partial g_0}\right] V(R, g_0(a), a) = 0 \tag{3.30}$$

This is the equivalent of the Callan-Symanzik equation (3.8) for lattice gauge theories, while the lattice form of β function is defined as:

$$\beta_L(g_0) = -a\frac{dg_0}{da}\Big|_{g,\mu} \tag{3.31}$$

where μ is the renormalization scale and g the renormalized coupling constant. The lattice β function expresses the rate of change of coupling constant under a variation of the lattice spacing.

Similar to 3.14, the asymptotic limit ($g_0 \to 0$) of the lattice β function is:

$$\beta_L(g_0) = -b_0 {g_0}^3 - b_1 {g_0}^5 - b_2^L {g_0}^7 + \mathcal{O}({g_0}^9) \tag{3.32}$$

as discussed before, the coefficients b_0, b_1 are universal, hence we suppress the superscript L.

Furthermore, the Λ_L parameter of the theory is a particular solution of the lattice version of Callan-Symanzik equation 3.30. Thus, repeating the procedure followed in

3.20 to 3.23, one can obtain the Λ_L parameter of a lattice gauge theory for the 2-loop corrections:

$$a\Lambda_L = \exp\Big[-\int^{g_0} \frac{dg}{\beta^L(g)}\Big] = \exp\Big(-\frac{1}{2b_0 g_0^2}\Big)(b_0 g_0^2)^{-b_1/(2b_0^2)}[1 + q g_0^2 + \mathcal{O}(g_0^4)] \quad (3.33)$$

where q is the correction factor

$$q = \frac{b_1^2 - b_0 b_2^L}{2b_0^3} \quad (3.34)$$

Chapter 4

Background field formalism

The background field formalism was first adopted in quantum gravity [51] and it has been a helpful method to study the renormalization of gauge theories since. The use of a background field leads to a gauge-invariant effective action with respect to the background field and as a consequence, numerical computations are technically simplified.

The functional integral considering a background gauge field, contains all required symmetry properties to establish renormalizability to all orders in perturbation theory in both dimensional (DR) and lattice regularization (LR) [52], [53]. Moreover, the introduction of the background field does not require any further counterterms besides those already needed in its absence.

In lattice gauge theories, the background field method is primarily used for the computation of the matching between different couplings. It has been the most systematic and economical way.

4.1 Classical action and gauge fixing

In this section, we consider a pure $SU(N)$ gauge theory in D dimensions, characterised by a gauge potential $A_\mu(x) = A^\alpha_\mu(x)T^\alpha$, where T^α are the generators of the algebra with the convention of $\mathrm{Tr}(T^aT^b) = \delta^{ab}/2$. The Yang-Mills action may be written as:

$$S[A] = -\frac{1}{2g_0^2}\int d^D(x)\mathrm{Tr}\left\{F_{\mu\nu}(x)F_{\mu\nu}(x)\right\} \tag{4.1}$$

where g_0 is the bare gauge coupling constant and $F_{\mu\nu}(x)$ the field strength tensor ($F_{\mu\nu}(x) = \partial_\mu A_\nu(x) - \partial_\nu A_\mu(x) + [A_\mu(x), A_\nu(x)]$). According to the background field technique, we separate the gauge field into two parts, the quantum field $Q_\mu(x) = Q^a_\mu(x)T^a$ and the background field, $B_\mu(x) = B^a_\mu(x)T^a$:

$$A_\mu(x) = B_\mu(x) + g_0 Q_\mu(x) \tag{4.2}$$

The background field is considered an arbitrary external source field, which is not required to satisfy the Yang-Mills equations, while the quantum field is the integration variable of the functional integral.

By substituting equation 4.2 back to the Yang-Mills action, we have to add a gauge fixing term which breaks the quantum gauge invariance, but in such a way that the background field is invariant under gauge transformations:

$$S_{gf}[B, Q] = -\lambda_0 \int d^D x \, \mathrm{Tr} \Big\{ D_\mu Q_\mu(x) D_\nu Q_\nu(x) \Big\} \tag{4.3}$$

where λ_0 is the bare gauge parameter and $D_\mu = \partial_\mu + iB_\mu$ is the covariant derivative.

The gauge-fixing term gives rise to the following Fadeev-Popov action:

$$S_{FP}[B, Q, c, \bar{c}] = -2 \int d^D x \, \mathrm{Tr} \Big\{ D_\mu \bar{c}(x) \Big(D_\mu + i g_0 Q_\mu(x) \Big) c(x) \Big\} \tag{4.4}$$

where $c(x)(\bar{c}(x)$ is the ghost (antighost) field.

As one can see from equations 4.4 and 4.3, external quantities are coupled only to $Q_\mu(x)$ and thus gauge invariance of $B_\mu(x)$ is always preserved.

The total action is given by,

$$S_{total}[B, Q, c, \bar{c}] = S[B + g_0 Q] + S_{gf}[B, Q] + S_{FP}[B, Q, c, \bar{c}] \tag{4.5}$$

and coincides with its standard form in the vanishing limit of the background field.

The partition function $Z[J, \eta, \bar{\eta}]$ ($J_\mu(x), \eta, \bar{\eta}$ are classical source fields) in the presence of the background field and is given by:

$$Z[B, J, \eta, \bar{\eta}] = \frac{1}{\mathcal{N}} \int D[Q] D[\bar{c}] D[c] \, e^{-S_{total}[B,Q,c,\bar{c}] + (J,Q) + (\bar{\eta},c) + (\eta,\bar{c})} \tag{4.6}$$

with the normalization factor $\mathcal{N}$ ensuring that $Z[0, 0, 0, 0] = 1$.

The gauge invariance property of the background field appears in the partition function as well, since $B_\mu(x)$ is not coupled to the source J, whereas all sources and ghost fields transform in the same way as Q does. In addition, Z can be expanded in powers of $B, J, \eta, \bar{\eta}$, with the coefficients being expectation values of products constructed by local operators, at vanishing sources. In the following, $Z[B, J, \eta, \bar{\eta}]$ will be considered as a well-defined formal power series of $B, J, \eta, \bar{\eta}$.

We can also write the expansion of the generating functional for the connected diagrams W:

$$W[B, J, \eta, \bar{\eta}] = \ln\left(Z[B, J, \eta, \bar{\eta}]\right) \tag{4.7}$$

The background field effective action, $\Gamma[B, Q^*, c^*, \bar{c}^*]$, can be derived by a Legendre transformation, and its expression is written as:

$$\Gamma[B, Q^*, c^*, \bar{c}^*] = W[B, J, \eta, \bar{\eta}] - (J, Q^*) - (\bar{\eta}, c^*) - (\eta, \bar{c}^*) \tag{4.8}$$

where

$$Q^* = \frac{\delta W}{\delta J}, \;\; c^* = \frac{\delta W}{\delta \bar{\eta}}, \;\; \bar{c}^* = -\frac{\delta W}{\delta \eta} \tag{4.9}$$

The functional $\Gamma[B, Q^*, c^*, \bar{c}^*]$ corresponds to the background field effective action considered as a functional of B and evaluated at $Q = 0$. It can be obtained from the calculation of the 1-particle-irreducible, Green's functions of the background field.

Similar to the partition function Z, equation 4.8 can be considered as a power series expansion of its arguments and obtain the vertex functions $\Gamma^{(j,k,l)}$ with j, k, l correspond to the number of background, quantum and ghost fields respectively, appearing in the vertex.

4.2 Background field and gauge fixing on lattice

We consider a four-dimensional hypercubic lattice characterized by its lattice spacing a. In the lattice action of a pure $SU(N)$ theory, gauge fields are introduced via the variables $U_\mu(x)$. The variables are defined on the links connecting two neighboring lattice sites and they are constructed in such a way that the Yang-Mills action is recovered in the continuum limit ($a \to 0$) of the lattice gluon action.

The implementation of the background field method on lattice theories is not sole. Each different selection leads to the same action in the continuum limit if the lattice theory is renormalized, and thus the exact way of introducing the background field is not important. So we proceed as follows; link variables are separated into a background field $B_\mu(x)$ and a quantum field $Q_\mu(x)$, similar to 4.2:

$$\begin{aligned} U_\mu(x) &= U^Q_\mu(x) U^B_\mu(x), \\ U^Q_\mu(x) &\equiv e^{ig_0 Q_\mu(x)}, \\ U^B_\mu(x) &\equiv e^{iag_0 B_\mu(x)} \end{aligned} \tag{4.10}$$

Since the gauge link is now a product of two different field links, there is freedom in interpreting the gauge transformation:

$$[U_\mu(x)]^\Lambda = \Lambda(x) U_\mu(x) \Lambda^{-1}(x + a\hat{\mu}); \tag{4.11}$$

This transformation can be viewed in two ways. The first one considers the quantum field as a matter field which transforms purely locally, while the background field transforms as a true gauge field:

$$\begin{aligned} [U^Q_\mu(x)]^\Lambda &= \Lambda(x) U^Q_\mu(x) \Lambda^{-1}(x) \\ [U^B_\mu(x)]^\Lambda &= \Lambda(x) U^B_\mu(x) \Lambda^{-1}(x + a\hat{\mu}) \end{aligned} \tag{4.12}$$

The second one considers the background field as invariant, while the quantum field is now the true gauge field:

$$\begin{aligned} [U^Q_\mu(x)]^\Lambda &= \Lambda(x) U^Q_\mu(x) \Lambda^{-1}(x + a\hat{\mu}) \\ [U^B_\mu(x)]^\Lambda &= U^B_\mu(x) \end{aligned} \tag{4.13}$$

Let us call the first interpretation of gauge transformations "background gauge transformations" and the second one "quantum gauge transformations". As the background is an external field, which is not involved in the path integration, the gauge-fixing term, which ensures the finiteness of path integrals, can be chosen to preserve the gauge invariance under background transformations. A proper choice

(see [54]) is the following gauge fixing term:

$$S_{gf} = \lambda_0 a^4 \sum_{x,\mu,\nu} \mathrm{Tr}\, \left\{ D^-_\mu Q_\mu(x) D^-_\nu Q_\nu(x) \right\} \tag{4.14}$$

where the lattice covariant derivative D^-_μ is written as:

$$D^-_\mu Q_\nu(x) = \frac{1}{a}\Big[U^{B^{-1}}_\mu(x - a\hat{\mu})\; Q_\nu(x - a\hat{\mu})\; U^B_\mu(x - a\hat{\mu}) - Q_\nu(x) \Big] \tag{4.15}$$

This term preserves the gauge invariance of the background field in the action, even though it breaks the gauge invariance of the quantum field.

By examining how the gauge-fixing term changes when a gauge transformation of the form specified in Eq. 4.13 is applied, i.e., $\delta\left(D^\mu Q_\mu(x)\right)/\delta\Lambda(x)$, we can derive the Faddeev-Popov action. Here, we only present the relevant terms of the action for our calculations, up to $\mathcal{O}(g_0^2)$:

$$S_{FP} = 2a^4 \sum_{x,\mu} \mathrm{Tr} \Big\{ (D^+_\mu \omega(x))^\dagger \Big(D^+_\mu \omega(x) + i g_0 \left[Q_\mu(x), \omega(x) \right] + \frac{1}{2} i g_0 a \left[Q_\mu(x), D^+_\mu \omega(x) \right] \\ - \frac{1}{12} g_0^2 a^2 \left[Q_\mu(x), \left[Q_\mu(x), D^+_\mu \omega(x) \right] \right] + \cdots \Big) \Big\} \tag{4.16}$$

where $\omega(\omega^\dagger)$ is the ghost (antighost) field and

$$D^+_\mu \omega(x) = \frac{1}{a}\Big[U^B_\mu(x) \omega(x + a\hat{\mu}) U^{B^{-1}}_\mu(x) - \omega(x) \Big] \tag{4.17}$$

Finally, the change of integration variables from links to vector fields yields a Jacobian that can be rewritten as a measure term $S_{meas.}$ in the action:

$$S_{meas} = \frac{1}{12} N_c g_0^2 a^2 \sum_{x,\mu} \mathrm{Tr} \Big\{ Q_\mu(x) Q_\mu(x) + \cdots \Big\} \tag{4.18}$$

Note that the measure term is not affected by the presence of a background field.

Therefore the full action is given by:

$$S = S_{\mathrm{F}} + S_{\mathrm{G}} + S_{\mathrm{gf}} + S_{\mathrm{FP}} + S_{\mathrm{meas.}} \tag{4.19}$$

The background field and coupling constant renormalization are determined by the 2-point function of the background field; no renormalization for the quantum and

ghost fields is needed. The reason for this is that these fields appear only within the loops of a diagram (external lines correspond to background fields) and their renormalization factor would be canceled with those of the propagators. The gauge fixing parameter also needs to be redefined, since the longitudinal part of the propagator must be renormalized. The renormalized quantities can be written with respect to the bare ones:

$$B_0^\mu = \left[Z_B^{(X,Y)}\right]^{1/2} B^\mu \tag{4.20}$$

$$g_0 = Z_g^{(X,Y)} g \tag{4.21}$$

$$\lambda = Z_\lambda^{(X,Y)} \lambda_0 \tag{4.22}$$

where B^μ, g, and λ denote the renormalized values of the background field, coupling constant, and gauge parameter, respectively. Note that all renormalization factors depend on the regularization X (where $X = \mathrm{DR}$, LR, etc.) and on the renormalization scheme Y (where $Y = \overline{\mathrm{MS}}$, RI′, etc.), and should thus be properly represented as $Z^{X,Y}$ unless it is clear from the context.

Chapter 5

QCD running coupling

Let us first recall some concepts discussed in Chapter 3, related to the beta function in the massless case and to the background field method; these will be useful as we extend them to the case of nonzero fermion mass. The dependence of the renormalized coupling constant on the intrinsic scale of the renormalization scheme is given by the renormalized β-function:

$$\beta(g) \equiv \bar{\mu}\frac{dg}{d\bar{\mu}}\Big|_{a,g_0} \tag{5.1}$$

where a is the lattice spacing, $\bar{\mu} = \mu\,(4\pi/e^{\gamma_E})^{1/2}$ is the renormalization scale and g (g_0) is the renormalized (bare) coupling constant. We will employ the $\overline{\text{MS}}$ renormalization scheme in this work. In the asymptotic limit for QCD ($g \to 0$), one can write the expansion of β-function in powers of g_0:

$$\beta(g) = -b_0\, g^3 - b_1\, g^5 - b_2\, g^7 + \mathcal{O}({g_0}^9) \tag{5.2}$$

The bare β-function for the lattice regularization is defined as:

$$\beta_L(g_0) \equiv -a\frac{dg_0}{da}\Big|_{\bar{\mu},g} \tag{5.3}$$

Similar to Eq.5.2, the asymptotic high energy limit ($g_0 \to 0$) of the lattice bare β-function is:

$$\beta_L(g_0) = -b_0{g_0}^3 - b_1{g_0}^5 - b_2^L{g_0}^7 + \mathcal{O}({g_0}^9) \tag{5.4}$$

The first two coefficients b_0, b_1 are universal for massless gauge theories (see Chapter 3), in the sense that they do not depend on the regularization nor the renormalization

scheme. However, coefficients $b_i^L (i \geq 2)$ depend on the renormalization scheme and must be determined perturbatively.

Expressions of the coefficients b_0, b_1, and b_2 can be found in Ref. [55]:

$$b_0 = \frac{1}{(4\pi)^2}\Big(\frac{11}{3}N_c - \frac{2}{3}N_f\Big) \tag{5.5}$$

$$b_1 = \frac{1}{(4\pi)^4}\Big[\frac{34}{3}N_c^2 - N_f\Big(\frac{13}{3}N_c - \frac{1}{N_c}\Big)\Big] \tag{5.6}$$

$$b_2 = \frac{1}{(4\pi)^6}\Big[\frac{2857}{54}N_c^3 + N_f\Big(-\frac{1709}{54}N_c^2 + \frac{187}{36} + \frac{1}{4N_c^2}\Big) + N_f^2\Big(\frac{56}{27}N_c - \frac{11}{18N_c}\Big)\Big] \tag{5.7}$$

where N_c is number of color and N_f is number of flavor.

The bare coupling constant g_0 is related to the renormalized coupling constant g through the renormalization factor Z_g [1]:

$$g_0 = Z_g(g_0^2, a\bar{\mu})g \tag{5.8}$$

The renormalization factor Z_g is related to the $\overline{\text{MS}}$-renormalized $\beta(g)$ through:

$$\beta(g) = -g\mu\frac{d}{d\mu}\ln Z_g(g_0, a\mu)\Big|_{a,g_0} \tag{5.9}$$

while the lattice β-function $\beta_L(g_0)$ can be expressed as:

$$\beta_L(g_0) = -g_0 a\frac{d}{da}\ln Z_g(g_0, a\mu)\Big|_{\mu,g} \tag{5.10}$$

Due to the renormalizability of the theory ([56]) combined with dimensional arguments, the lattice β-function, as defined above, is independent of the renormalized fermionic masses. Thus, the arguments of the massless case for the beta function remain valid even in the case of non-zero fermion mass.

Using Eqs. 5.9 and 5.10, one can derive an exact relation, valid to all orders of perturbation theory [57]:

$$\beta_L(g_0) = \Big(1 - g_0^2\frac{\partial}{\partial g_0^2}\ln Z_g^2\Big)^{-1} Z_g\,\beta(g_0 Z_g^{-1}) \tag{5.11}$$

[1] Hereafter, we omit the superscript $(L, \overline{MS})$ from $Z_g^{(L,\overline{MS})}$.

Writing Z_g^2 in the form of one- and two-loop coefficients:

$$Z_g^2(g_0, a\bar{\mu}) = 1 + {g_0}^2 L_0(a^2\bar{\mu}^2) + {g_0}^4 L_1(a^2\bar{\mu}^2) + \mathcal{O}({g_0}^6) \tag{5.12}$$

follows that $L_0(a^2\bar{\mu}^2) = b_0 \ln(a^2\bar{\mu}^2) + l_0$ and $L_1(a^2\bar{\mu}^2) = b_1 \ln(a^2\bar{\mu}^2) + l_1$. Substituting back to 5.11, we extract a relation for the lattice coefficient b_2^L:

$$b_2^L = b_2 - b_1 l_0 + b_0 l_1. \tag{5.13}$$

Thus, the evaluation of b_2^L requires the determination of the 2-loop quantity l_1 and the 1-loop quantity l_0. Specifically, the following references can be found in the literature on the calculation of b_2^L; using Wilson gluons [58, 59], Symnazik improved gluons [60], Wilson fermions [57], clover fermions [61], and overlap fermions [62].

Moreover, coefficient constant l_0 is further related to the ratio of the Λ parameters associated with the particular lattice regularization and the $\overline{\text{MS}}$ scheme:

$$\frac{\Lambda_L}{\Lambda_{\overline{\text{MS}}}} = \exp\left(\frac{l_0}{2b_0}\right) \tag{5.14}$$

5.1 Lattice QCD with $\mathcal{O}(a)$ improvement

Let us revisit some concepts regarding the precision determination of the strong coupling constant as discussed in Chapter 2. The world average of the strong-coupling constant (α_s), evaluated at the Z-boson mass scale, includes various determinations, each classified based on their methodological approach (e.g, hadron collisions, τ decays, etc.). The most accurate determinations arise from lattice QCD, providing a result of $\alpha_s(m_Z^2) = 0.01184 \pm 0.0008$ [33]. However, employing lattice QCD introduces systematic uncertainties in the precise determination of α_s. These uncertainties are associated with perturbative truncation, discretization errors in continuum limit extrapolations, and finite volume effects.

Overcoming the limitations of simulations is challenging without employing a specific strategy to control systematic uncertainties. Addressing this challenge, a recent lattice QCD strategy has been proposed, named as the decoupling method [44]. This method enables the connection of an experimentally well-measured low-energy quantity with the high-energy regime of QCD, where perturbation theory can be safely applied. Thus,

it effectively eliminates systematic errors in a controlled way, as opposed to most "large volume" approaches.

As seen in Chapter 2, the decoupling strategy requires linking observables at different quark masses, and thus it is crucial to keep a constant lattice spacing up to order $\mathcal{O}(a)^2$. So, there is a need to study a lattice theory that respects $\mathcal{O}(a)$ improvements.

In an $\mathcal{O}(a)$ improved lattice theory, one has to properly impose renormalization conditions in a way that correlation functions of the renormalized field converge to the continuum limit as $\mathcal{O}(a^2)$. A simple strategy is to choose all renormalization conditions defined at the same point (g_0, am_0) in the bare parameter space. In this scheme, transformations of the bare parameters and rescaling of the bare fields do not affect renormalization quantities. Hence, the corresponding counterterms of $\mathcal{O}(a)$ can be ignored and so this category of renormalization schemes is automatically compatible with $\mathcal{O}(a)$ improvement. However, in this manner, the renormalized coupling constant and renormalized fields implicitly depend on the quark mass. This can be avoided though, by using mass-independent renormalization schemes [63].

In mass-independent schemes, renormalization conditions are defined at zero quark mass. As a result, renormalized quark masses are decoupled from the running coupling and it is convenient to study its scale evolution (β-function) since the arguments of the massless theory will remain the same. Then, the issue is that the theory of finite mass quark must be related to the massless theory. This link is usually established through the bare parameters. Thus, there is a need for reparametrization of the bare theory, so that we can preserve the $\mathcal{O}(a)$ improvement.

To set up a general mass-independent renormalization scheme respecting $\mathcal{O}(a)$ improvement, we introduce a modified bare coupling through:

$$\tilde{g}_0^2 = g_0^2(1 + b_g(g_0^2)\, am_q) \tag{5.15}$$

while the subtracted mass, m_q, is given by:

$$m_q = m_0 - m_c(g_0^2) \tag{5.16}$$

The parameter $m_c(g_0^2)$ is the critical value of the bare quark mass at which the renormalized quark masses vanish. Note that $m_c(g_0^2)$ depends on how the physical quark mass is defined, but its exact form should differ at $\mathcal{O}(a^2)$. Nevertheless, order

a^2 corrections are considered negligible. At $m_0 = m_c$, the modified and ordinary bare coupling coincide. Moreover, $b_g(g_0^2)$ in Eq.5.15 must be appropriately selected so as to remove any remaining cutoff effects of $\mathcal{O}(a)$. The bottom line is that the scaling required for g_0 depends on the quark mass, while $\tilde{g}_0$ scales independently of the quark mass.

For heavier quarks in decoupling methods, values of am_q increase, emphasizing the significance of determining $b_g(g_0^2)$ in both perturbation and non-perturbation theories. Non-perturbative calculations of $b_g(g_0^2)$ have been recently carried out [64]. Currently, in perturbation theory $b_g(g_0^2)$ is only known to 1-loop order [63], which introduces a significant systematic error to the precision of the strong coupling constant due to the truncated perturbative result [44].

In this context, the renormalized coupling g within a mass-independent scheme, compatible with $\mathcal{O}(a)$ improvement, is related to the bare parameters through:

$$\tilde{g}_0 = Z_g(\tilde{g}_0^2, a\bar{\mu})g \tag{5.17}$$

where Z_g is a power expansion of $\tilde{g}_0$. Meanwhile, the bare lattice β function, defined by Eq. 5.3, is now transformed as:

$$\beta_L(\tilde{g}_0) \equiv -a\frac{d\tilde{g}_0}{da}\Big|_{\bar{\mu},g} \tag{5.18}$$

Consequently, statements made in the context of the massless theory remain valid to the massive case, except for the necessity to use the modified bare coupling constant as defined in Eq. 5.15 for all quantities defined in the preceding section.

5.2 Formulation

5.2.1 Improved lattice action

Our computations are carried out within the lattice regularization, utilizing the clover improved action (Sheikholeslami-Wohlert) [65] for fermions. The clover action reads,

in standard notation:

$$\begin{aligned} S_{\rm F} &= \sum_f \sum_x (4r + m_0)\bar{\psi}_f(x)\psi_f(x) \\ &- \frac{1}{2}\sum_f \sum_{x,\mu} \left[\bar{\psi}_f(x)\,(r-\gamma_\mu)\,U_{x,x+\mu}\psi_f(x+\mu) + \bar{\psi}_f(x+\mu)\,(r+\gamma_\mu)\,U_{x+\mu,x}\psi_f(x)\right] \\ &- \frac{1}{4}\,c_{\rm SW}\sum_f \sum_{x,\mu,\nu} \bar{\psi}_f(x)\sigma_{\mu\nu}\hat{F}_{\mu\nu}(x)\psi_f(x), \end{aligned} \tag{5.19}$$

where r is the Wilson parameter, f is a flavor index, $\sigma_{\mu\nu} = [\gamma_\mu, \gamma_\nu]/2$, m_0 is the Lagrangian quark mass[2] and c_{SW} is the clover parameter. In the following calculations, r is set to 1 as customary, and c_{SW} is considered as a free parameter for wider applicability of results. Powers of the lattice spacing a have been omitted and may be directly reinserted by dimensional counting. The tensor $\hat{F}_{\mu\nu}$ is proportional to a lattice representation of the gluon field tensor, defined through:

$$\hat{F}_{\mu\nu} \equiv \frac{1}{8}\,(Q_{\mu\nu} - Q_{\nu\mu}) \tag{5.20}$$

where $Q_{\mu\nu}$ is the sum of the plaquette loops:

$$\begin{aligned} Q_{\mu\nu} &= U_{x,x+\mu}U_{x+\mu,x+\mu+\nu}U_{x+\mu+\nu,x+\nu}U_{x+\nu,x} \\ &+ U_{x,x+\nu}U_{x+\nu,x+\nu-\mu}U_{x+\nu-\mu,x-\mu}U_{x-\mu,x} \\ &+ U_{x,x-\mu}U_{x-\mu,x-\mu-\nu}U_{x-\mu-\nu,x-\nu}U_{x-\nu,x} \\ &+ U_{x,x-\nu}U_{x-\nu,x-\nu+\mu}U_{x-\nu+\mu,x+\mu}U_{x+\mu,x} \end{aligned} \tag{5.21}$$

For the gauge fields we employ a class of Symanzik improved gauge actions [66], involving Wilson loops with 4 and 6 links (1×1 plaquettes and 1×2 rectangles, respectively), which is given by the relation

$$S_{\rm G} = \frac{2}{g_0^2}\left[c_0 \sum_{\rm plaq.} \mathrm{Re\,Tr}\,\{1 - U_{\rm plaq.}\} + c_1 \sum_{\rm rect.} \mathrm{Re\,Tr}\,\{1 - U_{\rm rect.}\}\right] \tag{5.22}$$

The coefficients c_0 and c_1 can in principle be chosen arbitrarily, subject to the following normalization condition, which ensures the correct classical continuum limit of the

[2]For simplicity of notation, we denote all flavor masses by m_0; the case of different flavor masses can be trivially recovered from our results.

action:

$$c_0 + 8c_1 = 1 \tag{5.23}$$

For the numerical evaluation, particular choices of values for $\{c_0, c_1\}$ are employed in our calculations as shown in Table 5.1.

Gluon action	c_0	c_1
Wilson	1	0
TL Symanzik	5/3	$-1/12$
Iwasaki	3.648	-0.331

TABLE 5.1: Commonly used sets of values for Symanzik coefficients.

5.2.2 Theoretical setup

The most convenient and economical approach to computing Z_g^2 involves employing the background field method discussed in Chapter 2. In this method, link variables are decomposed into a background field $B_\mu(x)$ and a quantum field $Q_\mu(x)$ (refer to Eq. 4.10).

The fact that exact gauge invariance is preserved in the background field formalism, leads to a relation between the renormalization factors of background field Z_B and of coupling constant Z_g [67]:

$$Z_B(g_0^2, a\mu)\ Z_g^2(g_0^2, a\mu) = 1 \tag{5.24}$$

where $B_0^\mu = Z_B(g_0^2, a\mu)^{1/2} B^\mu$. In this framework, the relation between the lattice bare coupling constant and the renormalized one can be extracted by the evaluation of Z_B, instead of Z_g^2, with no need to calculate any 3-point Green's functions. Note that the inclusion of quark masses adds a layer of complexity to this calculation.

Henceforth we consider the 1-particle-irreducible (1-PI) 2-point Green's function of background field, both in the continuum ($\Gamma_{\rm R}^{\rm BB}(p, m, \lambda)_{\mu\nu}^{ab}$) and on the lattice ($\Gamma_{\rm L}^{\rm BB}(p, m_q, \lambda_0)_{\mu\nu}^{ab}$), in the presence of a fermion mass [3] . These functions can be expressed in terms of scalar amplitudes $\nu_R(p, m, \lambda)$, $\nu(p, m_q, \lambda_0)$. Following the

[3]We adopt the notation $\Gamma^{\rm BB}$ for the vertex function, in contrast to the $\Gamma^{(2,0,0)}$ notation used in Chapter 2.

notation of Ref.[58] the Green's functions of the background field in the continuum are given as:

$$\begin{aligned}\Gamma^{\mathrm{BB}}_{\mathrm{R}}(p,m,\lambda)^{ab}_{\mu\nu} &= -\delta^{ab}(\delta_{\mu\nu}p^2 - p_\mu p_\nu)\left(1-\nu_{\mathrm{R}}(p,m,\lambda)\right)/g^2\ ,\\ \nu_{\mathrm{R}}(p,m,\lambda) &= \sum_{\ell=1}^{\infty} g^{2\ell}\nu^{(\ell)}_{\mathrm{R}}(p,m(g_0^2),\lambda(g_0^2))\end{aligned} \tag{5.25}$$

where $\nu^{(\ell)}_{\mathrm{R}}(p,m(g_0^2),\lambda(g_0^2))$ can be written as:

$$\nu^{(\ell)}_{\mathrm{R}}(p,m(g_0^2),\lambda(g_0^2))) = \nu^{(\ell)}_{\mathrm{R}}(p,0,\lambda(g_0^2))) + \Delta\nu^{(\ell)}_{\mathrm{R}}(p,m(g_0^2),\lambda(g_0^2))) \tag{5.26}$$

where λ is the inverse $\overline{\mathrm{MS}}$-renormalized gauge parameter, m is the renormalized mass (where $m = Z_m(g_0^2)\, m_q$) and $\nu^{(\ell)}_{\mathrm{R}}(p,0,\lambda(g_0^2)))$ is the result corresponding to the massless case.

Similarly, the Green's functions of the background field in the lattice are given as:

$$\begin{aligned}\sum_\mu \Gamma^{\mathrm{BB}}_{\mathrm{L}}(p,m_q,\lambda_0)^{ab}_{\mu\mu} &= -\delta^{ab}3\hat{p}^2\left(1-\nu(p,m_q,\lambda_0)\right)/g_0^2\ ,\\ \nu(p,m_q,\lambda_0) &= \sum_{\ell=1}^{\infty} g_0^{2\ell}\nu^{(\ell)}(p,m_q,\lambda_0)\end{aligned} \tag{5.27}$$

where $\hat{p}^2 = \sum_\mu \hat{p}_\mu^2$, $\hat{p}_\mu = (2/a)\sin(ap_\mu/2)$, and λ_0 is the inverse bare gauge parameter. The amplitude $\nu^{(\ell)}(p,m_q,\lambda_0)$ can be written as:

$$\begin{aligned}\nu^{(\ell)}(p,m_q,\lambda_0) &= \nu^{(\ell)}_0(p,m_q,\lambda_0) + a\, m_q\, \nu^{(\ell)}_1(p,m_q,\lambda_0) + \mathcal{O}(a^2\, m_q^2)\\ &= \nu^{(\ell)}_0(p,0,\lambda_0) + \Delta\nu^{(\ell)}_0(p,m_q,\lambda_0)\\ &\qquad + a\, m_q\left(\nu^{(\ell)}_1(p,0,\lambda_0) + \Delta\nu^{(\ell)}_1(p,m_q,\lambda_0)\right) + \mathcal{O}(a^2\, m_q^2)\end{aligned} \tag{5.28}$$

where $\nu^{(\ell)}_0(p,0,\lambda_0)$ represents the outcome to the massless theory without considering the $\mathcal{O}(a)$ improvement. The tensor structure of these Green's functions, as given above, is implied by the symmetries of the theory.

As discussed in Ref.[52], the continuum and lattice Green's functions are related by $\Gamma^{\mathrm{BB}}_{\mathrm{R}} = \Gamma^{\mathrm{BB}}_{\mathrm{L}}$. Thus, using the Eqs.(5.24),(5.25), and (5.27) we can express Z_g^2 in terms of $\nu_R(p)$, $\nu(p)$:

$$Z_g^2 = Z_B^{-1} = \frac{1-\nu(p,m_q,\lambda_0)}{1-\nu_{\mathrm{R}}(p,m,\lambda)} \tag{5.29}$$

In the computation, we used an arbitrary bare gauge-fixing parameter. Therefore the gauge parameter must be explicitly renormalized. To find a similar relation to Eq. 5.29 for the renormalization factor Z_λ (where $\lambda = Z_\lambda(g_0^2)\ \lambda_0$), we need to introduce the scalar terms $\omega_{\mathrm{R}}(p,m)$ and $\omega(p,m_q)$ into the definition of the quantum field self-energy in the continuum ($\Gamma_{\mathrm{R}}^{\mathrm{QQ}}(p,m,\lambda)_{\mu\nu}^{ab}$) and on the lattice ($\Gamma_{\mathrm{L}}^{\mathrm{QQ}}(p,m_q,\lambda_0)_{\mu\nu}^{ab}$), respectively. The Green's functions of the quantum field in the continuum are given as:

$$\begin{aligned}\Gamma_{\mathrm{R}}^{\mathrm{QQ}}(p,m,\lambda)_{\mu\nu}^{ab} &= -\delta^{ab}\left[(\delta_{\mu\nu}p^2 - p_\mu p_\nu)\,(1-\omega_{\mathrm{R}}(p,m)) + \lambda\ p_\mu p_\nu\right]\ ,\\ \omega_{\mathrm{R}}(p,m) &= \sum_{\ell=1}^{\infty} g^{2\ell}\omega_{\mathrm{R}}^{(\ell)}(p,m(g_0^2))\end{aligned} \tag{5.30}$$

where $\omega_{\mathrm{R}}^{(\ell)}(p,m(g_0^2))$ can be written as:

$$\omega_{\mathrm{R}}^{(\ell)}(p,m(g_0^2)) = \omega_{\mathrm{R}}^{(\ell)}(p,0) + \Delta\omega_{\mathrm{R}}^{(\ell)}(p,m(g_0^2)) \tag{5.31}$$

where $\omega_{\mathrm{R}}^{(\ell)}(p,0)$ is the result corresponding to the massless case.

Similarly, the Green's functions of the quantum field in the lattice are given as:

$$\begin{aligned}\sum_{\mu}\Gamma_{\mathrm{L}}^{\mathrm{QQ}}(p,m_q,\lambda_0)_{\mu\mu}^{ab} &= -\delta^{ab}\hat{p}^2\left[3\,(1-\omega(p,m_q)) + \lambda_0\right]\ ,\\ \omega(p,m_q) &= \sum_{\ell=1}^{\infty} g_0^{2\ell}\omega^{(\ell)}(p,m_q)\end{aligned} \tag{5.32}$$

where the amplitude $\omega^{(\ell)}(p,m_q)$ can be written as:

$$\begin{aligned}\omega^{(\ell)}(p,m_q) &= \omega_0^{(\ell)}(p,m_q) + a\,m_q\ \omega_1^{(\ell)}(p,m_q) + \mathcal{O}(a^2\,m_q^2)\\ &= \omega_0^{(\ell)}(p,0) + \Delta\omega_0^{(\ell)}(p,m_q) + a\,m_q\left(\omega_1^{(\ell)}(p,0) + \Delta\omega_1^{(\ell)}(p,m_q)\right) + \mathcal{O}(a^2\,m_q^2)\end{aligned} \tag{5.33}$$

where $\omega_0^{(\ell)}(p,0)$ is the result corresponding to the massless case.

The relation between the continuum and lattice Green's functions is now given by $\Gamma_{\mathrm{R}}^{\mathrm{QQ}} = Z_\lambda^{-1}\Gamma_{\mathrm{L}}^{\mathrm{QQ}}$ [52]. Hence, using the Eqs.(5.30), and (5.32) we can express Z_λ in terms of $\omega_R(p,m)$, $\omega(p,m_q)$:

$$Z_\lambda = \frac{1-\omega(p,m)}{1-\omega_R(p,m_q)} \tag{5.34}$$

Expressed in terms of the perturbative expansions given by Eqs. (5.25), (5.27), (5.30), and (5.32), and utilizing the relations provided by Eqs. (5.29) and (5.34), the renormalization factor Z_g^2 in the asymptotic limit ($g_0 \to 0$) of the mass-independent renormalization scheme ($m \to 0$) takes the following form:

$$Z_g^2 = \left[1 + g_0^2\left(\nu_R^{(1)} - \nu^{(1)}\right) + g_0^4\left(\nu_{\rm R}^{(2)} - \nu^{(2)}\right) + g_0^4\left(\omega_{\rm R}^{(1)} - \omega^{(1)}\right)\lambda\frac{\partial\nu_{\rm R}^{(1)}}{\partial\lambda} + \mathcal{O}(g_0^6, m^2)\right]_{\substack{\lambda=\lambda_0,\\ m=m_q}} \tag{5.35}$$

with $\nu_{\rm R}^{(\ell)}(p, m, \lambda)$, $\nu^{(\ell)}(p, m_q, \lambda_0)$, $\omega_{\rm R}^{(\ell)}(p, m)$ and $\omega^{(\ell)}(p, m_q)$ given by Eqs. (5.26), (5.28), (5.31), and (5.33) respectively. Although $\nu_{\rm R}^{(1)}(p, m, \lambda)$ is required for a general gauge λ, in all other cases, we can choose the Feynman gauge, $\lambda = \lambda_0 = 1$. This choice significantly simplifies the computations, particularly in lattice regularization.

The amplitudes $\nu_{\rm R}^{(1)}(p, 0, \lambda), \omega_{\rm R}^{(1)}(p, 0), \nu_{\rm R}^{(2)}(p, 0, \lambda)$ calculated in dimensional regularization for the massless case, have been already known in the literature [54, 57].

$$\nu_{\rm R}^{(1)}(p, 0, \lambda) = \frac{N_c}{16\pi^2}\left[-\frac{11}{3}\ln(\frac{p^2}{\bar{\mu}^2}) + \frac{205}{36} + \frac{3}{2}\lambda^{-1} + \frac{1}{4}\lambda^{-2}\right] + \frac{N_f}{16\pi^2}\left[\frac{2}{3}\ln(\frac{p^2}{\bar{\mu}^2}) - \frac{10}{9}\right], \tag{5.36}$$

$$\omega_{\rm R}^{(1)}(p, 0) = \frac{N_c}{16\pi^2}\left[\left(-\frac{13}{6} + \frac{1}{2}\lambda^{-1}\right)\ln(\frac{p^2}{\bar{\mu}^2}) + \frac{97}{36} + \frac{1}{2}\lambda^{-1} + \frac{1}{4}\lambda^{-2}\right] + \frac{N_f}{16\pi^2}\left[\frac{2}{3}\ln(\frac{p^2}{\bar{\mu}^2}) - \frac{10}{9}\right], \tag{5.37}$$

$$\begin{aligned}\nu_{\rm R}^{(2)}(p, 0, \lambda) = \frac{N_c^2}{(16\pi^2)^2}\Bigg[&\left(\frac{34}{3} - \frac{13}{4}\lambda^{-1} - \frac{1}{3}\lambda^{-2} + \frac{1}{4}\lambda^{-3} - \frac{1}{16}\lambda^{-4}\right)\ln(\frac{p^2}{\bar{\mu}^2}) + \left(\frac{2687}{72} - \frac{57}{8}\right)\\ &+ \left(-\frac{187}{48} + \frac{5}{4}\zeta(3)\right)\lambda^{-1} + \left(-\frac{161}{144} - \frac{1}{8}\right)\lambda^{-2} - \frac{3}{16}\lambda^{-3} - \frac{1}{16}\lambda^{-4}\Bigg]\\ &+ \underbrace{\frac{N_f}{(16\pi^2)^2}\left[N_c\left(3\ln(\frac{p^2}{\bar{\mu}^2}) - \frac{401}{36}\right) + \frac{1}{N_c}\left(-\ln(\frac{p^2}{\bar{\mu}^2}) + \frac{55}{12} - 4\zeta(3)\right)\right]}_{\text{for } \lambda = 1}\end{aligned} \tag{5.38}$$

Moreover, the amplitudes $\nu_0^{(1)}(p, 0, \lambda_0)$, $\omega_0^{(1)}(p, 0)$ and $\nu_0^{(2)}(p, 0, \lambda_0)$ have been calculated before using a variety of lattice actions (in agreement up to 5 - 6 decimal places) by

[57, 58, 60, 61], in general gauge λ_0:

$$\nu_0^{(1)}(p,0,\lambda_0) = \frac{N_c}{16\pi^2}\Big[-\frac{11}{3}\ln(a^2p^2) + c_{N_c}^{\nu(1)} + \frac{3}{2}\lambda_0^{-1} + \frac{1}{4}\lambda_0^{-2}\Big] + \frac{1}{N_c}\frac{1}{16\pi^2}\, c_{1/N_c}^{\nu(1)} + \frac{N_f}{16\pi^2}\Big[\frac{2}{3}\ln(a^2p^2) + c_{N_f}^{\nu(1)}\Big] + \mathcal{O}(a^2p^2), \tag{5.39}$$

$$\omega_0^{(1)}(p,0) = \frac{N_c}{16\pi^2}\Big[\Big(-\frac{13}{6} + \frac{1}{2}\lambda_0^{-1}\Big)\ln(a^2p^2) + c_{N_c}^{\omega(1)} + c_{\lambda_0^{-1}N_c}^{\omega(1)}\lambda_0^{-1} + \frac{1}{4}\lambda_0^{-2}\Big] + \frac{1}{N_c}\frac{1}{16\pi^2}c_{1/N_c}^{\omega(1)} + \frac{N_f}{16\pi^2}\Big[\frac{2}{3}\ln(a^2p^2) + c_{N_f}^{\omega(1)}\Big] + \mathcal{O}(a^2p^2), \tag{5.40}$$

where

$$c_{\lambda_0^{-1}N_c}^{\omega(1)} = -0.88629444(4), \tag{5.41}$$

$$c_{N_f}^{\nu(1)} = c_{N_f}^{\omega(1)} = -2.16850086(2) + 0.79694512(11)\; c_{SW} - 4.712691443(4)\; c_{SW}^2 \tag{5.42}$$

and the numerical constants $c_i^{\nu(1)}$, $c_i^{\omega(1)}$ $(i = N_c, 1/N_c)$ are listed in Table 5.2 for different gluon actions.

Gluon action	$c_{N_c}^{\nu(1)}$	$c_{1/N_c}^{\nu(1)} = c_{1/N_c}^{\omega(1)}$	$c_{N_c}^{\omega(1)}$
Wilson	32.5328199(5)	-19.7392089(2)	22.3156745(1)
TL Symanzik	18.860597(3)	-6.6594802(3)	10.308794(3)
TILW, βc_0 =8.60	10.5954557(3)	1.3040804(4)	3.06253640(3)
TILW, βc_0 =8.45	10.2868675(4)	1.5985007(6)	2.7923321(3)
TILW, βc_0 =8.30	9.8615392(2)	2.0038705(5)	2.4199523(3)
TILW, βc_0 =8.20	9.5977109(3)	2.2550514(4)	2.1889929(4)
TILW, βc_0 =8.10	9.2575332(5)	2.5786980(4)	1.8912290(2)
TILW, βc_0 =8.00	8.8354866(3)	2.9797868(4)	1.5218513(2)
Iwasaki	-1.152587(2)	11.888842(1)	-8.5190295(6)
DBW2	-25.693965(165)	32.281461(3)	-29.853124(130)

TABLE 5.2: Numerical coefficients for the quantities $\nu^{(1)}(p)$ and $\omega^{(1)}(p)$.

Note that the fermionic contributions in $\omega_0^{(1)}(p,0)$, as well as the contributions of the form $1/N_c$, are identical to those in $\nu_0^{(1)}(p,0)$.

The quantities l_0 and l_1 can be also expressed in terms of $\nu_R(p)$, $\nu(p)$, $\omega_R(p)$, $\omega(p)$:

$$l_0 = -b_0 \ln(a^2\bar{\mu}^2) + \left[\nu_R^{(1)} - \nu^{(1)}\right]_{\lambda=\lambda_0}, \tag{5.43}$$

$$l_1 = -b_1 \ln(a^2\bar{\mu}^2) + \left[\nu_R^{(2)} - \nu^{(2)} + \lambda \frac{\partial \nu_R^{(1)}}{\partial \lambda}\left(\omega_R^{(1)} - \omega^{(1)}\right)\right]_{\lambda=\lambda_0}. \tag{5.44}$$

The resulting one-loop quantity l_0, as well as the ratio $\Lambda_L/\Lambda_{\overline{\rm MS}}$, are given by:

$$l_0 = \frac{N_c}{16\pi^2} c_{N_c}^{l_0} + \frac{1}{N_c}\frac{1}{16\pi^2}\, c_{1/N_c}^{\ell_0} + \frac{N_f}{16\pi^2} c_{N_f}^{l_0}, \tag{5.45}$$

$$\frac{\Lambda_L}{\Lambda_{\overline{\rm MS}}} = \exp\left[\frac{N_c c_{N_c}^{\ell_0} + \frac{1}{N_c}\, c_{1/N_c}^{l_0} + N_f c_{N_f}^{l_0}}{\frac{22}{3}\, N_c - \frac{4}{3}\, N_f}\right] \tag{5.46}$$

where

$$c_{N_c}^{l_0} = \frac{205}{306} - c_{N_c}^{\nu^{(1)}}, \tag{5.47}$$

$$c_{1/N_c}^{l_0} = -c_{1/N_c}^{\nu^{(1)}}, \tag{5.48}$$

$$c_{N_f}^{l_0} = -3.27961197(2) + 0.79694512(11)\; c_{SW} - 4.712691443(4)\; c_{SW}^2 \tag{5.49}$$

Finally, the relation between the renormalized running coupling g and the bare running coupling g_0 can be expressed as:

$$g^2 = \left\{ g_0^2 - g_0^4\left(\nu_{\rm R}^{(1)} - \nu^{(1)}\right) + g_0^6\left[\left(\nu_{\rm R}^{(1)} - \nu^{(1)}\right)^2 - \nu_{\rm R}^{(2)} + \nu^{(2)} - \lambda\frac{\partial \nu_{\rm R}^{(1)}}{\partial \lambda}\left(\omega_{\rm R}^{(1)} - \omega^{(1)}\right)\right] + \mathcal{O}(g_0^8)\right\}_{\substack{\lambda=\lambda_0,\\ m=m_q}} \tag{5.50}$$

Writing $b_g(g_0)$ as an expansion in powers of g_0 in Eq.5.15:

$$\tilde{g}_0^2 = g_0^2\left[1 + a m_q\left(b_g^{(1)} g_0^2 + b_g^{(2)} g_0^4 + \mathcal{O}(g_0^6)\right)\right] \tag{5.51}$$

we can reparameterize the bare coupling constant so fermion mass will be decoupled from the renormalized running coupling:

$$g^2 = \Bigg\{ \tilde{g}_0^2 - \tilde{g}_0^4 \left[\left(\nu_{\mathrm{R}}^{(1)} - \nu_0^{(1)} \right) + a m_q \left(b_g^{(1)} - \nu_1^{(1)} \right) \right] + (4\pi)^2 \tilde{g}_0^6 \Bigg[\left(\nu_{\mathrm{R}}^{(1)} - \nu_0^{(1)} \right)^2 - \nu_{\mathrm{R}}^{(2)} + \nu_0^{(2)} - \lambda \frac{\partial \nu_{\mathrm{R}}^{(1)}}{\partial \lambda} \left(\omega_{\mathrm{R}}^{(1)} - \omega_0^{(1)} \right) + a m_q \Big(\nu_1^{(2)} - b_g^{(2)} + 2 \left(\nu_0^{(1)} - \nu_R^{(1)} \right) \left(\nu_1^{(1)} - b_g^{(1)} \right) + \lambda \frac{\partial \nu_{\mathrm{R}}^{(1)}}{\partial \lambda} \omega_1^{(1)} \Big) \Bigg] + \mathcal{O}(\tilde{g}_0^8) \Bigg\}_{\substack{\lambda=\lambda_0, \\ m=m_q}} \tag{5.52}$$

Therefore, $b_g^{(1)}$ is given by:

$$b_g^{(1)} = \nu_1^{(1)} \tag{5.53}$$

and at 2-loop order, $b_g^{(2)}$ must be:

$$b_g^{(2)} = \nu_1^{(2)} + \lambda \frac{\partial \nu_R^{(1)}}{\partial \lambda} \omega_1^{(1)} \tag{5.54}$$

5.3 One-loop Calculations

As already discussed, the most efficient way of calculating Z_g^2 is to consider the 2-point Green's function of the background field. We are only interested in calculating diagrams having a fermion propagator as seen in Fig.5.1, since these are associated with the $\mathcal{O}(am)$ effects of the strong coupling constant.

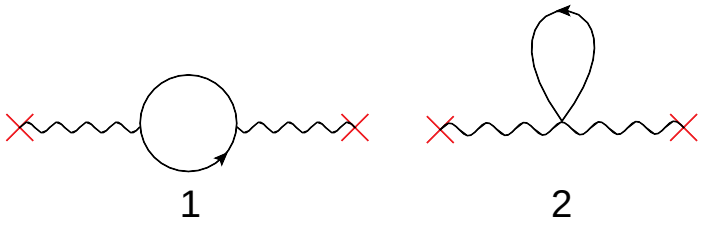

FIGURE 5.1: One-loop Feynman diagrams for fermion contributions to $\Gamma_{\mathrm{L,F}}^{\mathrm{BB,1loop}}$. A solid line represents quarks. Wavy lines ending on a cross represent background gluons. Each diagram is meant to be symmetrized over the color indices, Lorentz indices, and momenta of the two external background fields.

The one-loop result of the fermion contributions ('F') to 2-pt lattice Green's function is:

$$\Gamma^{\mathrm{BB,1loop}}_{\mathrm{L,F}}(p,m_q)^{ab}_{\mu\nu} = \delta^{ab}\left(\delta_{\mu\nu}p^2 - p_\nu p_\mu\right)\Bigg\{F_1(ap) + F_2\left(\frac{m_q^2}{p^2}\right) + am_q\left[F_3(ap) + F_4\left(\frac{m_q^2}{p^2}\right)\right] + \mathcal{O}\left(a^2m_q^2\right)\Bigg\} \tag{5.55}$$

where:

$$F_1(ap) = N_f\left\{-0.0137322 + 0.0050467\,c_{sw} - 0.0298435\,c_{sw}^2 + \frac{2}{3}\frac{1}{16\pi^2}\log(a^2p^2)\right\}$$

$$F_2\left(\frac{m_q^2}{p^2}\right) = \frac{N_f}{16\pi^2}\Bigg\{\frac{8}{3}\frac{m_q^2}{p^2} - \frac{8}{3}\left(-\frac{1}{2} + \frac{m_q^2}{p^2}\right)\sqrt{1+4\frac{m_q^2}{p^2}}\,\mathrm{arccoth}\left(\sqrt{1+4\frac{\mathrm{m_q^2}}{\mathrm{p^2}}}\right) + \frac{2}{3}\log\left(\frac{m_q^2}{p^2}\right)\Bigg\}$$

$$F_3(ap) = N_f\left\{0.0272837 - 0.0223503c_{sw} + 0.0070667c_{sw}^2 - (1-c_{sw})\frac{2}{16\pi^2}\log\left(a^2p^2\right)\right\}$$

$$F_4\left(\frac{m_q^2}{p^2}\right) = \frac{N_f}{16\pi^2}\Bigg\{4\left[(-1+c_{sw})\left(1+4\frac{m_q^2}{p^2}\right) + 4\left(\frac{m_q^2}{p^2}\right)^2\right]\frac{\mathrm{arccoth}\left(\sqrt{1+4\frac{\mathrm{m_q^2}}{\mathrm{p^2}}}\right)}{\sqrt{1+4\frac{m_q^2}{p^2}}} - (1-c_{sw})2\log\left(\frac{m_q^2}{p^2}\right) - 4\frac{m_q^2}{p^2}\Bigg\}$$

Since the above Green's function stems from diagrams of closed fermion loops, the one-loop results are independent of the Symanzik coefficients. Furthermore, incorporating stout links into the lattice action we find that the one-loop outcome is independent of the stout coefficient. This stems from the fact that after N successive smearing steps, the transverse part of a gluon field in 1-loop corrections is multiplied by a factor $(1 - wa^2\hat{p}^2)^N$ [68]. Eliminating terms of order $\mathcal{O}(a^2)$ should result in no contribution from the stout-smearing coefficient, as indicated by our findings.

In terms of the amplitudes $\nu^{(1)}(p, m_q, \lambda_0)$ in Eq.5.28, using Eq. 5.55 we find the following:

$$\begin{aligned}
\nu_0^{(1)}(p, 0, \lambda_0) &= \nu_0^{(1)}(p, 0, \lambda_0)|_{N_f=0} + F_1(p) \\
\Delta\nu_0^{(1)}(p, m_q, \lambda_0) &= \mathcal{O}\left(\frac{m_q^2}{p^2}\right) \\
\nu_1^{(1)}(p, 0, \lambda_0) &= F_3(p) \\
\Delta\nu_1^{(1)}(p, m_q, \lambda_0) &= \mathcal{O}\left(\frac{m_q^2}{p^2}\right)
\end{aligned} \tag{5.56}$$

The above amplitudes can be derived using two approaches; first, by evaluating the momentum integrals and subsequently performing a first-order Taylor expansion in mass, as outlined in this section, and second, by reversing the steps. Both methods yield identical results, with the latter being the most straightforward for lattice calculations. Consequently, for the 2-loop calculations, we will employ only the second method.

Using Eq.5.53 we find the first coefficient of the $b_g(g_0^2)$ as:

$$b_g^{(1)} = N_f \left\{ 0.0272837 - 0.0223503 c_{sw} + 0.0070667 c_{sw}^2 - (1 - c_{sw}) \frac{2}{16\pi^2} \log\left(a^2 p^2\right) \right\} + \mathcal{O}\left(\frac{m_q^2}{p^2}\right) \tag{5.57}$$

For the tree-level Sheikholeslami-Wohlert coefficient, $c_{sw} = 1 + \mathcal{O}(g_0^2)$, we obtain the well established result [63]:

$$b_g^{(1)} = 0.012000 N_f \tag{5.58}$$

To incorporate a mass-dependent running coupling, it is necessary to consider the terms of $\mathcal{O}\left(m_q^2/p^2\right)$ in the amplitudes of Eq. 5.56. For heavy fermions, taking the limit $z \to \infty$ (where $z \equiv m_q^2/p^2$) and setting $c_{sw} = 1 + \mathcal{O}(g_0^2)$, we obtain:

$$\begin{aligned}
\Delta\nu_0^{(1)}(p, m_q, \lambda_0) &= \frac{N_f}{16\pi^2} \left\{ \frac{10}{9} + \frac{4}{3}\log(z) + \frac{2}{15z^2} \right\} + \mathcal{O}\left(\frac{1}{z^4}\right) \\
\Delta\nu_1^{(1)}(p, m_q, \lambda_0) &= \frac{N_f}{16\pi^2} \left\{ -\frac{2}{3} + \frac{2}{15z^2} \right\} + \mathcal{O}\left(\frac{1}{z^4}\right)
\end{aligned} \tag{5.59}$$

Using the above relations and Eq.5.52, one can find the logarithmic mass dependence of the mass-depended renormalized running coupling in the limit of heavy fermions, as determined in Ref.[69].

5.4 Two-loop Calculations

To derive the two-loop amplitude $\nu^{(2)}$ of the fermion contribution, we are computing the 2-point lattice Green's function of twenty Feynman diagrams, as shown in Figure 5.2.

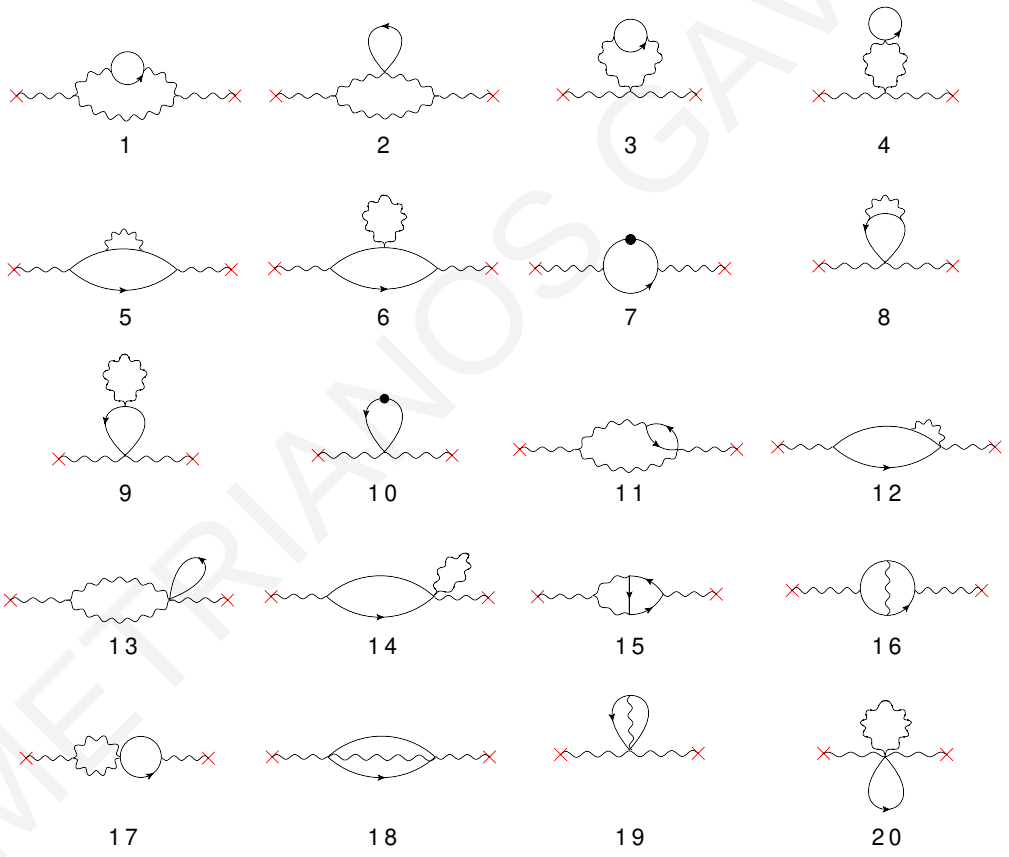

FIGURE 5.2: Two-loop Feynman diagrams for the fermion contributions to $\Gamma^{\mathrm{BB,2loop}}_{\mathrm{L,F}}$. A wavy (solid) line represents gluons (quarks). Wavy lines ending on a cross represent background gluons. A solid circle is the one-loop fermion mass counterterm. Each diagram is meant to be symmetrized over the color indices, Lorentz indices, and momenta of the two external background fields.

The tree-level fermion propagator in momentum space is given by:

$$\langle \psi \bar{\psi} \rangle = \frac{-i \mathring{\not{p}} + M(p,m)}{\mathring{p}^2 + M(p,m)^2}, \tag{5.60}$$

where: $\not{\hat{p}} = \sum_\mu \gamma_\mu \frac{1}{a}\sin(ap_\mu)$ and $M(p,m) = m + \frac{2}{a}\sum_\mu \sin^2(ap_\mu/2)$.

As mentioned in Section 5.3, we proceed by first expanding the denominator of Eq. (5.60) with respect to mass up to $\mathcal{O}(a)$ corrections:

$$\frac{1}{\mathring{p}^2 + M(q,m)^2} = \frac{1}{\mathring{p}^2 + M(p,0)^2}\left(1 - \frac{4m\frac{1}{a}\sum_\mu \sin^2(ap_\mu/2)}{\mathring{p}^2 + M(p,0)^2} + \mathcal{O}(a^2m^2)\right) \tag{5.61}$$

One main difficulty in this computation, as compared to the massless case, stems from the fact that the fermion propagator now contains contributions of $\mathcal{O}(p^{-2})$; this amplifies the presence of potential IR divergences, which must be carefully addressed. Also, the sheer number of terms which must be integrated over the two loop momenta is of the order of $\sim 10^6$; this has necessitated the creation of special-purpose integration routines, to overcome the severe constraints on CPU and memory. However, it is essential to note also that the computational challenges were further amplified by the distinct methodologies and manipulations required for each diagram. Particularly, the "diamond" diagrams (diagrams 15 and 16 in Figure 5.2) stand out as the most challenging within this computation.

The two-loop results regarding fermion contributions to the 2-point lattice Green's function has the following form:

$$\sum_\rho \Gamma^{\mathrm{BB,2loop}}_{\mathrm{L,F}}(p,m_q)^{ab}_{\rho\rho} = \delta^{ab}\, 3p^2 \sum_j \left[G_{0,j}(p) + am_q\, G_{1,j}(p) + \mathcal{O}(a^2m^2)\right] \tag{5.62}$$

The index j runs over the diagrams shown in Fig. 5.2. Since two-loop diagrams can have a maximum of 4 fermionic vertices, $G_{i,j}(p)$ is a polynomial in c_{SW} of degree up to 4.

On general grounds, we expect:

$$G_{i,j}(p) = c_{0,i,j} + c_{1,i,j}\, a^2 \sum_\mu \frac{p_\mu^4}{p^2} + a^2p^2\left\{c_{2,i,j}\left(\frac{\ln(a^2p^2)}{(4\pi)^2}\right)^2 + c_{3,i,j}\frac{\ln(a^2p^2)}{(4\pi)^2} + c_{4,i,j}\right\} + \mathcal{O}(a^4p^4) \tag{5.63}$$

where $\hat{p}^2 = 4\sum_\mu \sin^2(p_\mu/2)$, and the most general dependence of $c_{n,i,j}$ on N_c, N_f, $c_{\rm SW}$ is given by:

$$c_{n,i,j} = \sum_{k=0}^{4} N_f\, c_{\rm SW}^k \left(\frac{1}{N_c} c_{n,i,j}^{(-1,k)} + N_c\, c_{n,i,j}^{(1,k)} \right). \tag{5.64}$$

It's worth mentioning that specific diagrams exhibit infrared convergence only when considered in pairs: (1, 2), (3, 4). We have assessed these pairs accordingly, ensuring careful handling to prevent divergences in intermediate results.

Here, we briefly outline some validation checks that can be conducted on our calculations. Various constraints on the coefficients $c_{n,i,j}$ can be used for both verifying the algebraic expressions and the numerical outcomes:

$\underline{c_{0,i,j}}$: According to gauge invariance:

$$\sum_i c_{0,i,j} = 0 \tag{5.65}$$

We can verify this condition through three methods [57]: a formal derivation of a Ward identity type, wherein vertices with background fields at zero momentum are expressed in terms of appropriate derivatives of inverse propagators. This yields not only the aforementioned equation but also additional constraints:

$$\begin{aligned}
&2c_{0,i,20} + c_{0,i,14} = 0 \\
&c_{0,i,20} + c_{0,i,14} + c_{0,i,9} + c_{0,i,6} = 0 \\
&(c_{0,i,19} + c_{0,i,18})|_{N_c^2=2} = 0 \\
&c_{0,i,4} + c_{0,i,2} + c_{0,i,3} + \frac{1}{2} c_{0,i,15} + c_{0,i,1} = 0 \\
&c_{0,i,11} = 0 \\
&c_{0,i,7} + c_{0,i,10} = 0 \\
&(c_{0,i,8} + c_{0,i,5})(N_c^2 - 2) + c_{0,i,12}(N_c^2 - 1) - c_{0,i,16}(N_c^2 - 1)(N_c^2 - 2) = 0
\end{aligned} \tag{5.66}$$

These conditions hold for any value of the fermion mass m and Wilson parameter r. Secondly, we can confirm all the above identities through algebraic manipulation of the complete expression for each coefficient. Thirdly, we can substitute the numerical results for the coefficients into each identity, consistently obtaining zero within the error estimates.

$\underline{c_{1,i,j}}$: If Lorentz invariance is to be restored in the continuum limit, the sum of these terms must disappear. Only diagrams 1 and 2 contribute non-zero values, and we have verified that their combined sum equals zero.

$\underline{c_{2,0,j}}$: We verified that these coefficients align with those of the continuum:

$$c_{2,0,16} = \frac{1}{3}\frac{1}{N_c}N_f\,, \qquad c_{2,0,15} = \frac{4}{3}N_c N_f\,, \qquad c_{2,0,1} = -\frac{5}{3}N_c N_f\,, \qquad c_{2,0,5} = \frac{1}{3}\frac{N_c^2-1}{N_c}N_f \tag{5.67}$$

For all other diagrams: $c_{2,0,j} = 0$.

$\underline{c_{3,0,j}}$: The overall contribution from single logarithms must coincide the continuum result:

$$\sum_j c_{3,0,j} = \left(3N_c - \frac{1}{N_c}\right) N_f \tag{5.68}$$

Again, this can be checked both algebraically and numerically.

The preliminary results for each diagram are presented in Tables 5.3-5.15. Diagrams not appearing in these Tables give vanishing contributions.

j	$c_{0,0,j}^{(-1,0)}$	$c_{0,0,j}^{(-1,1)}$	$c_{0,0,j}^{(-1,2)}$
	−0.00068730(28)	0.00162886(15)	0.000162221(21)
5	−0.00026913(31)	0.00145195(15)	0.000138480(16)
	0.00039527(32)	0.00114316(15)	0.000099190(8)
	−0.00316447(8)	0	0
6	−0.00262031(8)	0	0
	−0.001935441(31)	0	0
	0.00112494(14)	−0.00072330(7)	−0.000323395(23)
8	0.00082062(8)	−0.00069047(7)	−0.000272079(26)
	0.000268266(33)	−0.00060490(4)	−0.000189186(22)
	0.00158227(5)	0	0
9	0.00131017(4)	0	0
	0.000967735(27)	0	0
	0.00022981(15)	−0.0000802(5)	0
12	−0.000101289(23)	−0.0000677(4)	0
	−0.0005336(5)	−0.00004800(35)	0
	0.00316443073(21)	0	0
14	0.00262027066(18)	0	0
	0.00193541596(13)	0	0
	−0.0005092(4)	0.00007030(14)	−0.00007632(17)
16	−0.00057771(31)	0.00005433(13)	−0.00006290(15)
	−0.0006570(8)	0.00003727(14)	−0.00004365(16)
	−0.00050773(6)	0	0
18	−0.00049253(6)	0	0
	−0.00043479(6)	0	0
	0.00039280(6)	0.000040203(15)	0
19	0.00054317(7)	0.000033948(12)	0
	0.00070176(9)	0.000024069(9)	0
	−0.00158227(5)	0	0
20	−0.00131017(4)	0	0
	−0.000967735(27)	0	0

TABLE 5.3: Coefficients $c_{0,0,j}^{(-1,k)}$,r=1. The three values of each diagram correspond to different Symanzik improved actions: Wilson action (first line), Tree-Level Symanzik (second line), and Iwasaki action (third line).

j	$c_{0,1,j}^{(-1,0)}$	$c_{0,1,j}^{(-1,1)}$	$c_{0,1,j}^{(-1,2)}$
	0.0050933(7)	−0.0048230(21)	−0.000199144(21)
5	0.0041580(10)	−0.0043157(22)	−0.000156729(29)
	0.00275792(11)	−0.0034206(23)	−0.000089821(24)
	0.0076499(7)	0	0
6	0.0063344(6)	0	0
	0.0046788(4)	0	0
	−0.0059980(13)	0.00193787(22)	0.00041980(6)
8	−0.0052415(12)	0.00176113(22)	0.00033840(5)
	−0.0040376(10)	0.00139419(18)	0.000211346(23)
	−0.0051000(6)	0	0
9	−0.0042230(5)	0	0
	−0.0031193(4)	0	0
	−0.0000539(8)	0.0006100(11)	0
12	0.00044375(28)	0.0005123(10)	0
	0.0011289(5)	0.0003603(8)	0
	−0.00509976855(25)	0	0
14	−0.00422280501(21)	0	0
	−0.00311909924(16)	0	0
	−0.0003874(26)	0.0014473(25)	0.00038181(25)
16	−0.0000495(22)	0.0012304(25)	0.00033267(28)
	0.000403(4)	0.0008971(21)	0.00025365(26)
	0.00057224(6)	0	0
18	0.00056020(6)	0	0
	0.000485524(31)	0	0
	−0.00054513(7)	−0.00030519(20)	0
19	−0.00078195(10)	−0.00025635(16)	0
	−0.00105013(9)	−0.00018026(11)	0
	0.00255002(30)	0	0
20	0.00211152(26)	0	0
	0.00155963(19)	0	0

TABLE 5.4: Coefficients $c_{0,1,j}^{(-1,k)}$,r=1. The three values of each diagram correspond to different Symanzik improved actions: Wilson action (first line), Tree-Level Symanzik (second line), and Iwasaki action (third line).

j	$c^{(1,0)}_{0,0,j}$	$c^{(1,1)}_{0,0,j}$	$c^{(1,2)}_{0,0,j}$
	−0.0020082(11)	0.00022193(21)	−0.0028072(12)
1+2	−0.0022026(10)	0.00023620(19)	−0.0030422(11)
	−0.0024047(6)	0.00025562(14)	−0.0033149(8)
	0.00145603(19)	−0.000215063(30)	0.00238751(11)
3+4	0.00146733(19)	−0.000220718(28)	0.00254495(29)
	0.00145912(19)	−0.000220758(9)	0.0025644(4)
	0.00068730(28)	−0.00162886(15)	−0.000162221(21)
5	0.00026913(31)	−0.00145195(15)	−0.000138480(16)
	−0.00039527(32)	−0.00114316(15)	−0.000099190(8)
	0.00316447(8)	0	0
6	0.00262031(8)	0	0
	0.001935441(31)	0	0
	−0.00112494(14)	0.00072330(7)	0.000323395(23)
8	−0.00082062(8)	0.00069047(7)	0.000272079(26)
	−0.000268266(33)	0.00060490(4)	0.000189186(22)
	−0.00158227(5)	0	0
9	−0.00131017(4)	0	0
	−0.000967735(27)	0	0
	0	−0.0000573(4)	0.0009552(14)
11	0.000157315(13)	−0.0000646(4)	0.0011115(14)
	0.000330707(26)	−0.0000792(4)	0.0016031(14)
	−0.00011491(7)	0.00029885(28)	0.00026804(9)
12	0.000050644(12)	0.00026594(28)	0.00024220(9)
	0.00026682(23)	0.00021724(26)	0.00018887(6)
	−0.00316443073(21)	0	0
14	−0.00262027066(18)	0	0
	−0.00193541596(13)	0	0
	0.001349(5)	0.0000436(8)	−0.00011568(14)
15	0.001556(5)	0.0000337(8)	−0.00011666(14)
	0.001802(4)	0.0000095(11)	−0.00010172(13)
	0.00045024(4)	0.0000402030(29)	−0.0077682(9)
18	0.00043918(4)	0.0000353047(26)	−0.0064232(8)
	0.00040291(4)	0.0000274085(20)	−0.0046228(6)
	−0.00039280(6)	−0.000160812(12)	0.0071560(5)
19	−0.00054317(7)	−0.000135791(10)	0.0057458(4)
	−0.00070176(9)	−0.000096275(7)	0.00372632(30)
	0.00158227(5)	0	0
20	0.00131017(4)	0	0
	0.000967735(27)	0	0

TABLE 5.5: Coefficients $c^{(1,k)}_{0,0,j}$,r=1. The three values of each diagram correspond to different Symanzik improved actions: Wilson action (first line), Tree-Level Symanzik (second line), and Iwasaki action (third line).

j	$c^{(1,0)}_{0,1,j}$	$c^{(1,1)}_{0,1,j}$	$c^{(1,2)}_{0,1,j}$
	0.0038168(26)	−0.0017134(28)	0.00060610(29)
1+2	0.0041574(25)	−0.0018097(26)	0.00065729(27)
	0.0045263(22)	−0.0019482(22)	0.00071661(19)
	−0.00297502(18)	0.00165076(33)	−0.00048649(8)
3+4	−0.00299543(19)	0.0016997(4)	−0.00052973(9)
	−0.00296564(21)	0.0017142(4)	−0.00054116(10)
	−0.0050933(7)	0.0048230(21)	0.000199144(21)
5	−0.0041580(10)	0.0043157(22)	0.000156729(29)
	−0.00275792(11)	0.0034206(23)	0.000089821(24)
	−0.0076499(7)	0	0
6	−0.0063344(6)	0	0
	−0.0046788(4)	0	0
	0.0059980(13)	−0.00193787(22)	−0.00041980(6)
8	0.0052415(12)	−0.00176113(22)	−0.00033840(5)
	0.0040376(10)	−0.00139419(18)	−0.000211346(23)
	0.0051000(6)	0	0
9	0.0042230(5)	0	0
	0.0031193(4)	0	0
	0	0.00053259(6)	−0.00022873(21)
11	−0.000249029(26)	0.00057339(6)	−0.00025542(21)
	−0.00052711(5)	0.00066218(9)	−0.0003586(5)
	0.0000269(4)	−0.00236349(11)	−0.0004656(8)
12	−0.00022187(14)	−0.00209473(19)	−0.0004043(7)
	−0.00056446(25)	−0.00170194(28)	−0.0003003(6)
	0.00509976855(25)	0	0
14	0.00422280501(21)	0	0
	0.00311909924(16)	0	0
	−0.002322(8)	−0.0000146(23)	−0.0001447(5)
15	−0.002296(7)	−0.0001814(33)	−0.0001358(5)
	−0.001325(7)	−0.0006773(30)	−0.0001268(4)
	−0.000558677(18)	−0.00030519(4)	0.0022034(4)
18	−0.000546553(5)	−0.000264678(34)	0.00180793(29)
	−0.000504270(6)	−0.000201129(25)	0.00127506(20)
	0.00054513(7)	0.00122076(16)	−0.0018550(5)
19	0.00078195(10)	0.00102539(13)	−0.00147783(35)
	0.00105013(9)	0.00072102(9)	−0.00094452(22)
	−0.00255002(30)	0	0
20	−0.00211152(26)	0	0
	−0.00155963(19)	0	0

TABLE 5.6: Coefficients $c^{(1,k)}_{0,1,j}$,r=1. The three values of each diagram correspond to different Symanzik improved actions: Wilson action (first line), Tree-Level Symanzik (second line), and Iwasaki action (third line).

j	$c_{4,0,j}^{(-1,0)}$	$c_{4,0,j}^{(-1,1)}$	$c_{4,0,j}^{(-1,2)}$	$c_{4,0,j}^{(-1,3)}$	$c_{4,0,j}^{(-1,4)}$
	0.00069295(5)	−0.0000201015(15)	0.00059633(5)	0	0
3+4	0.000109289(11)	$4.32917(25) \times 10^{-6}$	−0.0000204284(22)	0	0
	−0.000372439(27)	0.0000351782(10)	−0.00061565(6)	0	0
	0.0027(4)	0.00447(24)	0.001008(31)	−0.00068072(8)	0.0000140219(11)
5	0.0044(5)	0.00379(21)	0.000840(29)	−0.00058213(7)	$9.4883(8) \times 10^{-6}$
	0.0066(6)	0.00273(15)	0.000578(26)	−0.00042562(6)	$4.0157(8) \times 10^{-6}$
	−0.0154(7)	−0.00039098(5)	0.00231200(26)	0	0
6	−0.0127(6)	−0.00032375(4)	0.00191443(22)	0	0
	−0.0094(5)	−0.000239130(30)	0.00141406(17)	0	0
	−0.00011586(4)	0.000186623(13)	$5.9016(14) \times 10^{-6}$	0	0
12	$-5.59(4) \times 10^{-6}$	0.000143805(16)	$4.6789(11) \times 10^{-6}$	0	0
	0.000151014(25)	0.000073876(9)	$2.9442(7) \times 10^{-6}$	0	0
	−0.00106378758(4)	0.000826315389(28)	−0.00746086682(16)	0	0
14	−0.000880857132(34)	0.000623967525(24)	−0.00546527413(13)	0	0
	−0.000650629333(25)	0.000384844011(18)	−0.00313752882(10)	0	0
	−0.001111(5)	0.00125785(24)	0.00075480(25)	0.000166547(10)	−0.0000381711
16	−0.000780(5)	0.00110098(22)	0.00066396(23)	0.000146814(8)	−0.0000308278
	−0.000324(5)	0.00085197(17)	0.00053131(18)	0.000113649(5)	−0.0000202313
	0.000108788(6)	0	0	0	0
18	0.000105420(5)	0	0	0	0
	0.000095401(7)	0	0	0	0
	0	0.0000201015(12)	−0.00119266(7)	0	0
19	0	0.0000169738(10)	−0.00095763(6)	0	0
	0	0.0000120343(7)	−0.00062105(4)	0	0

TABLE 5.7: Coefficients $c_{4,0,j}^{(-1,k)}$,r=1. The three values of each diagram correspond to different Symanzik improved actions: Wilson action (first line), Tree-Level Symanzik (second line), and Iwasaki action (third line).

j	$c_{4,1,j}^{(-1,0)}$	$c_{4,1,j}^{(-1,1)}$	$c_{4,1,j}^{(-1,2)}$	$c_{4,1,j}^{(-1,3)}$	$c_{4,1,j}^{(-1,4)}$
	−0.00113873(15)	0.000152595(20)	−0.00015458(4)	0	0
3+4	−0.000153849(19)	−0.0000298762(19)	$1.08952(17) \times 10^{-6}$	0	0
	0.00068827(8)	−0.000256895(16)	0.000143724(28)	0	0
	0.01780(34)	−0.0363(22)	−0.00146(16)	0.00129413(13)	−0.000115914(12)
5	0.011334(33)	−0.0318(20)	−0.00171(15)	0.00116215(6)	−0.000099774(9)
	0.0022(5)	−0.0246(17)	−0.00200(13)	0.00094418(18)	−0.000073955(7)
	0.0737(31)	−0.00592703(25)	−0.00082124(15)	0	0
6	0.0611(26)	−0.00490781(26)	−0.00068002(12)	0	0
	0.0451(19)	−0.00362507(22)	−0.00050228(9)	0	0
	0.00003208(5)	−0.00037763(16)	0.00008612(13)	0	0
12	−0.00016569(6)	−0.00022383(4)	0.00007138(12)	0	0
	−0.00045518(6)	$4.225(31) \times 10^{-6}$	0.00004785(11)	0	0
	0.00211357914(13)	−0.00365949362(15)	0.00176668007(6)	0	0
14	0.00175012503(11)	−0.00276335794(12)	0.00129413795(5)	0	0
	0.00129269848(8)	−0.00170435438(9)	0.00074294446(4)	0	0
	0.00514(4)	0.00355(11)	−0.00210(9)	$8.256(9) \times 10^{-6}$	0.0000166996
16	0.0146(6)	0.00371(10)	−0.00196(8)	$-2.858(12) \times 10^{-6}$	0.0000137191
	0.0432(24)	0.00379(6)	−0.00173(5)	−0.000017944(21)	$9.44635486785388 \times 10^{-6}$
	−0.000151344(20)	0	0	0	0
18	−0.000145358(19)	0	0	0	0
	−0.000128649(17)	0	0	0	0
	0	−0.000152595(16)	0.00030916(6)	0	0
19	0	−0.000128174(13)	0.00024631(5)	0	0
	0	−0.000090128(8)	0.000157421(29)	0	0

TABLE 5.8: Coefficients $c_{4,1,j}^{(-1,k)}$,r=1. The three values of each diagram correspond to different Symanzik improved actions: Wilson action (first line), Tree-Level Symanzik (second line), and Iwasaki action (third line).

j	$c^{(1,0)}_{4,0,j}$	$c^{(1,1)}_{4,0,j}$	$c^{(1,2)}_{4,0,j}$	$c^{(1,3)}_{4,0,j}$	$c^{(1,5)}_{4,0,j}$
	−0.0010903(6)	0.00007742(9)	−0.0014856(5)	0	0
1+2	−0.0009526(6)	0.00006439(9)	−0.0013209(5)	0	0
	−0.0007641(5)	0.00004030(7)	−0.00105896(30)	0	0
	−0.00074284(11)	0.0000377508(29)	−0.00074562(7)	0	0
3+4	−0.000130647(20)	$-1.7160(7) \times 10^{-6}$	−0.000056858(11)	0	0
	0.00049279(7)	−0.000066534(9)	0.00078204(11)	0	0
	−0.0027(4)	−0.00447(24)	−0.001008(31)	0.00068072(8)	−0.0000140219(11)
5	−0.0044(5)	−0.00379(21)	−0.000840(29)	0.00058213(7)	$-9.4883(8) \times 10^{-6}$
	−0.0066(6)	−0.00273(15)	−0.000578(26)	0.00042562(6)	$-4.0157(8) \times 10^{-6}$
	0.0154(7)	0.00039098(5)	−0.00231200(26)	0	0
6	0.0127(6)	0.00032375(4)	−0.00191443(22)	0	0
	0.0094(5)	0.000239130(30)	−0.00141406(17)	0	0
	0.0000690696(32)	0.000040123(19)	−0.00055809(9)	0	0
11	0.0000694665(25)	0.000041335(12)	−0.00052884(9)	0	0
	0.000069021(7)	0.000043270(26)	−0.00052731(19)	0	0
	0.000057929(19)	−0.00022232(10)	−0.0001601650(29)	−0.0000140519(33)	0
12	$2.797(22) \times 10^{-6}$	−0.00015567(8)	−0.000114738(7)	−0.0000146039(33)	0
	−0.000075507(12)	−0.00007059(5)	−0.000062081(25)	−0.0000135287(29)	0
	0.00106378758(4)	−0.000939614357(27)	0.00880084109(16)	0	0
14	0.000880857132(34)	−0.000753148083(23)	0.00699307822(13)	0	0
	0.000650629333(25)	−0.000524268946(17)	0.00478649205(10)	0	0

	0.01216(22)	−0.0029943(8)	0.00029296(18)	−0.000169822(25)	0
15	0.01351(22)	−0.0031878(8)	0.00044870(21)	−0.00016299(4)	0
	0.01732(32)	−0.0035582(8)	0.00091398(33)	−0.00015735(7)	0
	0	−0.00016956(8)	0.00200515(32)	0	0
17	0	−0.00014250(8)	0.00168484(34)	0	0
	0	−0.00010318(8)	0.0012198(4)	0	0
	−0.000088930(22)	$4.360(6) \times 10^{-7}$	−0.000170561(22)	0	0
18	−0.000087444(22)	$5.690(6) \times 10^{-7}$	−0.000111322(10)	0	0
	−0.000082212(21)	$1.0483(6) \times 10^{-6}$	−0.000102964(11)	0	0
	0	$-5.0254(4) \times 10^{-6}$	0.000298165(23)	0	0
19	0	$-4.24346(31) \times 10^{-6}$	0.000239407(19)	0	0
	0	$-3.00858(21) \times 10^{-6}$	0.000155263(12)	0	0

TABLE 5.9: Coefficients $c^{(1,k)}_{4,0,j}$,r=1. The three values of each diagram correspond to different Symanzik improved actions: Wilson action (first line), Tree-Level Symanzik (second line), and Iwasaki action (third line).

j	$c^{(1,0)}_{4,1,j}$	$c^{(1,1)}_{4,1,j}$	$c^{(1,2)}_{4,1,j}$	$c^{(1,3)}_{4,1,j}$	$c^{(1,4)}_{4,1,j}$
	0.0022779(19)	−0.0011826(14)	0.00025340(12)	0	0
1+2	0.0020174(21)	−0.0010873(15)	0.00021920(13)	0	0
	0.0016425(23)	−0.0009012(16)	0.00016564(7)	0	0
	0.00127531(27)	−0.00028828(6)	0.00018090(4)	0	0
3+4	0.00019508(8)	0.0000162243(30)	0.0000173368(18)	0	0
	−0.00098527(9)	0.000537723(21)	−0.000171132(33)	0	0
	−0.01780(34)	0.0363(22)	0.00146(16)	−0.00129413(13)	0.000115914(12)
5	−0.011334(33)	0.0318(20)	0.00171(15)	−0.00116215(6)	0.000099774(9)
	−0.0022(5)	0.0246(17)	0.00200(13)	−0.00094418(18)	0.000073955(7)
	−0.0737(31)	0.00592703(25)	0.00082124(15)	0	0
6	−0.0611(26)	0.00490781(26)	0.00068002(12)	0	0
	−0.0451(19)	0.00362507(22)	0.00050228(9)	0	0
	−0.000105343(12)	−0.0002971(4)	0.00015842(5)	0	0
11	−0.000107988(4)	−0.0003025(4)	0.00014435(6)	0	0
	−0.000111859(15)	−0.00031521(34)	0.00013708(8)	0	0
	−0.000016042(26)	0.00083334(26)	$-5.8(1.9) \times 10^{-7}$	$-1.81(0.12) \times 10^{-6}$	0
12	0.000082843(29)	0.00064044(24)	−0.00002039(18)	$1.52(11) \times 10^{-6}$	0
	0.000227590(28)	0.00038125(23)	−0.00005439(18)	$5.89(9) \times 10^{-6}$	0
	−0.00211357914(13)	0.00416125932(15)	−0.00208397640(6)	0	0
14	−0.00175012503(11)	0.00333545827(12)	−0.00165591105(5)	0	0
	−0.00129269848(8)	0.00232182387(9)	−0.00113340718(4)	0	0

	−0.0199(4)	0.006549(17)	−0.0010149(5)	0.00004803(6)	0
15	−0.0240(4)	0.007169(17)	−0.0011078(8)	0.00009369(6)	0
	−0.0356(4)	0.00890(5)	−0.0013591(35)	0.00020187(9)	0
	0	0.0007509(4)	−0.00047487(15)	0	0
17	0	0.0006310(4)	−0.00039904(15)	0	0
	0	0.0004569(5)	−0.00028895(16)	0	0
	0.000128347(32)	$-3.9282(15) \times 10^{-6}$	0.000010186(8)	0	0
18	0.000126678(32)	$-4.5205(8) \times 10^{-6}$	$2.5432(30) \times 10^{-6}$	0	0
	0.000120257(31)	$-7.6210(18) \times 10^{-6}$	0.000017301(8)	0	0
	0	0.000038149(5)	−0.000077290(19)	0	0
19	0	0.000032044(4)	−0.000061576(15)	0	0
	0	0.0000225319(27)	−0.000039355(9)	0	0

TABLE 5.10: Coefficients $c^{(1,k)}_{4,1,j}$,r=1. The three values of each diagram correspond to different Symanzik improved actions: Wilson action (first line), Tree-Level Symanzik (second line), and Iwasaki action (third line).

j	$c_{3,0,j}^{(-1,0)}$	$c_{3,0,j}^{(-1,1)}$	$c_{3,0,j}^{(-1,2)}$
	0.005987949322865560(7)	0.0168125	0.00216441
5	0.011279691840390010(7)	0.0142852	0 .00205177
	0.018864013084219830(7)	0.0102781	0.00180472
	−0.0516445	0	0
6	−0.0427636	0	0
	−0.0315866	0	0
	0.00528244554(15)	−0.01449434464(6)	0
12	−0.00015727738(17)	−0.01261049781(6)	0
	−0.00813690678(30)	−0.00951504612(12)	0
	0.0516445	0	0
14	0.0427636	0	0
	0.0315866	0	0
	−0.0194564(16)	0.00500016(24)	−0.0058984(13)
16	−0.0204232(12)	0.00410192(5)	−0.0052439(9)
	−0.02198074(10)	0.00275597(12)	−0.00410844(24)

TABLE 5.11: Coefficients $c_{3,0,j}^{(-1,k)}$,r=1. The three values of each diagram correspond to different Symanzik improved actions: Wilson action (first line), Tree-Level Symanzik (second line), and Iwasaki action (third line).

j	$c_{3,1,j}^{(-1,0)}$	$c_{3,1,j}^{(-1,1)}$	$c_{3,1,j}^{(-1,2)}$	$c_{3,1,j}^{(-1,3)}$
	0	−0.17686885998176500(20)	−0.0435517	0
5	0	−0.163435963512354600(20)	−0.0388631	0
	0.078428741304771940(13)	−0.140479437381027000(20)	−0.0308436	0
	−0.01883007542(14)	0.06150748172(8)	−0.02174151702(13)	0
12	−0.0037152229(6)	0.0464924430(6)	−0.01891574666(11)	0
	0.02001163378(28)	0.02318904363(19)	−0.014272569341(18)	0
	−0.154933	0.327467	0	0
14	−0.128291	0.247277	0	0
	−0.0947597	0.152513	0	0
	0.038236(5)	−0.017618(32)	0.0248933(33)	−0.00520687(6)
16	0.045443(8)	−0.022879(31)	0.0224227(30)	−0.004845862(5)
	0.058106(5)	−0.033687(32)	0.0178267(21)	−0.00409382(7)

TABLE 5.12: Coefficients $c_{3,1,j}^{(-1,k)}$,r=1. The three values of each diagram correspond to different Symanzik improved actions: Wilson action (first line), Tree-Level Symanzik (second line), and Iwasaki action (third line).

j	$c^{(1,0)}_{3,0,j}$	$c^{(1,1)}_{3,0,j}$	$c^{(1,2)}_{3,0,j}$
	0.0813261088(8)	−0.0252335742(7)	0.14921733618(35)
1+2	0.0813261088(8)	−0.0252335742(7)	0.14921733618(35)
	0.0813261088(8)	−0.0252335742(7)	0.14921733618(35)
	−0.005987949322865560(7)	−0.0168125	−0.00216441
5	−0.011279691840390010(7)	−0.0142852	−0.00205177
	−0.018864013084219830(7)	−0.0102781	−0.00180472
	0.0516445	0	0
6	0.0427636	0	0
	0.0315866	0	0
	0	0.002523357011(34)	−0.02984346720(4)
11	0	0.002523357011(34)	−0.02984346720(4)
	0	0.002523357011(34)	−0.02984346720(4)
	−0.00264122277(7)	−0.005000260418(22)	0.010528965436(18)
12	0.00007863869(8)	−0.005199568630(25)	0.00975201723(8)
	0.00406845339(15)	−0.00491505806(32)	0.008155014073(31)
	−0.0516445	0	0
14	−0.0427636	0	0
	−0.0315866	0	0
	−0.021053(13)	0.0271101(26)	−0.0046299(7)
15	−0.017221(22)	0.0263235(33)	−0.0045076(7)
	−0.011226(9)	0.024289(4)	−0.0040462(6)
	0	0.0100951(27)	−0.119379(10)
17	0	0.0100951(27)	−0.119379(10)
	0	0.0100951(27)	−0.119379(10)

TABLE 5.13: Coefficients $c^{(1,k)}_{3,0,j}$,r=1. The three values of each diagram correspond to different Symanzik improved actions: Wilson action (first line), Tree-Level Symanzik (second line), and Iwasaki action (third line).

j	$c^{(1,0)}_{3,1,j}$	$c^{(1,1)}_{3,1,j}$	$c^{(1,2)}_{3,1,j}$	$c^{(1,3)}_{3,1,j}$
	−0.174414004(5)	0.1497470687(9)	−0.03533360140(4)	0
1+2	−0.174414004(5)	0.1497470687(9)	−0.03533360140(4)	0
	−0.174414004(5)	0.1497470687(9)	−0.03533360140(4)	0
	0	0.176868885998176500(20)	0.0435517	0
5	0	0.163435963512354600(20)	0.0388631	0
	−0.0784287413047719 40(13)	0.140479437381027000(20)	0.0308436	0
	0	−0.00167630123(4)	0.007066720288(32)	0
11	0	−0.00167630123(4)	0.007066720288(32)	0
	0	−0.00167630123(4)	0.007066720288(32)	0
	0.00941503771(7)	−0.00741987168(7)	−0.043181620961(25)	0.015793448154(27)
12	0.00185761146(29)	0.0014624225(4)	−0.0408514560(5)	0.01462802585(8)
	−0.01000581689(14)	0.01435074267(33)	−0.03504827712(25)	0.01223252112(9)
	0.154933	−0.372367	0	0
14	0.128291	−0.298471	0	0
	0.0947597	−0.207766	0	0
	−0.012751(24)	0.033406(18)	0.051912(5)	−0.00694526(34)
15	−0.019465(19)	0.038577(13)	0.048889(6)	−0.0067619(6)
	−0.03232(9)	0.049539(0.000023	0.041539(6)	−0.0060698(7)
	0	−0.111897(20)	0.028270(5)	0
17	0	−0.101166(19)	0.028270(5)	0
	0	−0.085583(22)	0.028270(5)	0

TABLE 5.14: Coefficients $c^{(1,k)}_{3,1,j}$,r=1. The three values of each diagram correspond to different Symanzik improved actions: Wilson action (first line), Tree-Level Symanzik (second line), and Iwasaki action (third line).

j	$c_{2,0,j}^{(-1,0)}$	$c_{2,1,j}^{(-1,0)}$	$c_{2,1,j}^{(-1,1)}$	$c_{2,0,j}^{(1,0)}$	$c_{2,1,j}^{(1,0)}$	$c_{2,1,j}^{(1,1)}$
	0	0	0	$-\frac{5}{3}$	5	-5
1+2	0	0	0	$-\frac{5}{3}$	5	-5
	0	0	0	$-\frac{5}{3}$	5	-5
	$-\frac{1}{3}$	$\frac{2}{3}$	1	$\frac{1}{3}$	$-\frac{2}{3}$	-1
5	$-\frac{1}{3}$	$\frac{2}{3}$	1	$\frac{1}{3}$	$-\frac{2}{3}$	-1
	$-\frac{1}{3}$	$\frac{2}{3}$	1	$\frac{1}{3}$	$-\frac{2}{3}$	-1
	0	0	0	0	0	$\frac{1}{2}$
11	0	0	0	0	0	$\frac{1}{2}$
	0	0	0	0	0	$\frac{1}{2}$
	0	0	0	0	0	1
12	0	0	0	0	0	1
	0	0	0	0	0	1
	0	0	0	$\frac{4}{3}$	-3	$-\frac{3}{2}$
15	0	0	0	$\frac{4}{3}$	-3	$-\frac{3}{2}$
	0	0	0	$\frac{4}{3}$	-3	$-\frac{3}{2}$
	$\frac{1}{3}$	0	-1	0	0	0
16	$\frac{1}{3}$	0	-1	0	0	0
	$\frac{1}{3}$	0	-1	0	0	0
	0	0	0	0	0	4
17	0	0	0	0	0	4
	0	0	0	0	0	4

TABLE 5.15: Coefficients $c_{2,i,j}^{(l,k)}$, r=1. The three values of each diagram correspond to different Symanzik improved actions: Wilson action (first line), Tree-Level Symanzik (second line), and Iwasaki action (third line).

Chapter 6

Hadron structure

Hadron structure is explained through the parton model, which revolutionized our understanding of the constituents and dynamics within hadrons. Proposed by Richard Feynman in 1969 [70, 71], the model treats hadrons as collections of point-like entities called partons, which include quarks and gluons. In high-energy experiments, when probing particles interact with the partons inside a target hadron, they experience scattering as if they are colliding with these constituent particles individually.

Within the framework of the parton model and QCD, information on this structure is achieved through the parton distribution functions (PDFs), which encode the distribution of a hadron's momentum and spin among its partons. Defined in a reference frame where the hadron has infinite momentum, the partons' momenta are nearly collinear with that of the hadron. This allows the hadron to be visualized as a stream of free partons, each carrying a fraction of the longitudinal momentum. However, these distributions cannot be directly measured in experiments, because individual quarks or gluons have not been detected in isolation, a consequence of QCD color confinement. Since the discovery of quarks within nucleons, significant experimental and computational resources have been dedicated to determining the distribution of quarks and gluons within hadrons. Two main methods are currently employed: global QCD analysis and lattice QCD [72].

6.1 Global PDF fits

The PDFs are classified as unpolarized (spin-averaged), and polarized (spin-dependent), where each can be obtained through the QCD factorization [73] of the cross-section from different high-energy processes, including deep-inelastic scattering (DIS) and Drell-Yan processes.

Specifically, let's examine the process $e + A \to e + X$ of the unpolarized DIS, occurring through the exchange of a virtual photon with momentum q^μ. Here, A denotes a hadron, and X represents the recoiling system. From the measured cross-section, we can extract the standard hadronic tensor $W^{\mu\nu}(q^\mu, p^\mu)$:

$$\begin{aligned} W^{\mu\nu} =& \frac{1}{4\pi} \int d^4y \, e^{iq\cdot y} \langle A | j_\mu(y) | X \rangle \langle X | j_\nu(0) | A \rangle \\ =& F_1(x, Q^2) \left(-g^{\mu\nu} + \frac{q^\mu q^\nu}{q^2} \right) + F_2(x, Q^2) \frac{(p^\mu - \frac{qp\cdot q}{q^2} q^\mu)(p^\nu - \frac{qp\cdot q}{q^2} q^\nu)}{p \cdot q} \end{aligned} \tag{6.1}$$

where p^μ is the momentum of the incoming hadron A, and $j_\mu(y)$ denotes the electromagnetic current. It's worth noting that in other processes, $j_\mu(y)$ can represent any electroweak current, and we should include more than two scalar structure functions F_i. Moreover, Q is the kinematic energy scale of the scattering, where $Q^2 = -q^\mu q_\mu$, and $x = \frac{Q^2}{2q\cdot p}$.

For large Q at a fixed x, factorization theorem allows expressing $W^{\mu\nu}$ as a convolution of a hard scattering coefficient and a parton distribution:

$$W^{\mu\nu}(q^\mu, p^\mu) = \sum_a \int_x^1 \frac{\mathrm{d}z}{z} f_{a/A}(z, \mu) H_a^{\mu\nu}(q^\mu, zp^\mu, \mu, \alpha_s(\mu)) + \mathcal{O}(Q^{-1}) \tag{6.2}$$

where a includes all possible types of partons (quarks, anti-quarks, and gluons), $f_{a/A}(z, \mu)$ is the parton distribution function, and $H_a^{\mu\nu}$ is the hard scattering coefficient. This coefficient is process-dependent and can be calculated in perturbation theory as a power series in $\alpha_s(Q)$ with finite coefficients. The expression $f_{a/A}(z, \mu)\mathrm{d}z$ is interpreted as the probability of finding a parton of type a in a hadron of type A carrying a fraction z to $z + \mathrm{d}z$ of the hadron's momentum. The distribution function $f_{a/A}$, characterizes the non-perturbative aspect of the process, revealing insights into the structure of hadrons. In this context of the unpolarized DIS process, the relevant distribution function is the unpolarized PDF. In contrast to the hard scattering coefficients, distribution functions are universal. They are not entirely

process-independent due to their reliance on the renormalization scale μ. Typically, both the distribution functions and hard scattering coefficients are defined within the $\overline{\text{MS}}$ scheme. However, when they are convoluted, the resulting physical observables are scheme-independent as expected.

We can project Eq.(6.2) onto individual structure functions:

$$\begin{aligned} F_1\left(x,Q^2\right) &= \sum_a \int_x^1 \frac{\mathrm{d}z}{z} f_{a/A}(z,\mu) H_{1a}\left(\frac{x}{z},\frac{Q}{\mu},\alpha_s(\mu)\right) + \mathcal{O}(Q^{-1}) \\ \frac{1}{x}F_2\left(x,Q^2\right) &= \sum_a \int_x^1 \frac{\mathrm{d}z}{z} f_{a/A}(z,\mu) \frac{z}{x} H_{2a}\left(\frac{x}{z},\frac{Q}{\mu},\alpha_s(\mu)\right) + \mathcal{O}(Q^{-1}), \end{aligned} \tag{6.3}$$

The extra factors of $1/x$ and z/x in the equation for F_2 are needed because of the dependence on the target momentum of the tensor multiplying F_2. Analogous expressions for the structure functions can be derived for other hard scattering processes as well.

The evolution in μ of the parton distribution functions is described by the DGLAP (Dokshitzer-Gribov-Lipatov-Altarelli-Parisi) evolution equations [74–76], which have the form of:

$$\frac{\partial f_a\left(x,\mu^2\right)}{\partial \ln \mu^2} = \sum_b \int_x^1 \frac{\mathrm{d}z}{z} P_{ab}\left(\frac{x}{z},\frac{Q}{\mu},\alpha_s(\mu)\right) f_b\left(z,\mu^2\right) \tag{6.4}$$

where P_{ab} is the DGLAP kernels, which describe the parton splitting $b \to a$. They can be expressed as powers of α_s.

Using Eq. 6.4, we can predict the evolution of parton distribution functions from a given scale μ_0. However, these evolution equations are incapable of directly predicting these at any particular μ_0. Thus, the initial scale μ_0 needs to be determined first, before comparing the QCD predictions of PDFs to other μ scales. This is a key aspect utilized in global QCD analyses.

Global PDF fits conduct a QCD analysis of hard-scattering measurements, typically incorporating a range of hadronic observables [77–83]. Parton distributions are parametrized at an initial energy scale, followed by their evolution to the scale of the data through the DGLAP equations. These distributions are then used to formulate theoretical predictions for the relevant observables.

Within this process, parton distributions are initially parameterized at an initial energy scale, followed by their evolution to the scale of the data through the DGLAP equations. These distributions are then used to formulate theoretical predictions for relevant observables. Typically, the factorization scale μ in the corresponding factorization formula is set equal to the characteristic scale of the process, Q. Finally, the determination of the best-fit parameters of PDFs is achieved through the minimization of a suitable metric, such as the log-likelihood χ^2.

However, global QCD analyses from high-energy experiments fall short of providing a complete picture of parton distributions. While they do offer accurate results in cases involving specific parton flavors, spin configurations, and kinematic regions, limitations within experimental programs or phenomenological models restrain a comprehensive determination. For instance, experiments face difficulties in accessing regions of small x values, while models struggle to capture the QCD dynamics [84–86].

6.2 PDFs from lattice QCD

To address the limitations of determining PDFs based on experimental data, the development of a theoretical systematic framework becomes necessary for studying the parton distributions. Currently, the only available method is through lattice QCD simulations.

The distribution functions can be defined as matrix elements in a hadron state of specific operators intended to count the number of quarks or gluons carrying a fraction x of the hadron's momentum. Typically, this definition is given in a light-cone reference frame, where the hadron carries momentum P^μ with plus and minus components, expressed as $P^\pm = (P^0 \pm P^3)/\sqrt{2}$, while its transverse components are set to zero.

We thus arrive at the definition for quark PDFs:

$$f^{\Gamma}_{q/A}(x) = \frac{1}{4\pi}\int dz^- \, \exp\left(-ixP^+z^-\right)\Big\langle P \,\Big|\, \overline{\psi}(z^-)\,\Gamma\, W(z^-,0)\,\psi(0) \,\Big|\, P\Big\rangle \tag{6.5}$$

where $z^\pm \equiv (z^0 \pm z^3)/\sqrt{2}$ denote the light-cone space coordinates, $|P\rangle$ represent the hadron state, and Γ takes values of γ^+, $\gamma_5\gamma^+$ or $\gamma^+\gamma^\perp$ (where $\gamma^+ \equiv (\gamma^0 + \gamma^i)/\sqrt{2}$ and $\gamma^\perp\cdot\gamma^+ = 0$), corresponding to the unpolarized, longitudinally polarized and transversely polarized types of PDFs respectively. The operator $W(z^-, 0)$, known as the light-cone

Wilson line, connects the light-like separated quark and antiquark fields, ensuring gauge invariance. Its expression is given by:

$$W\left(z^{-},0\right)=\mathcal{P}\exp\left[ig\int_{0}^{z^{-}}dy^{-}A^{+}\left(y^{-}\right)\right], \tag{6.6}$$

where $\mathcal{P}$ is the path order exponential, indicating the arrangement of gluon field operators $A^{+}(y^{-})$ along the path.

6.2.1 Mellin moments

In the Euclidean formulation of lattice QCD, direct determination of parton distributions is impossible since they are light-cone correlation functions. Instead, they can be obtained through the Mellin moments of PDFs. These moments correspond to matrix elements of local twist-two operators, where the twist is defined as the dimension minus the spin. While the leading-twist (twist-two) contributions have a probabilistic interpretation, the higher-twist contributions are influenced by soft dynamics. Typically, studies prioritize isolating the leading twist contributions due to their straightforward identification. While the higher-twist corrections have received less attention, there is an increasing interest in studying them, with efforts including exploration through lattice calculations.

The Mellin moments of the structure functions can be expressed, up to higher-twist effects, as:

$$\begin{aligned}\tilde{F}_{1}\left(n,Q^{2}\right)&=\int_{0}^{1}\frac{\mathrm{d}x}{x}x^{n}F_{1}\left(x,Q^{2}\right),\\ \tilde{F}_{2}\left(n,Q^{2}\right)&=\int_{0}^{1}\frac{\mathrm{d}x}{x}x^{n-1}F_{2}\left(x,Q^{2}\right).\end{aligned} \tag{6.7}$$

Using this notation, Eq. 6.3 transforms into:

$$\tilde{F}_{i}\left(n,Q^{2}\right)=\sum_{a}\tilde{f}_{a/A}(n,\mu)\tilde{H}_{ia}\left(n,\frac{Q}{\mu},\alpha_{s}(\mu)\right) \tag{6.8}$$

For integer values of n, the $\tilde{f}_{j/A}(n,\mu)$ are hadron matrix elements of specific local operators, calculated at a renormalization scale μ. Conversely, the structure-function moment $\tilde{F}_{2}\left(n,Q^{2}\right)$ can be described in relation to the hadron matrix element of a

product comprising two electromagnetic current operators, computed at two neighboring spacetime points. The equation above demonstrates an application of the operator product expansion (OPE). It expresses the product of the two operators using local operators and certain coefficients $\tilde{H}_{ia}\left(n, Q/\mu, \alpha_s(\mu)\right)$, known as Wilson coefficients, which can be calculated in perturbation theory.

In principle, the reconstruction of PDFs using an OPE is possible given a sufficient number of Mellin moments. However, in practice, only the lowest three moments have been accurately computed [87–90]. These moments are insufficient for fully reconstructing the momentum dependence of the PDFs without significant reliance on models. Despite their limitations, the lowest three moments are directly associated with measurable quantities like the axial charge and quark momentum fraction. Obtaining precise calculations of higher moments via lattice simulations is extremely challenging. The signal-to-noise ratio decreases due to the covariant derivatives in higher-twist operators. Additionally, higher moments encounter unavoidable power-law mixing under renormalization, making the reconstruction of full parton distributions from their moments practically unfeasible.

6.2.2 The x-dependence of PDFs

While the lowest three moments of PDFs can provide valuable benchmarks for lattice-QCD calculations and constraints in global PDF extractions, they are not in themselves sufficient to determine the x-dependence of PDFs. Various methods are being explored for extracting the x-dependence of PDFs on the lattice [91–95].

PDFs can be determined from hadronic tensors in the Euclidean path-integral by subtracting higher-twist contributions. The hadronic tensor method does not require large momentum, as it is frame-independence, allowing calculations in any momentum frame. It is also free of renormalization. The method relies on analyzing ratios of suitable four-point and two-point functions, which is computationally very challenging, as one has to suppress the gauge noise and isolate the ground state at the same time. Another difficulty is the reconstructing the hadronic tensor from Euclidean space to Minkowski space, a process that suffers from the inverse Laplace transform.

Another promising technique, termed "OPE without OPE," involves computing matrix elements of time-ordered products of local currents. This approach facilitates

the extraction of scalar functions related to DIS structure functions and avoids the computational complexity associated with four-point functions. It involves the Compton amplitude, critical for understanding nucleon structure, which can be directly computed in lattice QCD using the Feynman-Hellmann technique. By working at sufficiently large momentum transfers, twist-two contributions dominate, simplifying the computation process.

One notable approach is the quasi-distribution method, which employs the large momentum effective theory (LaMET) [96, 97]. Instead of directly computing light-cone correlation functions, this method calculates a Euclidean version of PDFs, called quasi-PDFs. These quasi-PDFs are defined as matrix elements of momentum-boosted hadrons coupled to gauge-invariant nonlocal operators, including a finite-length Wilson line. The resulting quasi-observable, which depends on the hadron's momentum but is independent of time, can be computed on the lattice and then renormalized nonperturbatively using an appropriate scheme. Finally, the renormalized quasi-PDF is matched to the standard PDF through a factorization formula, calculated in perturbation theory [98–102].

Another alternative framework to quasi-PDFs is the pseudo-ITDs. Like quasi-PDFs, pseudo-ITDs utilize matrix elements of boosted hadrons coupled to non-local operators. However, instead of using the variables z and P^z, the pseudo-ITDs approach employs Lorentz invariants z^2 and $\nu \equiv -p \cdot z$, where ν is historically known as Ioffe time. In Euclidean space, $\nu = zP^z\,\mathcal{M}(\nu, z^2)$. The matrix elements $\mathcal{M}(\nu, z^2)$ in this framework are referred to as Ioffe-time pseudo-distributions (pseudo-ITDs). One notable difference between quasi- and pseudo-distributions is their Fourier transforms. Quasi-distributions are Fourier transforms of $\mathcal{M}(P^z, z)$ in z, whereas pseudo-distributions are Fourier transforms of $\mathcal{M}(\nu, z^2)$ in ν. Similar also to quasi-distributions, the pseudo-distributions approach relies on factorizing pseudo-ITDs obtained on the lattice to extract light-cone ITDs, using a matching kernel calculable in perturbative QCD. However, the necessary matching in the pseudo-distributions approach is performed at the level of ITDs in coordinate space, while in the quasi-PDFs approach, it is done in momentum space.

In addition to the methods mentioned earlier, lattice cross-sections offer another path for extracting the x-dependence of PDFs from lattice-QCD calculations. Analogous to global QCD analyses of high-energy scattering data, lattice cross-sections involve analyzing data generated by lattice-QCD calculations of well-defined lattice

cross-sections. These cross-sections are defined as single-hadron matrix elements of time-ordered, renormalized, nonlocal operators, and they encapsulate the collision kinematics. The choice of operator determines the dynamical features of the lattice cross-section. A good lattice cross-section possesses three key properties: it is calculable in lattice QCD with Euclidean time, it converges to a well-defined continuum limit as the lattice spacing approaches zero, and it exhibits the same factorizable logarithmic collinear divergences as PDFs.

6.3 Three-dimensional structure of hadrons

PDFs are one-dimensional functions that depend only on the longitudinal momentum fraction carried by the partons, making them the most straightforward to compute among distribution functions. However, to describe the three-dimensional structure of hadrons, additional distribution functions are required [103]: the Generalized Parton Distributions (GPDs) [104–108], and the Transverse-Momentum-Dependent Distributions (TMD PDFs) [109–112].

GPDs describe the correlation functions of quarks and gluons, which involve off-diagonal matrix elements of operators positioned at a lightlike separation between the parton fields. Unlike the diagonal PDFs (see the quark definition in Eq. 6.5), GPDs should not be interpreted as parton densities; instead, they are to be perceived as probability amplitudes. Experimental access to GPDs is possible through exclusive processes like deeply virtual Compton scattering or meson electroproduction. They are significant in non-forward scattering phenomena, which effectively capture the transfer of momentum between the initial and final states of hadrons.

The definition of the quark GPDs is provided as [103]:

$$F^{\Gamma}_{q/A}(x,\xi,t) = \frac{1}{4\pi}\int dz^- \, \exp\left(ix\overline{P}^+ z^-\right)\Big\langle P' \,\Big|\, \overline{\psi}(-\frac{z^-}{2})\,\Gamma\, W(-\frac{z^-}{2},\frac{z^-}{2})\,\psi(\frac{z^-}{2}) \,\Big|\, P\Big\rangle\Big|_{\substack{z^+=0\\ z^T=0}} \tag{6.9}$$

where $P(P')$ is the incoming (outgoing) hadron momentum, $\overline{P} = (P + P')/2$, and $\Delta = P' - P$. They rely on two extra kinematic variables, apart from the fraction x: the momentum transfer squared $t = \Delta^2$, and the light-cone component of the longitudinal momentum transfer (skewness), $\xi \equiv -2\Delta^+/P$. It's worth noting that the transverse component of the longitudinal momentum transfer enters via t.

Extracting GPDs from experimental data poses several challenges due to the limited nature of the data and their coverage of a small kinematic region. These data sets are indirectly linked to GPDs through the Compton form factors, and it's particularly challenging to distinguish between different GPDs involved in the same high-energy process. The x-dependence of GPDs for fixed t and ξ values can be obtained from the lattice using the techniques established for PDFs. This approach has been recently investigated through the quasi- and pseudo-distributions approach.

The TMD PDFs extend the usual PDFs by including dependency on the transverse momentum of the parton $\mathbf{k_T}$, thus providing insight into the three-dimensional structure of hadrons. In other words, instead of having a number density $f(x)$ of partons per unit of lightcone momentum fraction x, there is now a density $f(x, \mathbf{k_T})$ of partons per unit of both the momentum fraction x and the (small) transverse momentum components. TMD PDFs emerge in processes that involve multiple kinematic scales, such as Drell-Yan, e^+e^- annihilation, and semi-inclusive deep inelastic scattering. As a result, a more intricate factorization framework is necessary [113].

For example, the quark TMDs are defined as [114]:

$$\Phi^{\Gamma}_{q/A}(x, \mathbf{k_T}) = \int_{-\infty}^{\infty} \frac{d^2\mathbf{z_T}}{(2\pi)^2} \int_{-\infty}^{\infty} \frac{dz^-}{4\pi} \exp(ixP^+z^- - i\mathbf{k_T}\cdot\mathbf{z_T}) \times \left\langle P \left| \overline{\psi}(0)\, \Gamma\, W_{\sqsubset}(z^\mu, 0)\, \psi(z^\mu) \right| P \right\rangle \Big|_{z^+=0} \tag{6.10}$$

where $z^\mu = (0, z^-, \mathbf{z_T})$ denotes the four-vector of the light-cone spatial coordinates, where $\mathbf{z_T}$ refers to the coordinates perpendicular to $z^\pm$. The quark and antiquark fields at positions 0 and z^μ are connected by the staple shaped Wilson line $W_{\sqsubset}(z^\mu, 0)$ which are defined by products of straight line segments:

$$\begin{aligned} W_{\sqsubset}(z^\mu, 0) &= W[0 \to -\infty\hat{n}_z \to -\infty\hat{n}_z + \mathbf{z_T} \to (z^-, \mathbf{z_T})] \\ &= W_{n_z}(z^\mu; -\infty, 0) W_{\hat{z}_T}(-\infty\hat{n}_z; 0, \mathbf{z_T}) W_{n_z}(0^\mu; 0, -\infty) \end{aligned} \tag{6.11}$$

The individual Wilson lines $W_n(x; a, b)$ are defined as path-ordered exponentials connecting the point $x^\mu + an^\mu$ to $x^\mu + bn^\mu$ along the direction n,

$$W_n(x^\mu; a, b) = \mathcal{P} \exp\left[-ig \int_a^b ds\, n^\mu \cdot A^0_\mu(x^\mu + s\, n^\mu) \right]. \tag{6.12}$$

Note that for W_n the subscript n is always a four-vector denoting the direction of the moving hadron.

According to Eq. 6.10 the light-cone quark TMD PDFs involve matrix elements of nonlocal operators with a staple-shaped Wilson line. These Wilson lines are infinite and have edges located on or near the light cone. Thus, directly determining the TMD PDFs in lattice QCD is unfeasible. To address this challenge, one can calculate correlation functions involving space-like separated partons, similar to the methodology used for PDFs and GPDs. These correlation functions can then be appropriately matched to their light-cone counterparts. Using the quasi-distributions approach, TMDs can be investigated through the lattice QCD [115–117]. Nevertheless, the field is still in its early stages, and significant progress is needed.

6.4 Gluon PDFs

While quark PDFs have been extensively studied both experimentally and theoretically, the investigation of gluon PDFs has been relatively limited. However, understanding gluon PDFs is essential as gluons play a critical role in various physical measurements. Gluonic contributions make a significant impact on the proton's spin [118–120]. Phenomenological data also suggest that gluon PDFs dominate over quark PDFs in the small-x region [121]. Global analysis finds that accurate calculations of the gluon-dependent quantities are essential for the cross-section of Higgs boson production, heavy quarkonium and jet production [122–125], as well as for providing theoretical input to the upcoming Electron-Ion Collider [126]. In this direction, first-principle calculations of gluon PDFs using lattice QCD can significantly complement the experimental investigations.

One complication in extracting gluon PDFs is the presence of mixing with quark flavor-singlet PDFs [127]. The disentanglement of the mixing will help to eliminate one of the sources of systematic uncertainties in simulations. In the case of Mellin moments of PDFs, the mixing arises during renormalization. When using quasi-PDFs or pseudo-ITDs approach, the mixing between the flavor-singlet quark and gluon PDFs should be resolved at the factorization level.

The definition of gluons PDFs is similar to Eq. 6.5:

$$f_{g/A}(x) = \frac{1}{2\pi x P^+} \int dz\, e^{-ixP^+z^-} \langle P|F_a^\nu(z^-)^+ W^{ab}(z^-,0)\, F_{b\nu}(0)^+|P\rangle. \tag{6.13}$$

where where $F_{\mu\nu}$ is the gluon field strength operator and W is defined in the adjoint representation.

The framework for extracting the x-dependence of quark distributions can also be applied to gluon PDFs. This concept has been recently explored in various studies concerning quasi-PDFs [99, 100, 128–130], the pseudo-ITDs [131–139], and lattice cross-sections [140]. However, ab initio calculations of gluon PDFs represent a novel and relatively uncharted territory.

An important aspect in the direct calculation of PDFs from lattice QCD is the nonperturbative renormalization of the quasi-PDFs. As regards quark quasi-PDFs, in Ref. [141] two important features of the Wilson-line operator matrix elements were revealed on the lattice: linear divergences in addition to logarithmic divergences, and mixing among certain subsets of the original operators during renormalization. Efforts to eliminate these linear divergences have been made using various methods, however a complete nonperturbative renormalization program has only recently been developed [142]. Similar effects are expected to be present in the renormalization of nonlocal gluon operators as well. A recent study [143], using the auxiliary field approach, showed that different components of nonlocal gluon operators have nontrivial renormalization patterns, making it challenging to accurately evaluate gluon quasi-PDFs. In addition, four gluon operators have been identified as multiplicatively renormalizable, making them suitable for defining some of the gluon quasi-PDFs. Related studies can be found in Refs. [99, 100, 144–146].

Chapter 7

Gluon nonlocal operators

7.1 Definition of operators

The nonlocal gluon operators under study are defined in the fundamental representation as:

$$O_{\mu\nu\rho\sigma}(x + z\hat{\tau}, x) \equiv 2\ \mathrm{Tr}\Big(F_{\mu\nu}(x + z\hat{\tau}) W(x + z\hat{\tau}, x) F_{\rho\sigma}(x) W(x, x + z\hat{\tau}) \Big) \tag{7.1}$$

where $F_{\mu\nu}$ is the gluon field strength tensor and $W(x, x + z\hat{\tau})$ denotes the straight Wilson line with length z. Its expression is given by the path-ordered ($\mathcal{P}$) exponential of the gauge field A_μ as follows:

$$W(x, x + z\hat{\tau}) \equiv \mathcal{P}\ \exp\left[ig \int_0^z A_\mu(x + \zeta\hat{\tau})\, d\zeta \right] \tag{7.2}$$

Without loss of generality, the Wilson line is chosen to lie along the z direction: $\tau = 3$; also, the origin of the axes is placed on one of the endpoints of the operator.

There are several relations among these operators, stemming both from their definition and from the symmetries of the QCD Lagrangian; these relations will be extensively discussed in Section 7.2.

Due to the antisymmetry of $F_{\mu\nu}$, for a fixed choice of the Wilson line, there are 36 nonlocal operators in total by selecting the indices of $O_{\mu\nu\rho\sigma}$ to be in any direction. However, only gluon operators that exhibit multiplicative renormalizability are appropriate for defining the gluon quasi-PDF [98]. Suitable candidates for the

unpolarized gluon quasi-PDF can be provided by [128]:

$$\tilde{f}^{(n)}_{g/H}(x, P^z) = \mathcal{N}^{(n)} \int \frac{dz}{2\pi x P^z} e^{izxP^z} \langle H(P)|O^{(n)}(z,0)|H(P)\rangle \tag{7.3}$$

where $\mathcal{N}^{(n)}$ is a renormalization factor, x is the longitudinal momentum fraction carried by the gluon, $P^\mu = (P^0, 0, 0, P^z)$ is the hadron momentum, and $H(P)$ stands for momentum-boosted hadron states. Potential candidates for the gluon operator are denoted here as $O^{(n)}(z, 0)$.

7.2 Symmetry properties

In this Section, we make use of all available symmetries [including space-time symmetries and local BRST (Becchi-Rouet-Stora-Tyutin) invariance] to pinpoint the possible mixing sets among nonlocal gluon operators. The first observation to be made is that all mixing operators will necessarily be of the same form as Eq. (7.1), possibly with different values for the Lorentz indices μ, ν, ρ, σ. This stems from the following arguments:

- Wilson lines renormalize multiplicatively [147] (see also Ref. [148] for smooth closed Wilson loops and Ref. [149] for Wilson loops involving singular points).
- There can be no mixing with nonlocal fermion operators, i.e. with operators having the generic form:

$$\bar{\Psi}(x + z\hat{\tau})\, \Gamma\, W(x + z\hat{\tau}, x)\, \Psi(x) \tag{7.4}$$

  where Ψ generically stands for a fermion field, possibly with one or more covariant derivatives, and Γ is a Dirac γ-matrix (or product thereof). The reason for this absence of mixing is that Ψ transforms under the fundamental, rather than the adjoint, representation of the global gauge group.[1]
- As in the case of local operators, there could, a priori, exist mixing with non-gauge invariant operators, in particular[127, 150]: BRST variations of other operators

[1] A more complicated alternative, in which Ψ could stand for a product of two fermion fields (and thus could transform under the adjoint representation) would lead to an operator of higher dimensionality and thus would be excluded from mixing.

[Class A]; operators which vanish by the equations of motion [Class B]; and *finite* mixing with any other operator having the same symmetry properties [Class C]. However, it can be verified by inspection that substitution of the field strength tensor $F_{\mu\nu}$, on either side of the Wilson line, by any combination of elementary fields, would violate one or more of the symmetries, first and foremost the local BRST symmetry.

Thus, in what follows we will investigate the mixing set, exclusively among operators shown in Eq. (7.1)

In lattice QCD, the action remains invariant under discrete transformations of charge conjugation ($\mathcal{C}$), parity ($\mathcal{P}$), and time reversal ($\mathcal{T}$) [151, 152]. In what follows, we present the analysis of the symmetry properties concerning the nonlocal gluon operators under $\mathcal{C}$, $\mathcal{P}$, $\mathcal{T}$ transformations, and transformations under the discrete rotational group. Since we consider the Wilson line direction as special, we study the residual three-dimensional rotational symmetry (or the discrete rotational octahedral symmetry on the lattice). The importance of this study lies in the fact that if two operators undergo different transformations, symmetries act as a safeguard, preventing them from mixing with each other under renormalization across all orders of perturbation theory. Conversely, operators lacking protection from symmetries are generally prone to mixing.

7.2.1 $\mathcal{C}$, $\mathcal{P}$, $\mathcal{T}$ transformations

First, let us review the transformations of fields under $\mathcal{C}$, $\mathcal{P}$, $\mathcal{T}$ symmetries. Since the operators under study (Eq. (7.1)) are made out of the gluon field strength tensor and the Wilson line, we only need to consider the transformations of links, U_μ. We work in Euclidean spacetime with coordinates $(x, y, z, t) = (1, 2, 3, 4)$ throughout this paper.

Charge conjugation $\mathcal{C}$ acts on lattice links as:

$$U_\mu(x) \xrightarrow{\mathcal{C}} U_\mu(x)^* = (U_\mu^\dagger(x))^\top \tag{7.5}$$

Since there is no distinction between time and space in the Euclidean formulation, the parity transformation, denoted as $\mathcal{P}_\mu$ with $\mu \in \{1, 2, 3, 4\}$, can be defined in any

direction [152].

$$\begin{aligned} U_\mu(x) &\xrightarrow{\mathcal{P}_\mu} U_\mu\left(\mathbb{P}_\mu(x)\right) \\ U_\nu(x) &\xrightarrow{\mathcal{P}_\mu} U_\nu^\dagger\left(\mathbb{P}_\mu(x) - \hat{\nu}\right) \ , \quad \nu \neq \mu \end{aligned} \tag{7.6}$$

where $\mathbb{P}_\mu(x)$ is the vector x with sign flipped except for the μ-direction.

Analogously, for any direction in Euclidean space one may define a time reversal transformation, denoted as $\mathcal{T}_\mu$:

$$\begin{aligned} U_\mu(x) &\xrightarrow{\mathcal{T}_\mu} U_\mu^\dagger(\mathbb{T}_\mu(x) - \hat{\mu}) \\ U_\nu(x) &\xrightarrow{\mathcal{T}_\mu} U_\nu(\mathbb{T}_\mu(x)) \, , \quad \nu \neq \mu \end{aligned} \tag{7.7}$$

where $\mathbb{T}_\mu(x)$ is the vector x with sign flipped in the μ-direction.

Utilizing the link transformations, we can construct the transformations of the gluon field strength tensor. For charge conjugation, we find that,

$$F_{\mu\nu}(x) \xrightarrow{C} -F_{\mu\nu}(x)^\top \tag{7.8}$$

By employing the above transformation relations and the cyclic property of traces, it can be shown that under charge conjugation the operators in Eq. (7.1) remain invariant.

Under parity transformations, the gluon field strength tensor transforms as:

$$\begin{aligned} F_{\mu\nu}(x) &\xrightarrow{\mathcal{P}_\mu} -F_{\mu\nu}(\mathbb{P}_\mu(x)) \\ &\xrightarrow{\mathcal{P}_\nu} -F_{\mu\nu}(\mathbb{P}_\nu(x)) \\ &\xrightarrow{\mathcal{P}_\rho} F_{\mu\nu}(\mathbb{P}_\rho(x)) \, , \quad \mu \neq \rho \neq \nu \end{aligned} \tag{7.9}$$

Finally, the transformation of the gluon field strength tensor under time reversal is as follows:

$$\begin{aligned} F_{\mu\nu}(x) &\xrightarrow{\mathcal{T}_\mu} -F_{\mu\nu}(\mathbb{T}_\mu(x)) \\ &\xrightarrow{\mathcal{T}_\nu} -F_{\mu\nu}(\mathbb{T}_\nu(x)) \\ &\xrightarrow{\mathcal{T}_\rho} F_{\mu\nu}(\mathbb{T}_\rho(x)) \, , \quad \mu \neq \rho \neq \nu \end{aligned} \tag{7.10}$$

Taking into consideration the antisymmetry of the gluon field strength tensor and the specified direction of the Wilson line (along the z direction), we observe the following operator transformations under parity:

$$\begin{aligned} O_{3\nu3\nu}(z,0) &\xrightarrow{\mathcal{P}_3} O_{3\nu3\nu}(z,0) \\ &\xrightarrow{\mathcal{P}_\nu} O_{3\nu3\nu}(-z,0) \\ &\xrightarrow{\mathcal{P}_\rho} O_{3\nu3\nu}(-z,0) \\ &\xrightarrow{\mathcal{P}_\rho} O_{3\nu3\nu}(-z,0) \end{aligned} \tag{7.11}$$

$$\begin{aligned} O_{\mu\nu\mu\nu}(z,0) &\xrightarrow{\mathcal{P}_3} O_{\mu\nu\mu\nu}(z,0) \\ &\xrightarrow{\mathcal{P}_\mu} O_{\mu\nu\mu\nu}(-z,0) \\ &\xrightarrow{\mathcal{P}_\nu} O_{\mu\nu\mu\nu}(-z,0) \\ &\xrightarrow{\mathcal{P}_\rho} O_{\mu\nu\mu\nu}(-z,0) \end{aligned} \tag{7.12}$$

$$\begin{aligned} O_{3\nu3\sigma}(z,0) &\xrightarrow{\mathcal{P}_3} O_{3\nu3\sigma}(z,0) \\ &\xrightarrow{\mathcal{P}_\nu} -O_{3\nu3\sigma}(-z,0) \\ &\xrightarrow{\mathcal{P}_\sigma} -O_{3\nu3\sigma}(-z,0) \\ &\xrightarrow{\mathcal{P}_\rho} O_{3\nu3\sigma}(-z,0) \end{aligned} \tag{7.13}$$

$$\begin{aligned} O_{\mu\nu\mu\sigma}(z,0) &\xrightarrow{\mathcal{P}_3} O_{\mu\nu\mu\sigma}(z,0) \\ &\xrightarrow{\mathcal{P}_\nu} -O_{\mu\nu\mu\sigma}(-z,0) \\ &\xrightarrow{\mathcal{P}_\sigma} -O_{\mu\nu\mu\sigma}(-z,0) \\ &\xrightarrow{\mathcal{P}_\mu} O_{\mu\nu\mu\sigma}(-z,0) \end{aligned} \tag{7.14}$$

$$\begin{aligned} O_{3\nu\mu\nu}(z,0) &\xrightarrow{\mathcal{P}_3} -O_{3\nu\mu\nu}(z,0) \\ &\xrightarrow{\mathcal{P}_\mu} -O_{3\nu\mu\nu}(-z,0) \\ &\xrightarrow{\mathcal{P}_\nu} O_{3\nu\mu\nu}(-z,0) \\ &\xrightarrow{\mathcal{P}_\rho} O_{3\nu\mu\nu}(-z,0) \end{aligned} \tag{7.15}$$

$$\begin{aligned} O_{\mu\nu3\nu}(z,0) &\xrightarrow{\mathcal{P}_3} -O_{\mu\nu3\nu}(z,0) \\ &\xrightarrow{\mathcal{P}_\mu} -O_{\mu\nu3\nu}(-z,0) \\ &\xrightarrow{\mathcal{P}_\nu} O_{\mu\nu3\nu}(-z,0) \\ &\xrightarrow{\mathcal{P}_\rho} O_{\mu\nu3\nu}(-z,0) \end{aligned} \tag{7.16}$$

$$\begin{aligned} O_{3\nu\mu\sigma}(z,0) &\xrightarrow{\mathcal{P}_3} -O_{3\nu\mu\sigma}(z,0) \\ &\xrightarrow{\mathcal{P}_\mu} -O_{3\nu\mu\sigma}(-z,0) \\ &\xrightarrow{\mathcal{P}_\nu} O_{3\nu\mu\sigma}(-z,0) \\ &\xrightarrow{\mathcal{P}_\sigma} O_{3\nu\mu\sigma}(-z,0) \end{aligned} \tag{7.17}$$

$$\begin{aligned} O_{\mu\sigma3\nu}(z,0) &\xrightarrow{\mathcal{P}_3} -O_{\mu\sigma3\nu}(z,0) \\ &\xrightarrow{\mathcal{P}_\mu} -O_{\mu\sigma3\nu}(-z,0) \\ &\xrightarrow{\mathcal{P}_\nu} O_{\mu\sigma3\nu}(-z,0) \\ &\xrightarrow{\mathcal{P}_\sigma} O_{\mu\sigma3\nu}(-z,0) \end{aligned} \tag{7.18}$$

Given that some of these transformations alter the sign of z, it is useful to consider the translation invariance of the Lagrangian, which imposes:

$$O_{\mu\nu\rho\sigma}(-z,0) \to O_{\mu\nu\rho\sigma}(0,z) \tag{7.19}$$

and the cyclic permutations on the trace of the operators in Eq. (7.1):

$$O_{\mu\nu\rho\sigma}(z,0) = O_{\rho\sigma\mu\nu}(0,z) \tag{7.20}$$

Taking advantage of Eqs. (7.19), and (7.20), it is convenient to perform a change of basis in the form of,

$$O^{\pm}_{\mu\nu\rho\sigma}(z,0) = \frac{1}{2}\left(O_{\mu\nu\rho\sigma}(z,0) \pm O_{\rho\sigma\mu\nu}(z,0)\right) \tag{7.21}$$

where now these operators are eigenstates of parity transformations (performed with respect to the midpoint of the operators) with eigenvalues of $+1$ (even, E) or -1 (odd, O). Note that $O^{-}_{\mu\nu\rho\sigma}(z,0)$ vanishes when $(\mu,\nu) = (\rho,\sigma)$. This way allows us to classify the 36 operators into several categories, each demonstrating distinct transformations under parity, as illustrated in Table 7.1.

Operators	$\mathcal{P}_1$	$\mathcal{P}_2$	$\mathcal{P}_3$	$\mathcal{P}_4$
$O^{+}_{3131}, O^{+}_{3232}, O^{+}_{3434}$ $O^{+}_{1212}, O^{+}_{1414}, O^{+}_{2424}$	E	E	E	E
$O^{+}_{3132}, O^{+}_{4142}$	E	E	E	O
$O^{+}_{3134}, O^{+}_{2124}$	O	E	E	O
$O^{+}_{3234}, O^{+}_{1214}$	E	O	E	O
$O^{-}_{3132}, O^{-}_{4142}$	O	O	E	E
$O^{-}_{3134}, O^{-}_{2124}$	E	O	E	E
$O^{-}_{3234}, O^{-}_{1214}$	O	E	E	E
$O^{+}_{3212}, O^{+}_{3414}$	O	E	O	E
$O^{+}_{3121}, O^{+}_{3424}$	E	O	O	E
$O^{+}_{3141}, O^{+}_{3242}$	E	E	O	O
$O^{-}_{3212}, O^{-}_{3414}$	E	O	O	O
$O^{-}_{3121}, O^{-}_{3424}$	O	E	O	O
$O^{-}_{3141}, O^{-}_{3242}$	O	O	O	E
$O^{+}_{3124}, O^{+}_{3241}, O^{+}_{3412}$	O	O	O	O
$O^{-}_{3124}, O^{-}_{3241}, O^{-}_{3412}$	E	E	O	E

TABLE 7.1: Categories of operators exhibiting different parity transformations. The arguments of the operators are omitted.

Thus, operators belonging to different categories cannot mix among themselves. The mixing pattern will be further reduced in the following subsection, by taking into account octahedral symmetry. Given that time reversal transformations are merely a composition of 3 parity transformations (and vice versa), they provide no further information on the mixing pattern.

7.2.2 Rotational octahedral point group

The rotational octahedral point group refers to a symmetry group that describes the discrete rotational symmetry of an octahedron or a cube. This group consists of 24 elements, corresponding to rotations by various angles with respect to different axes. It possesses five irreducible representations, including two 1-dimensional representations denoted as A_1 and A_2, one 2-dimensional representation labeled as E, and two 3-dimensional representations labeled as T_1 and T_2. The character table can be found in Appendix A.

Taking into account the classification of operators in Table 7.1, we can explore whether they share the same irreducible representations.

Let us start with the operator triplet $O^+_{3131}, O^+_{3232}, O^+_{3434}$: it supports a 3-dimensional reducible representation. Under the operation $C_2(z)$, defined as a 180° rotation around the z axis which transforms $x \to -x, y \to -y, z \to z$, we find that:

$$C_2(z) \begin{pmatrix} O^+_{3131} \\ O^+_{3232} \\ O^+_{3434} \end{pmatrix} = \begin{pmatrix} O^+_{3131} \\ O^+_{3232} \\ O^+_{3434} \end{pmatrix} \tag{7.22}$$

Thus, $C_2(z)$ operation can be represented by a 3×3 identity matrix:

$$C_2(z) \equiv \begin{pmatrix} 1 & 0 & 0 \\ 0 & 1 & 0 \\ 0 & 0 & 1 \end{pmatrix} \tag{7.23}$$

By applying $C_2(x)$ and $C_2(y)$ operations, one can arrive at the same conclusion. The resulting transformation matrix of Eq. 7.23 has a character value of 3, indicating a 3-dimensional reducible representation, as shown in Table A.1. This representation can be decomposed into a one-dimensional representation (A_1) and a two-dimensional representation (E). Various choices for the basis elements of E are possible, for example: For checking purposes, we study the transformation of the aforementioned

$$\begin{array}{ll} A_1: & O^+_{3131} + O^+_{3232} + O^+_{3434} \\ E: & \begin{pmatrix} 2O^+_{3434} - O^+_{3131} - O^+_{3232} \\ O^+_{3131} - O^+_{3232} \end{pmatrix} \end{array}$$

2-dimensional representation under the $C_4(z)$ operation:

$$C_4(z)\begin{pmatrix} 2O^+_{3434} - O^+_{3131} - O_{3232} \\ O^+_{3131} - O^+_{3232} \end{pmatrix} = \begin{pmatrix} 2O^+_{3434} - O^+_{3232} - O^+_{3131} \\ O^+_{3232} - O^+_{3131} \end{pmatrix} \tag{7.24}$$

where the operation $C_4(z)$ is defined in a manner such that it can be represented through a 2×2 matrix having a character value of 0. Its form is given as:

$$C_4(z) \equiv \begin{pmatrix} 1 & 0 \\ 0 & -1 \end{pmatrix} \tag{7.25}$$

Similar reasoning can be applied to the operators O^+_{1212}, O^+_{1414}, and O^+_{2424}. In this case, we can identify the following operators, supporting irreducible representations:

$$\begin{aligned} A_1 &: \quad O^+_{1212} + O^+_{1414} + O^+_{2424} \\ E &: \quad \begin{pmatrix} 2O^+_{1212} - O^+_{1414} - O^+_{2424} \\ O^+_{1414} - O^+_{2424} \end{pmatrix} \end{aligned}$$

For completeness, we examine the impact of $C_4(z)$ operation on the above 2-dimensional representation:

$$C_4(z)\begin{pmatrix} 2O^+_{1212} - O^+_{1414} - O^+_{2424} \\ O^+_{1414} - O^+_{2424} \end{pmatrix} = \begin{pmatrix} 2O^+_{2121} - O^+_{2424} - O^+_{1414} \\ O^+_{2424} - O^+_{1414} \end{pmatrix} \tag{7.26}$$

It is evident that the $C_4(z)$ transformation matrix is equivalent to Eq. 7.25.

Proceeding analogously, we can draw conclusions about the rest of the categories of Table 7.1. For the second and third set of categories, we can identify operators supporting the three-dimensional irreducible representations T_1 and T_2:

$$\begin{aligned} T_1 &: \quad \begin{pmatrix} O^-_{3132} \\ O^-_{3431} \\ O^-_{3234} \end{pmatrix} \quad , \quad \begin{pmatrix} O^-_{4142} \\ O^-_{2421} \\ O^-_{1214} \end{pmatrix} \\ T_2 &: \quad \begin{pmatrix} O^+_{3132} \\ O^+_{3431} \\ O^+_{3234} \end{pmatrix} \quad , \quad \begin{pmatrix} O^+_{4142} \\ O^+_{2421} \\ O^+_{1214} \end{pmatrix} \end{aligned}$$

Concerning the remaining categories, the analysis becomes somewhat more intricate; we can construct linear combinations of these operators that support the following irreducible representations:

$$
\begin{aligned}
T_1: &\quad \begin{pmatrix} O^+_{3212}+O^+_{3414} \\ O^+_{3121}+O^+_{3424} \\ O^+_{3141}+O^+_{3242} \end{pmatrix} \quad , \quad \begin{pmatrix} O^-_{3212}+O^-_{3414} \\ O^-_{3121}+O^-_{3424} \\ O^-_{3141}+O^-_{3242} \end{pmatrix} \\
T_2: &\quad \begin{pmatrix} O^+_{3212}-O^+_{3414} \\ O^+_{3121}-O^+_{3424} \\ O^+_{3141}-O^+_{3242} \end{pmatrix} \quad , \quad \begin{pmatrix} O^-_{3212}-O^-_{3414} \\ O^-_{3121}-O^-_{3424} \\ O^-_{3141}-O^-_{3242} \end{pmatrix} \\
A_1: &\quad O^+_{3124}+O^+_{3241}+O^+_{3412} \quad , \quad O^-_{3124}+O^-_{3241}+O^-_{3412} \\
E: &\quad \begin{pmatrix} 2O^+_{3412}-O^+_{3241}-O^+_{3124} \\ O^+_{3124}-O^+_{3241} \end{pmatrix} \quad , \quad \begin{pmatrix} 2O^-_{3412}-O^-_{3241}-O^-_{3124} \\ O^-_{3124}-O^-_{3241} \end{pmatrix}
\end{aligned}
$$

Combining our findings from the octahedral point group and parity transformations, we arrange the 36 operators into 16 groups, as shown in Table 7.2. We notice that the operators in groups $\{1,\ 2\}$ have exactly the same behavior under parity transformations and the octahedral group: consequently, they have the potential to mix under renormalization. The same conclusion applies to the operators in groups $\{3,\ 4\}$, $\{5,\ 6\}$, $\{7,\ 8\}$. By the same arguments, operators in groups 9-16 cannot possibly mix; thus, quantum corrections result in a mere multiplicative renormalization for these operators. Finally, we note that, in groups containing multiplets (doublets or triplets) the renormalization and mixing coefficients are the same for each component of the multiplet.

We emphasize that all the above findings, being based on symmetry properties alone, are valid beyond perturbation theory. Thus, by making use of the operators of Table 7.2 in numerical simulations, one can avoid unnecessary contamination from spurious mixing contributions.

It is worth mentioning that the same mixing pattern will be observed in the continuum, where octahedral symmetry is replaced by $O(3)$ symmetry. This is because every mixing pair contains one operator with at least one index along the z-axis and one operator with no such index; such operators cannot be related via a continuum transformation, and thus they can still mix, just as on the lattice. However, in the continuum some of the Z factors of different groups will coincide; this is related to the fact that the E and T_2 representations of the cubic group combine into the spin-2 representation of the $O(3)$ group, and therefore the corresponding renormalization factors must be equal. In

Group	Operators	$\mathcal{P}_1$	$\mathcal{P}_2$	$\mathcal{P}_3$	$\mathcal{P}_4$	Irreducible Repr.
1	$O^+_{3131}+O^+_{3232}+O^+_{3434}$	E	E	E	E	A_1
2	$O^+_{1212}+O^+_{1414}+O^+_{2424}$	E	E	E	E	A_1
3	$\begin{pmatrix} 2O^+_{3434}-O^+_{3131}-O^+_{3232} \\ O^+_{3131}-O^+_{3232} \end{pmatrix}$	E	E	E	E	E
4	$\begin{pmatrix} 2O^+_{1212}-O^+_{1414}-O^+_{2424} \\ O^+_{1414}-O^+_{2424} \end{pmatrix}$	E	E	E	E	E
5	$\begin{pmatrix} O^-_{3132} \\ O^-_{3431} \\ O^-_{3234} \end{pmatrix}$	E E O	E O E	E E E	O E E	T_1
6	$\begin{pmatrix} O^-_{4142} \\ O^-_{2421} \\ O^-_{1214} \end{pmatrix}$	E E O	E O E	E E E	O E E	T_1
7	$\begin{pmatrix} O^+_{3132} \\ O^+_{3431} \\ O^+_{3234} \end{pmatrix}$	O O E	O E O	E E E	E O O	T_2
8	$\begin{pmatrix} O^+_{4142} \\ O^+_{2421} \\ O^+_{1214} \end{pmatrix}$	O O E	O E O	E E E	E O O	T_2
9	$\begin{pmatrix} O^+_{3212}+O^+_{3414} \\ O^+_{3121}+O^+_{3424} \\ O^+_{3141}+O^+_{3242} \end{pmatrix}$	O E E	E O E	O O O	E E O	T_1
10	$\begin{pmatrix} O^-_{3212}+O^-_{3414} \\ O^-_{3121}+O^-_{3424} \\ O^-_{3141}+O^-_{3242} \end{pmatrix}$	E O O	O E O	O O O	O O E	T_1
11	$\begin{pmatrix} O^+_{3212}-O^+_{3414} \\ O^+_{3121}-O^+_{3424} \\ O^+_{3141}-O^+_{3242} \end{pmatrix}$	O E E	E O E	O O O	E E O	T_2
12	$\begin{pmatrix} O^-_{3212}-O^-_{3414} \\ O^-_{3121}-O^-_{3424} \\ O^-_{3141}-O^-_{3242} \end{pmatrix}$	E O O	O E O	O O O	O O E	T_2
13	$O^+_{3124}+O^+_{3241}+O^+_{3412}$	O	O	O	O	A_1
14	$O^-_{3124}+O^-_{3241}+O^-_{3412}$	E	E	O	E	A_1
15	$\begin{pmatrix} 2O^+_{3412}-O^+_{3241}-O^+_{3124} \\ O^+_{3124}-O^+_{3241} \end{pmatrix}$	O	O	O	O	E
16	$\begin{pmatrix} 2O^-_{3412}-O^-_{3241}-O^-_{3124} \\ O^-_{3124}-O^-_{3241} \end{pmatrix}$	E	E	O	E	E

TABLE 7.2: Groups of operators exhibiting different parity transformations, along with the corresponding representation of the octahedral group.

particular:

$$\begin{aligned} &Z_{3\,3}^{\mathrm{DR},\overline{\mathrm{MS}}} = Z_{7\,7}^{\mathrm{DR},\overline{\mathrm{MS}}}, \qquad Z_{3\,4}^{\mathrm{DR},\overline{\mathrm{MS}}} = Z_{7\,8}^{\mathrm{DR},\overline{\mathrm{MS}}}, \qquad Z_{4\,3}^{\mathrm{DR},\overline{\mathrm{MS}}} = Z_{8\,7}^{\mathrm{DR},\overline{\mathrm{MS}}}, \\ &Z_{4\,4}^{\mathrm{DR},\overline{\mathrm{MS}}} = Z_{8\,8}^{\mathrm{DR},\overline{\mathrm{MS}}}, \qquad Z_{11\,11}^{\mathrm{DR},\overline{\mathrm{MS}}} = Z_{15\,15}^{\mathrm{DR},\overline{\mathrm{MS}}}, \qquad Z_{12\,12}^{\mathrm{DR},\overline{\mathrm{MS}}} = Z_{16\,16}^{\mathrm{DR},\overline{\mathrm{MS}}} \end{aligned} \tag{7.27}$$

Chapter 8

Perturbative renormalization of gluon nonlocal operators

8.1 Formulation

8.1.1 Lattice action

We consider a nonabelian gauge theory of $SU(N_c)$ group and N_f multiplets of fermions. To simplify our calculations, we employ the Wilson plaquette gauge action for gluons:

$$S = \frac{2}{g^2} \sum_{\text{plaq.}} \text{Re Tr}\,\{1 - U_{\text{plaq.}}\} + S_F \tag{8.1}$$

where

$$U_{\text{plaq.}} = U_\mu(x) U_\nu(x + a\hat{\mu}) U_\mu^\dagger(x + a\hat{\nu}) U_\nu^\dagger(x) \tag{8.2}$$

and a stands for the lattice spacing. For simplicity, we will often omit a in what follows; its presence can always be inferred by dimensional reasoning. The fermionic part of the action, S_F, only enters the one-loop calculation through the gluon field renormalization factor (see Sec. 8.2). For the sake of definiteness, we will use the clover-improved Wilson fermion action [65]; however, adapting our results to any other fermion action is trivial to one-loop order.

A standard lattice discretization of the Wilson line in Eq. 7.1, using gluon links $U_\tau(x)$, can be formulated as follows:

$$W(x, x + z\hat{\tau}) = \prod_{\ell=0}^{n\mp 1} U_{\pm\tau}(x + \ell a\hat{\tau}), \qquad n \equiv z/a \tag{8.3}$$

where $U_{-\tau}(x) \equiv U_\tau^\dagger(x - a\hat{\tau})$ and upper (lower) signs correspond to $n > 0$ ($n < 0$). Alternative discretization methods incorporate smeared gluon links, such as stout, HYP, and Wilson flow.

Furthermore, on the lattice, $F_{\mu\nu}$ is determined by the standard clover discretization of the gluon field strength tensor, defined as follows:

$$\hat{F}_{\mu\nu} \equiv -\frac{i}{8g}\left(Q_{\mu\nu} - Q_{\nu\mu}\right) \tag{8.4}$$

where $Q_{\mu\nu}$ is defined as the sum of the open plaquette loops:

$$\begin{aligned} Q_{\mu\nu} = {} & U_\mu(x)U_\nu(x + a\hat{\mu})U_\mu^\dagger(x + a\hat{\nu})U_\nu^\dagger(x) \\ & + U_\nu(x)U_\mu^\dagger(x + a\hat{\nu} - a\hat{\mu})U_\nu^\dagger(x - a\hat{\mu})U_\mu(x - a\hat{\mu}) \\ & + U_\mu^\dagger(x - a\hat{\mu})U_\nu^\dagger(x - a\hat{\mu} - a\hat{\nu})U_\mu(x - a\hat{\mu} - a\hat{\nu})U_\nu(x - a\hat{\nu}) \\ & + U_\nu^\dagger(x - a\hat{\nu})U_\mu(x - a\hat{\nu})U_\nu(x + a\hat{\mu} - a\hat{\nu})U_\mu^\dagger(x). \end{aligned} \tag{8.5}$$

We expect that improved gauge actions, such as the Symanzik improved action, or the implementation of stout-smeared links, will not have an impact on determining the mixing pattern under renormalization of the nonlocal operators.

8.1.2 Renormalization of operators

To study the renormalization of the nonlocal gluon operators, we choose, for convenience, to calculate the following one-particle-irreducible (1-PI) two-point bare amputated Green's functions [1]:

$$\delta^{(4)}(q + q')\Lambda_O(q, z) = \langle A_\alpha^a(q) \left(\int d^4x\, O_{\mu\nu\rho\sigma}(x + z\hat{\tau}, x)\right) A_\beta^b(q')\rangle_{\text{amp}} \tag{8.6}$$

[1] For simplicity, we omit color and Lorentz indices whenever they can be understood from the context. The Green's functions under study typically depend on seven Lorentz indices: two from the external gluon fields, four from the operators, and one indicating the direction of the Wilson line.

where operator $O_{\mu\nu\rho\sigma}$ is defined by Eq. (7.1), and $A^a_\alpha(q)$, $A^b_\beta(q')$ are two external gluon fields. [Use has been made of the fact that, the renormalization of $O_{\mu\nu\rho\sigma}(x + z\hat{\tau}, x)$ is x-independent due to translational invariance.]

In general, the nonlocal gluon operators may undergo mixing under renormalization. Their mixing pattern could be determined by the symmetries of the theory, as we explore in the next section. Consequently, we define the renormalization mixing matrix Z, which relates the bare operators to their renormalized counterparts, as follows:

$$O^R_{(i)} = \sum_j \left(Z^{-1}\right)_{ij} O_{(j)} \tag{8.7}$$

Here, we use i and j as generic indices, to list operators within a mixing set. Note that all renormalization factors depend on the regularization X (where X = DR [dimensional regularization], LR [lattice regularization] etc.) and on the renormalization scheme Y (where $Y = \overline{\text{MS}}$, RI′, etc.), and should thus be properly represented as $Z^{X,Y}$ unless it is clear from the context.

The corresponding renormalized amputated Green's functions are expressed as:

$$\Lambda^R_{O_{(i)}} = Z_A \sum_j \left(Z^{-1}\right)_{ij} \Lambda_{O_{(j)}}\,, \qquad A^R_\mu = Z_A^{-1/2} A_\mu \tag{8.8}$$

where A_μ (A^R_μ) is the bare (renormalized) gluon field. The perturbative expansions of the operators' renormalization matrix Z and the gluon field renormalization factor Z_A are given by:

$$Z_{ij} = \delta_{ij} + g^2 z_{ij} + \mathcal{O}\left(g^4\right)\,, \qquad Z_A = 1 + g^2 z_A + \mathcal{O}\left(g^4\right) \tag{8.9}$$

To determine the mixing matrix elements z_{ij} on the lattice, we perform calculations in the $\overline{\text{MS}}$ scheme employing both dimensional and lattice regularization. Subsequent to the computation of the $\overline{\text{MS}}$ renormalized Green's functions in DR, the process of extracting $z^{LR,\overline{\text{MS}}}_{ij}$ follows from the requirement that the renormalized Green's functions be independent of the regularization:

$$\Lambda^{\text{DR},\overline{\text{MS}}}_{O_{(i)}} = \left.\Lambda^{\text{LR},\overline{\text{MS}}}_{O_{(i)}}\right|_{a\to 0} \tag{8.10}$$

Here, $\Lambda_{O_{(i)}}^{\mathrm{DR},\overline{\mathrm{MS}}}$ ($\Lambda_{O_{(i)}}^{\mathrm{LR},\overline{\mathrm{MS}}}$) denotes the $\overline{\mathrm{MS}}$ renormalized Green's function of operator $O_{(i)}$, computed in dimensional (lattice) regularization.

After replacing the right-hand side of the above equation with the expressions provided in Eqs. (8.8), and (8.9), we obtain:

$$\Lambda_{O_{(i)}}^{\mathrm{DR},\overline{\mathrm{MS}}} - \Lambda_{O_{(i)}}^{\mathrm{LR}} = g^2 \left(z_A^{\mathrm{LR},\overline{\mathrm{MS}}} - z_{ii}^{\mathrm{LR},\overline{\mathrm{MS}}} \right) \Lambda_{O_{(i)}}^{\mathrm{tree}} - g^2 \sum_{j \neq i} z_{ij}^{\mathrm{LR},\overline{\mathrm{MS}}} \Lambda_{O_{(j)}}^{\mathrm{tree}} + \mathcal{O}\left(g^4\right) \tag{8.11}$$

where $\Lambda_{O_{(i)}}^{\mathrm{LR}}$ denotes the bare Green's function in LR. The Green's functions appearing on the left-hand side of Eq. (8.11) represent the main calculations of this study. In the absence of mixing, the renormalization matrix $Z_{ij}^{\mathrm{LR},\overline{\mathrm{MS}}}$ becomes diagonal ($z_{ij}^{\mathrm{LR},\overline{\mathrm{MS}}} = 0, \quad \text{for } i \neq j$) and thus the operators are multiplicative renormalized.

8.1.3 Conversion factors

Apart from the commonly used $\overline{\mathrm{MS}}$ scheme, typically employed in phenomenological studies, we also adopt the modified regularization-invariant (RI′) scheme (see Subsection 8.2.1.2). Nonperturbative calculations of the renormalization factors cannot be directly performed within the $\overline{\mathrm{MS}}$ scheme since its definition is perturbative. Instead, they can be computed within a suitably defined variant of the RI′ scheme, which is applicable in both nonperturbative and perturbative studies. Then, quantities that are renormalized in the RI′ scheme, calculated in lattice nonperturbatively, can be converted to the $\overline{\mathrm{MS}}$ scheme through appropriate conversion factors between RI′ and $\overline{\mathrm{MS}}$. These conversion factors, denoted as $\mathcal{C}^{\overline{\mathrm{MS}},\mathrm{RI}'}$, can only be determined using perturbation theory and are regularization independent:

$$\mathcal{C}^{\overline{\mathrm{MS}},\mathrm{RI}'} \equiv \left(Z^{\mathrm{LR},\overline{\mathrm{MS}}}\right)^{-1} \left(Z^{\mathrm{LR},\mathrm{RI}'}\right) = \left(Z^{\mathrm{DR},\overline{\mathrm{MS}}}\right)^{-1} \left(Z^{\mathrm{DR},\mathrm{RI}'}\right) \tag{8.12}$$

Hence, the evaluation of $\mathcal{C}^{\overline{\mathrm{MS}},\mathrm{RI}'}$ can be performed in DR, where computations are notably simpler compared to LR. Note that the conversion factors generally depend on the length of the Wilson line and the components of the RI′ renormalization-scale four-vector. It is understood that, in the presence of mixing among n operators, the conversion factor will be an $n \times n$ matrix.

The Green's functions in RI′ can be directly converted to $\overline{\text{MS}}$ through:

$$\Lambda^{\overline{\text{MS}}}_{O_{(i)}} = \frac{Z_A^{\text{LR},\overline{\text{MS}}}}{Z_A^{\text{LR,RI}'}} \sum_j \left[\left(Z^{\text{LR},\overline{\text{MS}}} \right)^{-1} Z^{\text{LR,RI}'} \right]_{ij} \Lambda^{RI'}_{O_{(j)}} = \frac{1}{\mathcal{C}_A^{\overline{\text{MS}},\text{RI}'}} \sum_j \left[\mathcal{C}^{\overline{\text{MS}},\text{RI}'} \right]_{ij} \Lambda^{RI'}_{O_{(j)}} \tag{8.13}$$

where the value of gluon field conversion factor $\mathcal{C}_A^{\overline{\text{MS}},\text{RI}'} \equiv Z_A^{\text{LR,RI}'}/Z_A^{\text{LR},\overline{\text{MS}}} = Z_A^{\text{DR,RI}'}/Z_A^{\text{DR},\overline{\text{MS}}}$ is given by [153]:

$$\mathcal{C}_A^{\overline{\text{MS}},\text{RI}'} = 1 + \frac{g^2}{16\pi^2} \frac{(97 + 18(1-\beta) + 9(1-\beta)^2)\, N_c - 40 N_f}{36} \tag{8.14}$$

where β is the standard gauge parameter: $\beta = 0(1)$ corresponds to the Feynman (Landau) gauge.

In nonperturbative investigations of Green's functions using physical nucleon states through lattice simulations, the normalization of external states is conducted without involving gluon field renormalization Z_A. Consequently, the only required conversion factor in this case is $\mathcal{C}^{\overline{\text{MS}},\text{RI}'}$.

8.2 Perturbative Calculation - Results

In this section, we provide the one-loop results for the $\overline{\text{MS}}$ renormalized Green's functions of the operators, along with the renormalization factors in $\overline{\text{MS}}$ and the conversion factors between the RI′ and $\overline{\text{MS}}$ schemes. Our calculations have been performed in both DR and LR. Due to the very lengthy expressions of the renormalized Green's functions and conversion factors, we include them as Supplemental Material, provided in the form of a *Mathematica* input file named "`Renormalized_Greens_Functions_and_Conversion_Factors.m`". The Feynman diagrams corresponding to the one-loop two-point Green's functions Λ_O of Eq. (8.6) are illustrated in Fig. 8.1. Diagrams 1 and 2 contain two gluon fields stemming from the operator insertion (denoted as a blue-filled rectangle), while diagrams 3 to 6 (7 to 15) contain three (four) gluon fields stemming from the operator, which can be from either side (i.e., emerging from either $F_{\mu\nu}$) or from the center (i.e., originating from the Wilson line) of the operator.

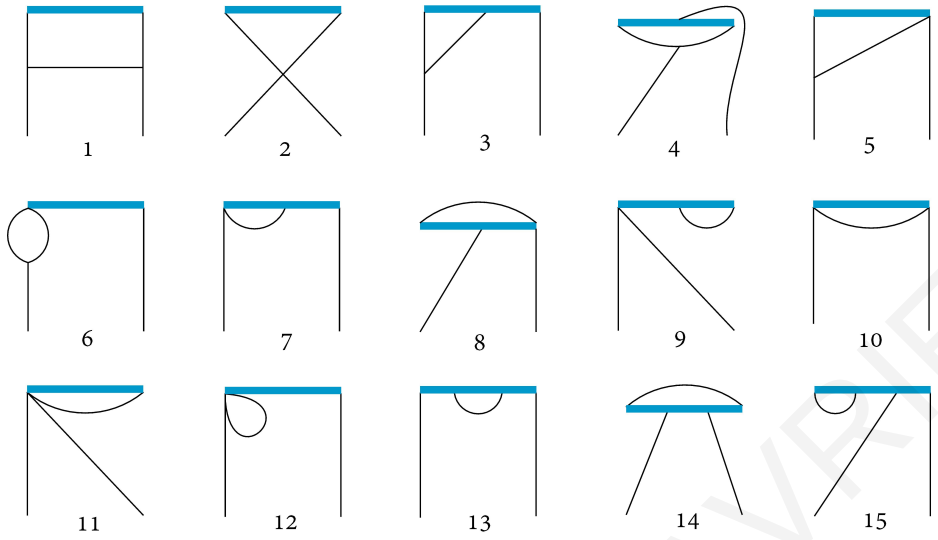

FIGURE 8.1: Feynman diagrams contributing to the one-loop calculation of the Green's functions of the nonlocal operators. Mirror diagrams are not shown, for compactness. Solid lines represent gluons. The operator insertion is denoted by a solid box.

8.2.1 Dimensional Regularization

We first present our results from DR. The computations are performed in D-dimensional Euclidean spacetime, where $D = 4 - 2\epsilon$ and ϵ is the regularization parameter. In contrast to two-point Green's functions involving local operators, the integration results become significantly more complicated due to the presence of both the external momentum q and the length of the Wilson line z in the integrands. Additionally, there is a nontrivial dependence on the preferred direction of the Wilson line, leading to further complexity. We apply new techniques, similar to [154], for handling one-loop tensor integrals with an exponential factor in D dimensions. For the elimination of the poles in ϵ, we adopt the $\overline{\text{MS}}$ scheme.

8.2.1.1 Renormalization Functions

We start by considering the amputated tree-level Green's functions of Eq. (8.6), which read:

$$\begin{aligned}\Lambda^{\text{tree}}_{O_{\mu\nu\rho\sigma}} = \delta^{ab}\big(&+ q_\mu q_\rho\ \delta_{\alpha\nu}\delta_{\beta\sigma}\ e^{-izq_3} + q_\mu q_\rho\ \delta_{\alpha\sigma}\delta_{\beta\nu}\ e^{izq_3} \\ &- q_\nu q_\rho\ \delta_{\alpha\mu}\delta_{\beta\sigma}\ e^{-izq_3} - q_\nu q_\rho\ \delta_{\alpha\sigma}\delta_{\beta\mu}\ e^{izq_3} \\ &- q_\mu q_\sigma\ \delta_{\alpha\nu}\delta_{\beta\rho}\ e^{-izq_3} - q_\mu q_\sigma\ \delta_{\alpha\rho}\delta_{\beta\nu}\ e^{izq_3} \\ &+ q_\nu q_\sigma\ \delta_{\alpha\mu}\delta_{\beta\rho}\ e^{-izq_3} + q_\nu q_\sigma\ \delta_{\alpha\rho}\delta_{\beta\mu}\ e^{izq_3}\big)\end{aligned} \tag{8.15}$$

where z is the length of the Wilson line. Notice that, as expected, the above expression is antisymmetric in $\{\mu,\nu\}$ and $\{\rho,\sigma\}$; also, it is symmetric under $(\mu,\nu)\leftrightarrow(\rho,\sigma)$ and under $(\alpha,\beta,q)\leftrightarrow(\beta,\alpha,-q)$.

Subsequently, we proceed to the 1-loop calculations. In DR, diagrams 11, 12 do not exist. We find that only diagrams 3, 6, and 13, contribute to the $1/\epsilon$ terms, and therefore the renormalization function of the operators in $\overline{\text{MS}}$ is not affected by the remaining diagrams. However, they contribute to the renormalized Green's functions and the conversion factors. Below we present the $\mathcal{O}(1/\epsilon)$ contributions of the perturbative calculation:

$$\Lambda^{\text{1-loop}}_{O_{\mu\nu\rho\sigma}}\Big|_{\mathcal{O}(1/\epsilon)} = \frac{g^2 N_c}{16\epsilon\pi^2}\left(\delta_{\mu 3}+\delta_{\nu 3}+\delta_{\rho 3}+\delta_{\sigma 3}-\frac{1}{2}\beta\right)\Lambda^{\text{tree}}_{O} \tag{8.16}$$

The computation was carried out in an arbitrary covariant gauge, allowing for a direct verification of the gauge invariance of the renormalization factors. It should be noted that, at the one-loop level in DR, the pole terms are proportional to the tree-level values for each one of the operators, indicating no mixing with operators of equal or lower dimension.

The renormalization factor of the gluon field in (DR, $\overline{\text{MS}}$) is given by [153]:

$$Z_A^{\text{DR},\overline{\text{MS}}} = 1+\frac{g^2}{16\epsilon\pi^2}\left(\frac{13N_c}{6}-\frac{N_c}{2}(1-\beta)-\frac{2}{3}N_f\right) \tag{8.17}$$

Using the $\overline{\text{MS}}$ renormalization condition and Eqs. (8.8), (8.16), and (8.17), the renormalization function of the operators turns out to be diagonal, both in the original basis ($O_{\mu\nu\rho\sigma}$) and in the basis of Table 7.2. Its value is:

$$Z_{O_{\mu\nu\rho\sigma}}^{\text{DR},\overline{\text{MS}}} = 1+\frac{g^2}{16\epsilon\pi^2}\left(\left(\frac{5}{3}+\delta_{\mu 3}+\delta_{\nu 3}+\delta_{\rho 3}+\delta_{\sigma 3}\right)N_c-\frac{2}{3}N_f\right) \tag{8.18}$$

[We recall that the cases $\mu=\nu$ and $\rho=\sigma$ give a vanishing operator; thus, it is understood that $\mu\neq\nu$ and $\rho\neq\sigma$ in Eq. (8.18).] We observe that this result depends on the choice of indices for the operators, specifically whether they align with the direction of the Wilson line or not. In the basis of Table 7.2, the diagonal matrix $Z_{ij}^{\text{DR},\overline{\text{MS}}}$ takes the form:

$$Z_{ij}^{\text{DR},\overline{\text{MS}}} = \delta_{ij}\left[1+\frac{g^2}{16\epsilon\pi^2}\left(\left(\frac{5}{3}+\omega_i\right)N_c-\frac{2}{3}N_f\right)\right] \tag{8.19}$$

where ω_i is defined as follows:

$$\omega_i = \begin{cases} 0 & \text{for } i = 2, 4, 6, 8 \\ 1 & \text{for } i = \text{9-16} \\ 2 & \text{for } i = 1, 3, 5, 7 \end{cases} \tag{8.20}$$

At this point, we remind the reader that groups containing multiplets share the same renormalization factor for each component within the multiplet. Note that Eq. 8.19 is compatible with rotational symmetry arguments in the continuum described by Eq. 7.27. Our results agree with previous studies using the auxiliary-field formulation [143, 144, 146].

As expected from gauge invariance in $\overline{\text{MS}}$, the β dependence disappears in the renormalization function of the operators, upon taking into account the gluon field renormalization function. Gauge invariance cannot be ensured in all schemes due to the presence of gauge-dependent renormalized external fields in the Green's functions.

It is worth mentioning that the renormalization function of the operators is independent of the length of the Wilson line (z). There is no dimensionless factor dependent on z that could emerge in the pole part because the leading pole at each loop cannot depend on external momenta or the renormalization scale. Consequently, z independence is expected to persist at all orders in perturbation theory.

8.2.1.2 RI′ renormalization prescription

In a RI′ scheme, there exists significant flexibility in defining normalization conditions in Green's functions, particularly in cases involving operator mixing. These variations only differ by finite terms. Hence, it is convenient to adopt a minimal prescription, containing the smallest possible set of operators prone to mixing, typically consistent with the mixing pattern identified by symmetries. This includes groups {1, 2}, {3, 4}, {5, 6}, {7, 8} of Table 7.2. However, such a scheme must be independent of the regularization method, incorporating any potential additional finite or power-divergent mixing, as encountered, for instance, in lattice regularization.

A practical choice for a RI′-like scheme suitable for nonperturbative studies is to consider four 2×2 mixing matrices, since there are four mixing pairs of operators, alongside eight 1×1 matrices for operators that are multiplicatively renormalizable.

However, renormalization conditions for operator 13 cannot be set, as the bare Green's function under study is zero. To properly select its renormalization conditions, further calculations involving other Green's functions, such as three-point Green's functions, are required. Consequently, we need to impose a total of 23 conditions to identify the elements of these matrices. The proposed renormalization conditions for this variant of the RI' scheme are as follows (where α and β are the Lorentz indices of the external gluons, cf. Eq. 8.6):

$$\left.\frac{\mathrm{Tr}\left[\Lambda^{\mathrm{RI}'}_{O_{(i)}}(\bar{q},z)\right]}{N_c^2-1}\right|_{\substack{\bar{q}_3=\bar{q}_4=0,\\ \alpha=\beta=3}} = \left.\frac{\mathrm{Tr}\left[\Lambda^{\mathrm{tree}}_{O_{(i)}}(\bar{q},z)\right]}{N_c^2-1}\right|_{\substack{\bar{q}_3=\bar{q}_4=0,\\ \alpha=\beta=3}} = \begin{cases} 2\bar{q}^2 & \text{for } i=1 \\ -2\bar{q}^2 & \text{for } i=3 \\ 2\bar{q}_1\bar{q}_2 & \text{for } i=7 \\ 0 & \text{for } i=2,4,8 \end{cases} \tag{8.21}$$

$$\left.\frac{\mathrm{Tr}\left[\Lambda^{\mathrm{RI}'}_{O_{(i)}}(\bar{q},z)\right]}{N_c^2-1}\right|_{\substack{\bar{q}_3=\bar{q}_4=0,\\ \alpha=\beta=4}} = \left.\frac{\mathrm{Tr}\left[\Lambda^{\mathrm{tree}}_{O_{(i)}}(\bar{q},z)\right]}{N_c^2-1}\right|_{\substack{\bar{q}_3=\bar{q}_4=0,\\ \alpha=\beta=4}} = \begin{cases} 2\bar{q}^2 & \text{for } i=2 \\ -2\bar{q}^2 & \text{for } i=4 \\ 2\bar{q}_1\bar{q}_2 & \text{for } i=8 \\ 0 & \text{for } i=1,3,7 \end{cases} \tag{8.22}$$

$$\left.\frac{\mathrm{Tr}\left[\Lambda^{\mathrm{RI}'}_{O_{(i)}}(\bar{q},z)\right]}{N_c^2-1}\right|_{\substack{\bar{q}_1=0,\\ \alpha=1,\beta=3}} = \left.\frac{\mathrm{Tr}\left[\Lambda^{\mathrm{tree}}_{O_{(i)}}(\bar{q},z)\right]}{N_c^2-1}\right|_{\substack{\bar{q}_1=0,\\ \alpha=1,\beta=3}} = \begin{cases} i\sin\left(z\bar{q}_3\right)\bar{q}_2\bar{q}_3 & \text{for } i=5 \\ 0 & \text{for } i=6 \end{cases} \tag{8.23}$$

$$\left.\frac{\mathrm{Tr}\left[\Lambda^{\mathrm{RI}'}_{O_{(i)}}(\bar{q},z)\right]}{N_c^2-1}\right|_{\substack{\bar{q}_1=0,\\ \alpha=1,\beta=4}} = \left.\frac{\mathrm{Tr}\left[\Lambda^{\mathrm{tree}}_{O_{(i)}}(\bar{q},z)\right]}{N_c^2-1}\right|_{\substack{\bar{q}_1=0,\\ \alpha=1,\beta=4}} = \begin{cases} 0 & \text{for } i=5 \\ i\sin\left(z\bar{q}_3\right)\bar{q}_2\bar{q}_4 & \text{for } i=6 \end{cases} \tag{8.24}$$

$$\left.\frac{\mathrm{Tr}\left[\Lambda^{\mathrm{RI}'}_{O_{(i)}}(\bar{q},z)\right]}{N_c^2-1}\right|_{\substack{\bar{q}_3=\bar{q}_4=0,\\ \alpha=1,\beta=3}} = \left.\frac{\mathrm{Tr}\left[\Lambda^{\mathrm{tree}}_{O_{(i)}}(\bar{q},z)\right]}{N_c^2-1}\right|_{\substack{\bar{q}_3=\bar{q}_4=0,\\ \alpha=1,\beta=3}} = \bar{q}_2^2 \qquad \text{for } i=9,11 \tag{8.25}$$

$$\left.\frac{\mathrm{Tr}\left[\Lambda^{\mathrm{RI}'}_{O_{(i)}}(\bar{q},z)\right]}{N_c^2-1}\right|_{\substack{\bar{q}_1=\bar{q}_4=0,\\ \alpha=1,\beta=3}} = \left.\frac{\mathrm{Tr}\left[\Lambda^{\mathrm{tree}}_{O_{(i)}}(\bar{q},z)\right]}{N_c^2-1}\right|_{\substack{\bar{q}_1=\bar{q}_4=0,\\ \alpha=1,\beta=3}} = i\sin\left(z\bar{q}_3\right)\bar{q}_2^2 \qquad \text{for } i=10,12 \tag{8.26}$$

$$\left.\frac{\mathrm{Tr}\left[\Lambda^{\mathrm{RI}'}_{O_{(i)}}(\bar{q},z)\right]}{N_c^2-1}\right|_{\substack{\bar{q}_1=\bar{q}_4=0,\\ \alpha=4,\beta=1}} = \left.\frac{\mathrm{Tr}\left[\Lambda^{\mathrm{tree}}_{O_{(i)}}(\bar{q},z)\right]}{N_c^2-1}\right|_{\substack{\bar{q}_1=\bar{q}_4=0,\\ \alpha=4,\beta=1}} = \begin{cases} 2i\sin\left(z\bar{q}_3\right)\bar{q}_2\bar{q}_3 & \text{for } i=14 \\ i\sin\left(z\bar{q}_3\right)\bar{q}_2\bar{q}_3 & \text{for } i=16 \end{cases} \tag{8.27}$$

$$\left.\frac{\mathrm{Tr}\left[\Lambda^{\mathrm{RI}'}_{O_{(i)}}(\bar{q},z)\right]}{N_c^2-1}\right|_{\substack{\bar{q}_3=\bar{q}_4=0,\\ \alpha=3,\beta=4}} = \left.\frac{\mathrm{Tr}\left[\Lambda^{\mathrm{tree}}_{O_{(i)}}(\bar{q},z)\right]}{N_c^2-1}\right|_{\substack{\bar{q}_3=\bar{q}_4=0,\\ \alpha=3,\beta=4}} = \frac{\bar{q}_1\bar{q}_2}{2} \qquad \text{for } i=15 \tag{8.28}$$

where the momentum of the external gluon fields is represented by q_ν, while the four-vector $\bar{q}_\nu$ denotes the RI' renormalization scale. The trace in the above equations is performed across color space. It is important to note that considering only the magnitude of $\bar{q}$ doesn't fully define the renormalization prescription. Various directions within $\bar{q}$ correspond to distinct renormalization schemes, interconnected through finite renormalization factors. In our proposed conditions, we select certain values for the Lorentz indices α, β and we set specific components of $\bar{q}$ to zero. With this choice, we isolate, in each condition, one of the possible Lorentz structures appearing in the Green's functions $\Lambda_{O(i)}$, in a way as to lead to a solvable system of conditions and to, as much as possible, simpler expressions. Other options can be tested by using our results for the Green's functions provided in the supplemental file.

For 'minus-type' operators (i.e., for mixing pair $\{5,6\}$ and operators 10,12,14, and 16 with multiplicative renormalization) we cannot select $\bar{q}_3 = 0$ (nor $\bar{q}_3 = \frac{\pi}{z}n$, where n is an integer) because $\sin(\bar{q}_3 z)$ which appears in their tree-level expression will vanish, thus making this expression noninvertible.

Note that the RI′ conditions are expressed in terms of amputated Green's functions. Consequently, in order to treat nonperturbative, non-amputated Green's functions, coming from lattice simulations, we must multiply each external gluon by an inverse gluon propagator. Such a propagator is non-invertible in the Landau gauge, which is

typically employed in simulations, however its inverse in the transverse subspace can be constructed in standard fashion, using singular value decomposition.

8.2.1.3 Conversion factors

The $\overline{\text{MS}}$-renormalized Green's functions are the fundamental ingredient for the construction of the conversion factors between $\overline{\text{MS}}$ and RI′ scheme, defined in Eqs. (8.21)–(8.28). These renormalized Green's functions are equal to the finite part of $\Lambda_O^{\text{1-loop}}$ and are complex expressions involving integrals over Bessel functions. By applying the renormalization conditions of the RI′ scheme in Eq. (8.13), one can straightforwardly derive the 2×2 conversion factors for the mixing pairs of operators found in Section 7.2, represented as $\mathcal{C}_{\{i,j\}}^{\overline{\text{MS}},\text{RI}'}$, where i and j denote the two operators belonging to a mixing pair. Due to the very lengthy expressions of the conversion factors, we present below only the explicit results for 'plus-type' operators (i.e., for mixing pairs $\{1,2\}$,$\{3,4\}$,$\{7,8\}$ and multiplicatively renormalizable operators 9, 11, and 15); the expressions are presented for a general gauge-fixing parameter (β) in terms of the quantities $F_1(\bar{q}^2, \bar{q}_3, z)$–$F_9(\bar{q}^2, \bar{q}_3, z)$ where $\bar{q}$ is the 4-vector renormalization scale dictated by the renormalization conditions of RI′ for each operator set. The quantities F_i are integrals of modified Bessel functions of the second kind, K_n, over a Feynman parameter, and are provided in Eqs. (B.1)–(B.9) of Appendix B.

The expressions for the 'minus-type' operators are provided in the supplementary *Mathematica* input file. They involve a double integral of modified Bessel functions, see Appendix B for an example.

Also, it is important to note that the conversion factors depend on the dimensionless quantities $z\overline{q}$ and $\overline{q}/\overline{\mu}$. The RI′ and $\overline{\text{MS}}$ renormalization scales ($\overline{q}$ and $\overline{\mu}$, respectively) have been left arbitrary.

$$\left[\mathcal{C}^{\overline{\text{MS}},\text{RI}'}_{\{1,2\}}\right]_{1,1} = 1 + \frac{g^2 N_c}{16\pi^2}\Bigg[\frac{67}{9} + (\beta+2)\left(2\gamma_E - \log(4) + \log\left(z^2\bar{q}^2\right)\right) + \frac{\beta-4}{2}\log\left(\frac{\bar{q}^2}{\bar{\mu}^2}\right) + \frac{F_2-F_3}{2}(261\beta+40) + (2-69\beta)(F_8-F_9) - \frac{10\text{Nf}}{9\text{Nc}} - \frac{\beta^2}{4} + \frac{F_7}{2}(23\beta-1) + \bar{q}^2|z|^2\frac{7\beta}{2}\left(3(F_3-2F_4+F_5) - (F_2-F_3)\right) + \frac{6}{\bar{q}^2|z|^2}(1-\beta+F_7) + \frac{F_1}{2}(-28\beta-11)\Bigg] \tag{8.29}$$

$$\left[\mathcal{C}^{\overline{\text{MS}},\text{RI}'}_{\{1,2\}}\right]_{1,2} = \frac{g^2 N_c}{16\pi^2}\Bigg[\frac{12}{\bar{q}^2|z|^2}\left((2\beta-1)F_7+1\right) + 4(\beta-2)(F_2-F_3) + 4(5\beta-1)(F_8-F_9) + 4F_1\Bigg] \tag{8.30}$$

$$\left[\mathcal{C}^{\overline{\text{MS}},\text{RI}'}_{\{1,2\}}\right]_{2,1} = \frac{g^2 N_c}{16\pi^2}\Bigg[\frac{37\beta}{2}(F_2-F_3) + \frac{F_7}{2}\left(-\frac{\beta}{2}-5\right) + (-5\beta-2)(F_8-F_9) + \frac{5F_1}{2} + \bar{q}^2|z|^2\frac{\beta}{2}\left(\frac{1}{2}(F_2-F_3) + 5(F_3-2F_4+F_5)\right) + \frac{2}{\bar{q}^2|z|^2}\left((\beta+3)-F_7\right)\Bigg] \tag{8.31}$$

$$\left[\mathcal{C}^{\overline{\text{MS}},\text{RI}'}_{\{1,2\}}\right]_{2,2} = 1 + \frac{g^2 N_c}{16\pi^2}\Bigg[\frac{31}{9} - \frac{\beta^2}{4} + (\beta+2)\left(2\gamma_E - \log(4) + \log\left(z^2\bar{q}^2\right)\right) + \frac{\beta}{2}\log\left(\frac{\bar{q}^2}{\bar{\mu}^2}\right) + (76\beta+14)(F_2-F_3) + (-105\beta-4)\frac{F_8-F_9}{2} - 14\beta F_1 + \frac{3F_7}{4}(13\beta+2) + \bar{q}^2|z|^2\frac{\beta}{2}\left(13(F_3-2F_4+F_5) - 5(F_2-F_3)\right) + \frac{4}{\bar{q}^2|z|^2}(4-\beta-14\beta F_7) - \frac{10\text{Nf}}{9\text{Nc}}\Bigg] \tag{8.32}$$

$$\left[\mathcal{C}^{\overline{\text{MS}},\text{RI}'}_{\{3,4\}}\right]_{1,1} = 1 + \frac{g^2 N_c}{16\pi^2}\Bigg[\frac{67}{9} + (\beta+2)\left(2\gamma_E - \log(4) + \log\left(z^2\bar{q}^2\right)\right) + \frac{\beta-4}{2}\log\left(\frac{\bar{q}^2}{\bar{\mu}^2}\right) - 7(2\beta+1)F_1 + (69\beta+8)\left(F_2 - F_3\right) + \frac{F_7}{4}(49\beta-2) - \frac{\beta^2}{4} + \bar{q}^2|z|^2\frac{7\beta}{2}\left(3\left(F_3 - 2F_4 + F_5\right) - \left(F_2 - F_3\right)\right) - \frac{10\text{Nf}}{9\text{Nc}} + (-99\beta-8)\frac{F_8 - F_9}{2}\Bigg] \tag{8.33}$$

$$\left[\mathcal{C}^{\overline{\text{MS}},\text{RI}'}_{\{3,4\}}\right]_{1,2} = \frac{g^2 N_c}{16\pi^2}\Bigg[2(5\beta-1)\left(F_2 - F_3\right) + 2(1-5\beta)\left(F_8 - F_9\right) - 2F_1\Bigg] \tag{8.34}$$

$$\left[\mathcal{C}^{\overline{\text{MS}},\text{RI}'}_{\{3,4\}}\right]_{2,1} = \frac{g^2 N_c}{16\pi^2}\Bigg[(-43\beta-6)\left(F_2 - F_3\right) + \frac{F_7}{2}(\beta-2) + 4(7\beta+1)\left(F_8 - F_9\right) + F_1 + \bar{q}^2|z|^2\frac{\beta}{2}\left(-\left(F_2 - F_3\right) - 10\left(F_3 - 2F_4 + F_5\right)\right) + \frac{4}{\bar{q}^2|z|^2}\left(F_7 - \beta - 3\right)\Bigg] \tag{8.35}$$

$$\left[\mathcal{C}^{\overline{\text{MS}},\text{RI}'}_{\{3,4\}}\right]_{2,2} = 1 + \frac{g^2 N_c}{16\pi^2}\Bigg[\frac{31}{9} - \frac{\beta^2}{4} + (\beta+2)\left(2\gamma_E - \log(4) + \log\left(z^2\bar{q}^2\right)\right) + \frac{\beta}{2}\log\left(\frac{\bar{q}^2}{\bar{\mu}^2}\right) - 2(7\beta+3)F_1 + (106\beta+8)\left(F_2 - F_3\right) + \frac{3F_7}{4}(13\beta+2) - \frac{10\text{Nf}}{9\text{Nc}} + \bar{q}^2|z|^2\frac{\beta}{2}\left(13\left(F_3 - 2F_4 + F_5\right) - 5\left(F_2 - F_3\right)\right) + \frac{4}{\bar{q}^2|z|^2}\left(1 - \beta - (8\beta+3)F_7\right) + (-105\beta-4)\frac{F_8 - F_9}{2}\Bigg] \tag{8.36}$$

$$\left[\mathcal{C}^{\overline{\text{MS}},\text{RI}'}_{\{7,8\}}\right]_{1,1} = 1 + \frac{g^2 N_c}{16\pi^2}\Bigg[\frac{67}{9} + (\beta+2)\left(2\gamma_E - \log(4) + \log\left(z^2\bar{q}^2\right)\right) + \frac{\beta-4}{2}\log\left(\frac{\bar{q}^2}{\bar{\mu}^2}\right) - 7(2\beta+1)F_1 + (69\beta+8)\left(F_2 - F_3\right) + \frac{F_7}{4}(49\beta-2) + \bar{q}^2|z|^2\frac{7\beta}{2}\left(3\left(F_3 - 2F_4 + F_5\right) - \left(F_2 - F_3\right)\right) + (-99\beta-8)\frac{F_8 - F_9}{2} - \frac{10\text{Nf}}{9\text{Nc}} - \frac{\beta^2}{4}\Bigg] \tag{8.37}$$

$$\left[\mathcal{C}^{\overline{\text{MS}},\text{RI}'}_{\{7,8\}}\right]_{1,2} = \frac{g^2 N_c}{16\pi^2}\Big[2(1-5\beta)\left(F_2 - F_3\right) + 2(5\beta-1)\left(F_8 - F_9\right) + 2F_1\Big] \tag{8.38}$$

$$\left[\mathcal{C}^{\overline{\text{MS}},\text{RI}'}_{\{7,8\}}\right]_{2,1} = \frac{g^2 N_c}{16\pi^2}\Big[2(1-5\beta)\left(F_2 - F_3\right) + 6\beta\left(F_8 - F_9\right) + 2F_1 - 2F_7\Big] \tag{8.39}$$

$$\left[\mathcal{C}^{\overline{\text{MS}},\text{RI}'}_{\{7,8\}}\right]_{2,2} = 1 + \frac{g^2 N_c}{16\pi^2}\Bigg[\frac{31}{9} - \frac{\beta^2}{4} + (\beta+2)\left(2\gamma_E - \log(4) + \log\left(z^2\bar{q}^2\right)\right) + \frac{\beta}{2}\log\left(\frac{\bar{q}^2}{\bar{\mu}^2}\right) + (-14\beta-3)F_1 + (69\beta+8)\left(F_2 - F_3\right) + \frac{F_7}{4}(41\beta+6) + \bar{q}^2|z|^2\frac{\beta}{2}\left(13\left(F_3 - 2F_4 + F_5\right) - 5\left(F_2 - F_3\right)\right) + (-95\beta-4)\frac{F_8 - F_9}{2} - \frac{10\text{Nf}}{9\text{Nc}}\Bigg] \tag{8.40}$$

$$\mathcal{C}_{(9)}^{\overline{\text{MS}},\text{RI}'} = 1 + \frac{g^2 N_c}{16\pi^2}\Bigg[\frac{49}{9} - \frac{\beta^2}{4} + (\beta+2)\left(2\gamma_E - \log(4) + \log\left(z^2\bar{q}^2\right)\right) + \frac{\beta-2}{2}\log\left(\frac{\bar{q}^2}{\bar{\mu}^2}\right) - 2(8\beta+1)F_1 + (125\beta-2)\left(F_2 - F_3\right) + (-153\beta-4)\,\frac{F_8-F_9}{2} + \frac{3F_7}{4}(15\beta+2) + \bar{q}^2|z|^2\frac{\beta}{2}\left(23\left(F_3 - 2F_4 + F_5\right) - 6\left(F_2 - F_3\right)\right) + \frac{\bar{q}^2}{\bar{q}_2^2}\left(2(\beta-2)F_1 + (12-13\beta)\left(F_2-F_3\right) + 21\beta\left(F_8-F_9\right) - \frac{\beta F_7}{2}\right) - \frac{10\text{Nf}}{9\text{Nc}} + \frac{4}{\bar{q}_2^2|z|^2}\left(1-\beta-3F_7\right)\Bigg] \tag{8.41}$$

$$\mathcal{C}_{(11)}^{\overline{\text{MS}},\text{RI}'} = 1 + \frac{g^2 N_c}{16\pi^2}\Bigg[\frac{49}{9} - \frac{\beta^2}{4} + (\beta+2)\left(2\gamma_E - \log(4) + \log\left(z^2\bar{q}^2\right)\right) + \frac{\beta-2}{2}\log\left(\frac{\bar{q}^2}{\bar{\mu}^2}\right) - 7(2\beta+1)F_1 + (79\beta+6)\left(F_2-F_3\right) + \frac{3F_7}{4}(15\beta+2) + \bar{q}^2|z|^2\frac{\beta}{2}\left(23\left(F_3-2F_4+F_5\right) - 6\left(F_2-F_3\right)\right) - \frac{10\text{Nf}}{9\text{Nc}} + (-101\beta-4)\,\frac{F_8-F_9}{2}\Bigg] \tag{8.42}$$

$$\mathcal{C}_{(15)}^{\overline{\text{MS}},\text{RI}'} = 1 + \frac{g^2 N_c}{16\pi^2}\Bigg[\frac{49}{9} - \frac{\beta^2}{4} + (\beta+2)\left(2\gamma_E - \log(4) + \log\left(z^2\bar{q}^2\right)\right) + \frac{\beta-2}{2}\log\left(\frac{\bar{q}^2}{\bar{\mu}^2}\right) + (7\beta+6)\left(F_2-F_3\right) + (45\beta+6)\,\frac{F_7-F_8}{2} + (-17\beta-4)\,\frac{F_8-F_9}{2} - 4F_1 + 144\beta\left(F_2-2F_3+F_4\right) - 84\beta\left(F_8-2F_9+F_{10}\right) + \bar{q}^2|z|^2\frac{\beta}{2}\Big(-12\left(F_2-2F_3+F_4\right) + 35\left(F_3-2F_4+F_5\right) - 24\left(F_4-2F_5+F_6\right)\Big) + (-28\beta-6)\left(F_1-F_2\right) - \frac{10\text{Nf}}{9\text{Nc}}\Bigg] \tag{8.43}$$

Plotting conversion factors for the parameters used in lattice simulations can offer very useful insights and visual representations. To facilitate this, we select specific values of the free parameters that correspond to the $N_f = 2 + 1 + 1$ ensemble of twisted-mass clover-improved fermions described in Ref. [139]. In this setup, the $\overline{\text{MS}}$ scale is fixed at $\overline{\mu} = 2$ GeV while the lattice volume is $L^3 \times T$ with $L = 32$ and $T = 64$ (in lattice units). The lattice spacing is $a = 0.0938$ fm, while $g^2 = 3.47625$ and $\beta = 1$ (Landau gauge).

The RI′ scale is defined in lattice units as $a\bar{q} = \left(\frac{2\pi}{L}n_1, \frac{2\pi}{L}n_2, \frac{2\pi}{L}n_3, \frac{2\pi}{T}\left(n_4 + \frac{1}{2}\right)\right)$, where n_i are integers. For the momentum scales, we choose isotropic spatial directions ($n_1 = n_2 = n_3$) when possible and introduce a nonzero twist of $1/2$ in the temporal component. This choice aligns with the antiperiodic boundary conditions applied to the fermion fields in the temporal direction. Additionally, we rescale the length of the Wilson line with the lattice spacing, denoted as z/a.

Depending on the choice of $\bar{q}$ the numerical values of the conversion factors can be excessively large. It is thus important to tune the values of $\bar{q}$ accordingly. Similarly to the continuum, most appropriate choices of values for $\bar{q}_3$ on the lattice will be: $\bar{q}_3 = \frac{2\pi}{aL}n_3$, where n_3 is an odd integer: these choices guarantee that tree-level Green's functions will be invertible for all integer values of z/a in the range $1 \leq z/a < L/2$.

As an example, we apply the following values for the plus-type operators: $n_1 = n_2 = 3$, $n_3 = 0$, and $n_4 = -1/2$. The conversion matrix elements for pair $\{7, 8\}$ are shown in Fig. 8.2; the other plus-type mixing pairs, i.e., $\{1, 2\}$ and $\{3, 4\}$, have similar qualitative behavior. The plus-type operators undergoing multiplicative renormalization (9,11, and 15) exhibit a similar graphical representation as demonstrated, for example, in Fig. 8.3, for operator 15.

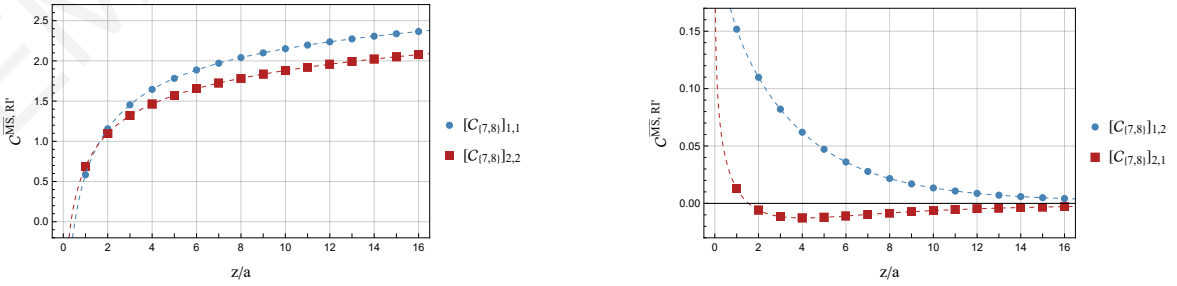

(A) Diagonal elements. (B) Nondiagonal elements.

FIGURE 8.2: Elements of $\mathcal{C}^{\overline{\text{MS}},\text{RI}'}_{\{7,8\}}$ conversion matrix as a function of z/a.

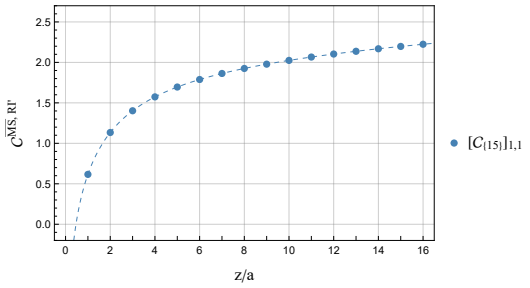

FIGURE 8.3: Conversion factor $\mathcal{C}^{\overline{\text{MS}},\text{RI}'}_{\{15\}}$ as a function of z/a

Furthermore, in Fig.8.4, the conversion matrix elements for the pair $\{5,6\}$ of minus-type operators are presented, where the values $n_2 = n_3 = 3$, $n_1 = 0$, and $n_4 = 5$ are employed. For the remaining minus-type operators, we have selected $n_1 = n_2 = 0$, $n_3 = 3$, and $n_4 = 5$; a representative plot is given in Fig.8.5 for operator 16. The rest of the multiplicatively renormalizable minus-type operators (10,12, and 14) follow the same format as operator 16.

The plots of Figs. 8.2–8.5 show the real part of the conversion factors as a function of z/a. They highlight data points at integer values of z/a ranging from 1 to $L/2 = 16$, while dashed lines connecting these points display the conversion factors for arbitrary noninteger values of z/a. The value at $z/a = 0$ has been excluded from the analysis; indeed, a singular behavior is expected at $z = 0$, where the nonlocal operator collapses to a local composite operator with additional contact singularities. The imaginary part of plus-type operators is strictly zero given our choice of renormalization conditions. For minus-type operators the imaginary part is negligible, having a magnitude less than 10^{-5}. In these plots, we include all possible positive values of z up to half the lattice size, focusing only on the positive directions of the Wilson line. By definition of the plus-type and minus-type operators and the selected RI′ renormalization conditions, the conversion factors are symmetric with respect to $z = 0$, and therefore, negative values of z are not shown in the plots.

We note here the divergent behavior shown in the plots of 'minus-type' operators (Figs. 8.4 and 8.5) for noninteger values of z/a; this is due to the unavoidable factor of $sin(z\bar{q}_3)$ in their tree-level expressions (cf. Eqs. (8.23, 8.24, 8.26, 8.27), which renders these expressions non-invertible for some noninteger z/a). Of course, z/a is necessarily an integer in the lattice definition of the operators, making these divergences inconsequential; however, this behavior points out the necessity for a

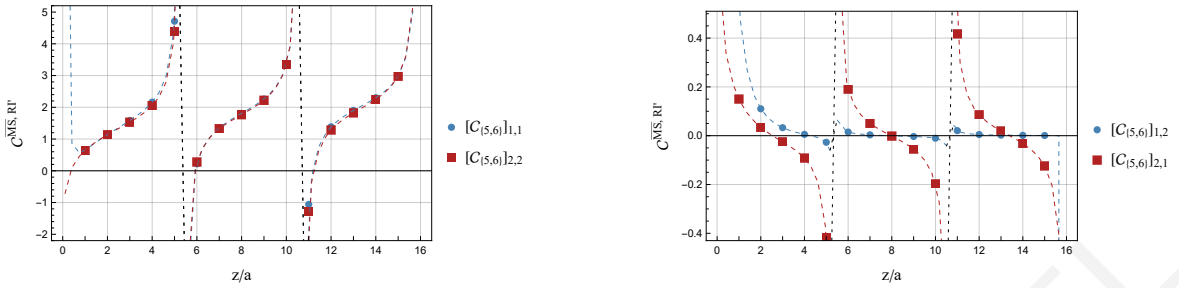

(A) Diagonal elements. (B) Nondiagonal elements.

FIGURE 8.4: Elements of $\mathcal{C}^{\overline{\text{MS}},\text{RI}'}_{\{5,6\}}$ conversion matrix as a function of z/a.

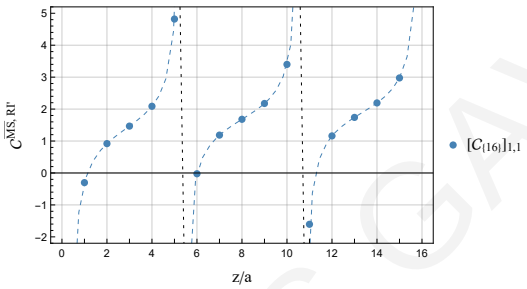

FIGURE 8.5: Conversion factor $\mathcal{C}^{\overline{\text{MS}},\text{RI}'}_{\{16\}}$ as a function of z/a

judicious choice of the renormalization 4-vector scale $\bar{q}$, as mentioned above, so that no divergences will occur at integer values of z/a.

8.2.2 Lattice Regularization

We now focus on computing the bare Green's functions, as given by Eq. (8.6), using lattice regularization. The tree-level Green's functions yield the same result as in dimensional regularization, shown in Eq. (8.15).

The 1-loop computation is considerably more complicated than in dimensional regularization due to the subtleties involved in extracting divergences from lattice integrals. To begin, we write the lattice expressions in the form of a sum of continuum integrals plus additional lattice corrections. Noteworthy, these additional terms, although they have a simple quadratic dependence on the external momentum q, are expected to have a nontrivial dependence on z as seen in nonlocal fermion operators [141].

Several diagrams (1, 2, 4, 5, 8, 10, and 14), as seen in Fig. 8.1, give precisely the same contributions as in DR. This aligns with expectations, considering that these

contributions are finite as $\epsilon \to 0$. Consequently, the limit $a \to 0$ can be applied right from the beginning, without inducing any lattice corrections. However, we must ensure that we eliminate the overall factor of $1/a^2$, attributed to the presence of the external gluons in the Green's functions, by extracting two powers of the external momentum, (aq).

As an example of the ensuing expressions, we present the one-loop lattice result for diagram 13, which is particularly simple, but includes all types of divergences found in our calculations:

$$\Lambda^{\mathrm{d13}}_{O_{\mu\nu\rho\sigma}} = \frac{g^2 N_c}{16\pi^2}\left(c_1 + c_2\,\beta - c_3\frac{|z|}{a} + 8\log\frac{|z|}{a}\,(2+\beta)\right)\Lambda^{\mathrm{tree}}_{O_{\mu\nu\rho\sigma}} \tag{8.44}$$

where $c_1 = 32.24812(2)$, $c_2 = 14.24059(4)$, and $c_3 = 79.81936(8)$. Note here the presence of both linear divergence and logarithmic divergence in a, features revealed in the nonlocal fermion operators as well. Other diagrams typically have more complicated tensorial structures than the tree level, and also contain a very complex dependence on the momenta of the Green's function, in terms of the integrals over Bessel functions shown in Appendix B. The complete expression for $\Lambda^{\overline{\mathrm{MS}}}$ can be found in the supplemental file.

The difference between the bare lattice Green's functions and the $\overline{\mathrm{MS}}$-renormalized ones, calculated up to one loop, is as follows:

$$\Lambda^{\mathrm{DR},\overline{\mathrm{MS}}}_{O_{\mu\nu\rho\sigma}} - \Lambda^{\mathrm{LR}}_{O_{\mu\nu\rho\sigma}} = \frac{g^2}{16\pi^2}\Bigg\{-\frac{4\pi^2}{N_c} + N_c\Bigg[\left(\alpha_1 + \log(a^2\bar{\mu}^2)\right)(\delta_{\mu 3}+\delta_{\nu 3}+\delta_{\rho 3}+\delta_{\sigma 3}) + \alpha_2 + \alpha_3\beta + \alpha_4\frac{|z|}{a} - \frac{\beta}{2}\log(a^2\bar{\mu}^2)\Bigg]\Bigg\}\Lambda^{\mathrm{tree}}_{O_{\mu\nu\rho\sigma}} \tag{8.45}$$

where $\alpha_1 = -8.37940$, $\alpha_2 = 36.04994$, $\alpha_3 = 1.38629$, and $\alpha_4 = 19.95484$. Despite the extremely complicated momentum dependence and the complex tensorial structure of both the $\overline{\mathrm{MS}}$ and the bare lattice Green's functions, their difference (Eq. 8.45) is proportional to the tree-level Green's function, indicating multiplicative renormalization without mixing in $\overline{\mathrm{MS}}$; the proportionality factor is momentum-independent, as expected. Note that the coefficient α_4 in front of the linear divergence has the same value with the corresponding divergent term in the quark nonlocal operators of an arbitrary Wilson line's shape [155]. This is a

consequence of the fact that linear divergence arises only from Wilson-line self-energy. As expected, the linear divergent term depends on the length of the Wilson lines and logarithmic divergences arise from the endpoints and contact points of the Wilson lines.

Using the above equation together with Eq. (8.11) one can extract the multiplicative renormalization and mixing coefficients in LR using the $\overline{\text{MS}}$-scheme. The value found for the of coefficient α_3 was expected, since all gauge dependence must disappear in the $\overline{\text{MS}}$ scheme for gauge-invariant operators: Indeed, this term will cancel against a similar term in $Z_A^{\text{LR},\overline{\text{MS}}}$ in Eq. (8.46). For clover-improved Wilson fermions the latter has the value [153]:

$$Z_A^{\text{LR},\overline{\text{MS}}} = 1 + \frac{g^2}{16\pi^2}\Bigg\{ -\frac{2\pi^2}{N_c} + N_f\left(e_1^A + e_2^A c_{SW} + e_3^A c_{SW}^2\right) + N_c\left(e_4^A + e_5^A\beta\right) + \left[\left(-\frac{5}{3} - \frac{\beta}{2}\right)N_c + \frac{2N_f}{3}\right]\log(a^2\bar{\mu}^2)\Bigg\}$$

where $e_1^A = -1.05739$, $e_2^A = 0.79694$, $e_3^A = -4.71269$, $e_4^A = 18.2349$, $e_5^A = 1.38629$, and c_{SW} is the standard clover coefficient [66].

At the one-loop level, the renormalization factors of the operators are found to be diagonal, in both original basis ($O_{\mu\nu\rho\sigma}$) and basis shown in Table 7.2, as observed in the case of DR. This implies that in the lattice theory at the 1-loop level, the nonlocal gluon operators under investigation are multiplicatively renormalized. By using Eq. 8.11, one can derive:

$$Z_{O_{\mu\nu\rho\sigma}}^{\text{LR},\overline{\text{MS}}} = 1 + \frac{g^2}{16\pi^2}\Bigg\{\frac{2\pi^2}{N_c} + N_f\left(e_1 + e_2\, c_{SW} + e_3\, c_{SW}^2 + \frac{2}{3}\log(a^2\bar{\mu}^2)\right) + N_c\left[e_4 + e_5\frac{|z|}{a} - \frac{5}{3}\log(a^2\bar{\mu}^2) - \left(e_6 + \log(a^2\bar{\mu}^2)\right)\left(\delta_{\mu 3} + \delta_{\nu 3} + \delta_{\rho 3} + \delta_{\sigma 3}\right)\right]\Bigg\}$$

where $e_1 = e_1^A = -1.05739$, $e_2 = e_2^A = 0.79694$, $e_3 = e_3^A = -4.71269$, $e_4 = -17.81504$, $e_5 = -\alpha_4 = -19.95484$, and $e_6 = \alpha_1 = -8.37940$. It is worth mentioning that the presence of c_{SW} in $Z_{O_{\mu\nu\rho\sigma}}^{\text{LR},\overline{\text{MS}}}$ is inherited from $Z_A^{\text{LR},\overline{\text{MS}}}$. As expected, $Z_{O_{\mu\nu\rho\sigma}}^{\text{LR},\overline{\text{MS}}}$ is gauge independent, and the cancellation of the gauge dependence was numerically confirmed up to $\mathcal{O}(10^{-5})$. This gives an estimate of the accuracy of the numerical loop integration.

Similarly to Eq. 8.19, in the basis of Table 7.2, the matrix $Z_{ij}^{\mathrm{LR},\overline{\mathrm{MS}}}$ takes the following diagonal form:

$$Z_{ij}^{\mathrm{LR},\overline{\mathrm{MS}}} = \delta_{ij}\Bigg[1 + \frac{g^2}{16\pi^2}\Bigg\{\frac{2\pi^2}{N_c} + N_f\left(e_1 + e_2\, c_{SW} + e_3\, c_{SW}^2 + \frac{2}{3}\log(a^2\bar{\mu}^2)\right) + N_c\left(e_4 + e_5\frac{|z|}{a} - \frac{5}{3}\log(a^2\bar{\mu}^2) - \big(e_6 + \log(a^2\bar{\mu}^2)\big)\,\omega_i\right)\Bigg\}\Bigg] \tag{8.46}$$

where ω_i is defined by Eq. 8.20.

Even though the one-loop lattice calculation shows a multiplicative renormalization for all the gluon nonlocal operators under study, we expect that mixing among pairs of operators, as dictated by the symmetries of QCD, will be revealed at higher orders. The absence of mixing at one loop, found in our calculation, provides a valuable input to the nonperturbative studies regarding the size of mixing contributions expected to arise in lattice simulations: Although a multiplicatively renormalizable operator is a better candidate to explore the hadron matrix elements of gluon PDFs, in practice, other operators, which can mix only at higher orders of perturbation theory, can be possible alternatives, if their mixing contributions are small enough compared to statistical errors, and thus, negligible.

Chapter 9

Conclusions

In this dissertation, we have performed a series of perturbative calculations using lattice perturbation theory. We have examined the discretization errors affecting the QCD running coupling in relation to the fermion mass, as well as the renormalization of gluon nonlocal operators. We summarize below our findings from these calculations and outline several paths for extending our work in the future.

In Chapter 5, we have presented the one-loop result of the fermion contributions of the two-point Green's functions of background gluon field using lattice perturbation theory. This calculation incorporates a finite fermion mass and respects the $\mathcal{O}(a)$ improvement. We have calculated the renormalization factor, Z_g, which relates the bare running coupling g_0 to the $\overline{\text{MS}}$-renormalized running coupling g. By employing the background field method we have found the discretization errors associated with the finite fermion mass. We have extracted the coefficient $b_g^{(1)}$ of the perturbative expansion of the reparameterized running coupling. We observed that the one-loop results are independent of the stout-smearing coefficient. The process of computing two-loop Feynman diagrams with a fermion propagator that contributes to the two-point Green's functions of the background field is at its final stage: all calculations are finished and consistency controls are being performed. The outcomes of these computations can be valuable for nonperturbative studies concerning the precision determination of the strong coupling constant. Specifically, our findings will assist research groups employing the decoupling method in eliminating uncertainties of $\mathcal{O}(am)$ introduced by truncating the perturbative results of $b_g(g_0^2)$.

In Chapter 8, we have studied the renormalization of the gluon nonlocal operators. By analyzing the symmetry properties of these operators, we have identified their mixing pattern under renormalization; some undergo mixing into pairs ($\{1,\ 2\}$, $\{3,\ 4\}$, $\{5,\ 6\}$, $\{7,\ 8\}$ for notation, see Table 7.2), while others are multiplicatively renormalizable (9-16). We have computed the two-point bare Green's functions of gluon nonlocal operators using both dimensional and lattice regularization methods. We have evaluated the renormalization factors in the $\overline{\text{MS}}$ scheme. At the one-loop level, the renormalization factors for the operators were found to be diagonal, both in the continuum and on the lattice. This suggests that in lattice theory, at the 1-loop level, the nonlocal gluon operators undergo multiplicative renormalization. This observation aligns with the pattern revealed by symmetry arguments, where mixing may occur between certain operators but not necessarily at all orders of perturbation theory. Additionally, we determined the conversion factors of these operators between the RI' and $\overline{\text{MS}}$ renormalization schemes. The RI' scheme was defined to be compatible with the mixing pattern of the operators and be practical for nonperturbative studies. The outcomes of this study are essential for exploring potential paths for investigating gluon PDFs through lattice QCD. Furthermore, it contributes valuable insights into the renormalization of general gluon nonlocal operators on the lattice, thereby facilitating the development of nonperturbative renormalization prescriptions.

Expanding on our calculations presented in Chapter 5, our next step involves conducting a comprehensive two-loop calculation including all Feynman diagrams contributing to the background field propagator. This will enable us to determine the three-loop beta function of the strong coupling constant using the clover and Symanzik improved actions. Another aspect we intend to incorporate into our analysis is the inclusion of stout smearing on gluon links, with a focus on finding its effects on two-loop calculations. Additionally, we plan to undertake a thorough one-loop evaluation of lattice artifacts proportional to the fermion mass at higher orders of lattice spacing, specifically of order $\mathcal{O}(a^2m^2)$.

Simultaneously, we intend to delve deeper into the realm of gluon nonlocal operators, as explored in Chapter 8. There is a number of possible extensions to this work. One particular direction is the study of higher-order effects beyond the one-loop level. Another extension regards using a number of improved lattice actions and investigating their effect on the renormalization factors. Further, the calculation of additional Green's functions and use of variant renormalization schemes will allow for

alternative ways of renormalizing the nonlocal operators, enabling stringent cross-checks when converting to $\overline{\rm MS}$; one possible variant scheme is a coordinate-space Gauge Invariant Renormalization scheme [156]. This broader investigation can provide a tight control of sources of systematic error, which is essential for nonperturbative studies.

Appendix A

Character Table of Octahedral point group

Table A.1 provides a comprehensive overview of the representations of the rotational octahedral point group. Each row corresponds to an irreducible representation, while the columns denote the classes of symmetry operations, including the identity operation (E) and rotations (C_n) along different axes. For our purposes it is sufficient to focus on classes C_2 representing 180° rotations about each of the 3 axes perpendicular to the Wilson line and C_4 representing 90° rotations about these axes.

	E	$8C_3$	$3C_2 = 3C_4^2$	$6C_2'$	$6C_4$
A_1	1	1	1	1	1
A_2	1	1	1	-1	-1
E	2	-1	2	0	0
T_1	3	0	-1	-1	1
T_2	3	0	-1	1	-1

TABLE A.1: Character table of the rotational octahedral point group.

Appendix B

Definition of Feynman parameter Integrals

In this appendix we provide a list of Feynman parameter integrals, featured in the expressions of the conversion factors, which lack a closed analytical form. Notably, all the integrals discussed in this context are convergent and their numerical calculation is straightforward.

These integrals depend on both the external momentum 4-vector q_ν and the length of the Wilson line, z. Within the integrands, we encounter modified Bessel functions of the second kind, denoted as K_0 and K_1. To simplify notation, we introduce the parameter $s \equiv \sqrt{q^2(1-x)x}$. All integrals are dimensionless by definition.

$$F_1(q^2, q_3, z) = \int_0^1 dx\, e^{-iq_3xz}\, K_0(s|z|) \tag{B.1}$$

$$F_2(q^2, q_3, z) = \int_0^1 dx\, e^{-iq_3xz}\, K_0(s|z|)\, x \tag{B.2}$$

$$F_3(q^2, q_3, z) = \int_0^1 dx\, e^{-iq_3xz}\, K_0(s|z|)\, x^2 \tag{B.3}$$

$$F_4(q^2, q_3, z) = \int_0^1 dx\, e^{-iq_3xz}\, K_0(s|z|)\, x^3 \tag{B.4}$$

$$F_5(q^2, q_3, z) = \int_0^1 dx\, e^{-iq_3xz}\, K_0(s|z|)\, x^4 \tag{B.5}$$

$$F_6(q^2, q_3, z) = \int_0^1 dx\, e^{-iq_3xz}\, K_0(s|z|)\, x^5 \tag{B.6}$$

$$F_7(q^2, q_3, z) = \int_0^1 dx\, e^{-iq_3xz}\, K_1(s|z|)\, s|z| \tag{B.7}$$

$$F_8(q^2, q_3, z) = \int_0^1 dx\, e^{-iq_3xz}\, K_1(s|z|)\, s|z|\, x \tag{B.8}$$

$$F_9(q^2, q_3, z) = \int_0^1 dx\, e^{-iq_3xz}\, K_1(s|z|)\, s|z|\, x^2 \tag{B.9}$$

For 'minus-type' operators there appear also double integrals of modified Bessel functions over both x and the parameter ζ; an example is provided below:

$$\int_0^1 dx \int_0^z d\zeta\, e^{-iq_3x\zeta}\, K_0(s|\zeta|)\, \frac{1}{|z|}$$

References

[1] D. d'Enterria, et al., The strong coupling constant: State of the art and the decade ahead, arXiv e-prints (3 2022). arXiv:2203.08271.

[2] K. G. Wilson, Confinement of Quarks, Phys. Rev. D 10 (1974) 2445–2459. doi:10.1103/PhysRevD.10.2445.

[3] R. L. Workman, et al., Review of Particle Physics, PTEP 2022 (2022) 083C01. doi:10.1093/ptep/ptac097.

[4] H. B. Nielsen, M. Ninomiya, Absence of Neutrinos on a Lattice. 1. Proof by Homotopy Theory, Nucl. Phys. B 185 (1981) 20, [Erratum: Nucl.Phys.B 195, 541 (1982)]. doi:10.1016/0550-3213(82)90011-6.

[5] B. Sheikholeslami, R. Wohlert, Improved continuum limit lattice action for qcd with wilson fermions, Nuclear Physics B 259 (4) (1985) 572–596. doi:https://doi.org/10.1016/0550-3213(85)90002-1.
URL https://www.sciencedirect.com/science/article/pii/0550321385900021

[6] J. B. Kogut, L. Susskind, Hamiltonian Formulation of Wilson's Lattice Gauge Theories, Phys. Rev. D 11 (1975) 395–408. doi:10.1103/PhysRevD.11.395.

[7] H. Neuberger, More about exactly massless quarks on the lattice, Phys. Lett. B 427 (1998) 353–355. arXiv:hep-lat/9801031, doi:10.1016/S0370-2693(98)00355-4.

[8] H. Neuberger, Exact chiral symmetry on the lattice, Ann. Rev. Nucl. Part. Sci. 51 (2001) 23–52. arXiv:hep-lat/0101006, doi:10.1146/annurev.nucl.51.101701.132438.

[9] R. Narayanan, H. Neuberger, Chiral fermions on the lattice, Phys. Rev. Lett. 71 (20) (1993) 3251. arXiv:hep-lat/9308011, doi:10.1103/PhysRevLett.71.3251.

[10] V. Furman, Y. Shamir, Axial symmetries in lattice QCD with Kaplan fermions, Nucl. Phys. B 439 (1995) 54–78. arXiv:hep-lat/9405004, doi:10.1016/0550-3213(95)00031-M.

[11] D. B. Kaplan, A Method for simulating chiral fermions on the lattice, Phys. Lett. B 288 (1992) 342–347. arXiv:hep-lat/9206013, doi:10.1016/0370-2693(92)91112-M.

[12] R. Frezzotti, P. A. Grassi, S. Sint, P. Weisz, Lattice QCD with a chirally twisted mass term, JHEP 08 (2001) 058. arXiv:hep-lat/0101001, doi:10.1088/1126-6708/2001/08/058.

[13] R. Frezzotti, G. C. Rossi, Chirally improving Wilson fermions. 1. O(a) improvement, JHEP 08 (2004) 007. arXiv:hep-lat/0306014, doi:10.1088/1126-6708/2004/08/007.

[14] R. Frezzotti, G. C. Rossi, Twisted mass lattice QCD with mass nondegenerate quarks, Nucl. Phys. B Proc. Suppl. 128 (2004) 193–202. arXiv:hep-lat/0311008, doi:10.1016/S0920-5632(03)02477-0.

[15] R. Frezzotti, G. C. Rossi, Chirally improving Wilson fermions, Nucl. Phys. B Proc. Suppl. 129 (2004) 880–882. arXiv:hep-lat/0309157, doi:10.1016/S0920-5632(03)02741-5.

[16] M. Luscher, Exact chiral symmetry on the lattice and the Ginsparg-Wilson relation, Phys. Lett. B 428 (1998) 342–345. arXiv:hep-lat/9802011, doi:10.1016/S0370-2693(98)00423-7.

[17] C. Morningstar, M. J. Peardon, Analytic smearing of SU(3) link variables in lattice QCD, Phys. Rev. D 69 (2004) 054501. arXiv:hep-lat/0311018, doi:10.1103/PhysRevD.69.054501.

[18] R. Horsley, H. Perlt, P. E. L. Rakow, G. Schierholz, A. Schiller, Perturbative determination of c(SW) for plaquette and Symanzik gauge action and stout link clover fermions, Phys. Rev. D 78 (2008) 054504. arXiv:0807.0345, doi:10.1103/PhysRevD.78.054504.

[19] A. Hasenfratz, F. Knechtli, Flavor symmetry and the static potential with hypercubic blocking, Phys. Rev. D 64 (2001) 034504. arXiv:hep-lat/0103029, doi:10.1103/PhysRevD.64.034504.

[20] S. Capitani, S. Durr, C. Hoelbling, Rationale for UV-filtered clover fermions, JHEP 11 (2006) 028. arXiv:hep-lat/0607006, doi:10.1088/1126-6708/2006/11/028.

[21] G. P. Lepage, Flavor symmetry restoration and Symanzik improvement for staggered quarks, Phys. Rev. D 59 (1999) 074502. arXiv:hep-lat/9809157, doi:10.1103/PhysRevD.59.074502.

[22] E. Follana, Q. Mason, C. Davies, K. Hornbostel, G. P. Lepage, J. Shigemitsu, H. Trottier, K. Wong, Highly improved staggered quarks on the lattice, with applications to charm physics, Phys. Rev. D 75 (2007) 054502. arXiv:hep-lat/0610092, doi:10.1103/PhysRevD.75.054502.

[23] K. Symanzik, Continuum Limit and Improved Action in Lattice Theories. 1. Principles and φ^4 Theory, Nucl. Phys. B 226 (1983) 187–204. doi:10.1016/0550-3213(83)90468-6.

[24] M. Luscher, P. Weisz, On-shell improved lattice gauge theories, Commun. Math. Phys. 98 (3) (1985) 433, [Erratum: Commun.Math.Phys. 98, 433 (1985)]. doi:10.1007/BF01205792.

[25] Y. Iwasaki, Renormalization Group Analysis of Lattice Theories and Improved Lattice Action. II. Four-dimensional non-Abelian SU(N) gauge model, arXiv e-prints (12 1983). arXiv:1111.7054.

[26] G. Martinelli, S. Petrarca, C. T. Sachrajda, A. Vladikas, Nonperturbative renormalization of two quark operators with an improved lattice fermion action, Phys. Lett. B 311 (1993) 241–248, [Erratum: Phys.Lett.B 317, 660 (1993)]. doi:10.1016/0370-2693(93)90562-V.

[27] G. Martinelli, C. Pittori, C. T. Sachrajda, M. Testa, A. Vladikas, A General method for nonperturbative renormalization of lattice operators, Nucl. Phys. B 445 (1995) 81–108. arXiv:hep-lat/9411010, doi:10.1016/0550-3213(95)00126-D.

[28] R. L. Workman, Others, Review of Particle Physics, PTEP 2022 (2022) 083C01. doi:10.1093/ptep/ptac097.

[29] P. D. Group, Review of Particle Physics, Progress of Theoretical and Experimental Physics 2020 (8), 083C01 (08 2020). arXiv:https://academic.oup.com/ptep/article-pdf/2020/8/083C01/34673722/ptaa104.pdf, doi:10.1093/ptep/ptaa104.
URL https://doi.org/10.1093/ptep/ptaa104

[30] S. Heinemeyer, S. Jadach, J. Reuter, Theory requirements for SM Higgs and EW precision physics at the FCC-ee, Eur. Phys. J. Plus 136 (9) (2021) 911. arXiv:2106.11802, doi:10.1140/epjp/s13360-021-01875-1.

[31] C. Anastasiou, C. Duhr, F. Dulat, E. Furlan, T. Gehrmann, F. Herzog, A. Lazopoulos, B. Mistlberger, High precision determination of the gluon fusion Higgs boson cross-section at the LHC, JHEP 05 (2016) 058. arXiv:1602.00695, doi:10.1007/JHEP05(2016)058.

[32] A. H. Hoang, What is the Top Quark Mass?, Ann. Rev. Nucl. Part. Sci. 70 (2020) 225–255. arXiv:2004.12915, doi:10.1146/annurev-nucl-101918-023530.

[33] Y. Aoki, et al., FLAG Review 2021, Eur. Phys. J. C 82 (10) (2022) 869. arXiv:2111.09849, doi:10.1140/epjc/s10052-022-10536-1.

[34] M. Dalla Brida, Past, present, and future of precision determinations of the QCD parameters from lattice QCD, Eur. Phys. J. A 57 (2) (2021) 66. arXiv:2012.01232, doi:10.1140/epja/s10050-021-00381-3.

[35] A. Bazavov, N. Brambilla, X. Garcia i Tormo, P. Petreczky, J. Soto, A. Vairo, Determination of α_s from the QCD static energy, Phys. Rev. D 86 (2012) 114031. arXiv:1205.6155, doi:10.1103/PhysRevD.86.114031.

[36] D. Boito, V. Mateu, Precise determination of α_s from relativistic quarkonium sum rules, JHEP 03 (2020) 094. arXiv:2001.11041, doi:10.1007/JHEP03(2020)094.

[37] K. Maltman, D. Leinweber, P. Moran, A. Sternbeck, The Realistic Lattice Determination of alpha(s)(M(Z)) Revisited, Phys. Rev. D 78 (2008) 114504. arXiv:0807.2020, doi:10.1103/PhysRevD.78.114504.

[38] E. Shintani, S. Aoki, H. Fukaya, S. Hashimoto, T. Kaneko, T. Onogi, N. Yamada, Strong coupling constant from vacuum polarization functions in three-flavor lattice QCD with dynamical overlap fermions, Phys. Rev. D 82 (7) (2010) 074505, [Erratum: Phys.Rev.D 89, 099903 (2014)]. arXiv:1002.0371, doi:10.1103/PhysRevD.82.074505.

[39] S. Zafeiropoulos, P. Boucaud, F. De Soto, J. Rodríguez-Quintero, J. Segovia, Strong Running Coupling from the Gauge Sector of Domain Wall Lattice QCD with Physical Quark Masses, Phys. Rev. Lett. 122 (16) (2019) 162002. arXiv:1902.08148, doi:10.1103/PhysRevLett.122.162002.

[40] K. Nakayama, H. Fukaya, S. Hashimoto, Lattice computation of the Dirac eigenvalue density in the perturbative regime of QCD, Phys. Rev. D 98 (1) (2018) 014501. arXiv:1804.06695, doi:10.1103/PhysRevD.98.014501.

[41] J. Komijani, P. Petreczky, J. H. Weber, Strong coupling constant and quark masses from lattice QCD, Prog. Part. Nucl. Phys. 113 (2020) 103788. arXiv:2003.11703, doi:10.1016/j.ppnp.2020.103788.

[42] M. Luscher, P. Weisz, U. Wolff, A Numerical method to compute the running coupling in asymptotically free theories, Nucl. Phys. B 359 (1991) 221–243. doi:10.1016/0550-3213(91)90298-C.

[43] R. Sommer, U. Wolff, Non-perturbative computation of the strong coupling constant on the lattice, Nucl. Part. Phys. Proc. 261-262 (2015) 155–184. arXiv:1501.01861, doi:10.1016/j.nuclphysbps.2015.03.013.

[44] M. Dalla Brida, R. Höllwieser, F. Knechtli, T. Korzec, A. Ramos, R. Sommer, Non-perturbative renormalization by decoupling, Phys. Lett. B 807 (2020) 135571. arXiv:1912.06001, doi:10.1016/j.physletb.2020.135571.

[45] K. G. Wilson, J. Kogut, The renormalization group and the ϵ expansion, Physics Reports 12 (2) (1974) 75–199. doi:https://doi.org/10.1016/0370-1573(74)90023-4.
URL https://www.sciencedirect.com/science/article/pii/0370157374900234

[46] M. E. Peskin, D. V. Schroeder, An Introduction to Quantum Field Theory, Westview Press, 1995, reading, USA: Addison-Wesley (1995) 842 p.

[47] C. G. Callan, Broken scale invariance in scalar field theory, Phys. Rev. D 2 (1970) 1541–1547. doi:10.1103/PhysRevD.2.1541.
URL https://link.aps.org/doi/10.1103/PhysRevD.2.1541

[48] K. Symanzik, Small distance behaviour in field theory and power counting, Communications in Mathematical Physics 18 (3) (1970) 227–246. doi:10.1007/BF01649434.

[49] R. Balian, J. Zinn-Justin, Methods in Field Theory: Les Houches Session XXVIII, Les Houches Summer School Proceedings Series, North-Holland Publishing Company, 1981.
URL https://www.worldscientific.com/doi/abs/10.1142/0004

[50] H. J. Rothe, Lattice Gauge Theories, 4th Edition, WORLD SCIENTIFIC, 2012. arXiv:https://www.worldscientific.com/doi/pdf/10.1142/8229, doi:10.1142/8229.
URL https://www.worldscientific.com/doi/abs/10.1142/8229

[51] B. S. DeWitt, Quantum theory of gravity. ii. the manifestly covariant theory, Phys. Rev. 162 (1967) 1195–1239. doi:10.1103/PhysRev.162.1195.
URL https://link.aps.org/doi/10.1103/PhysRev.162.1195

[52] M. Luscher, P. Weisz, Background field technique and renormalization in lattice gauge theory, Nucl. Phys. B 452 (1995) 213–233. arXiv:hep-lat/9504006, doi:10.1016/0550-3213(95)00346-T.

[53] H. Kluberg-Stern, J. B. Zuber, Renormalization of non-abelian gauge theories in a background-field gauge. i. green's functions, Phys. Rev. D 12 (1975) 482–488. doi:10.1103/PhysRevD.12.482.
URL https://link.aps.org/doi/10.1103/PhysRevD.12.482

[54] R. Ellis, G. Martinelli, Two-loop corrections to the Λ parameters of one-plaquette actions, Nuclear Physics B 235 (1) (1984) 93–114. doi:https://doi.org/10.1016/0550-3213(84)90150-0.
URL https://www.sciencedirect.com/science/article/pii/0550321384901500

[55] A. Z. O.V. Tarasov, A.A. Vladimirov, The gell-mann-low function of QCD in the three-loop approximation, Phys. Lett. B98 (1980) 429.

[56] T. Reisz, Lattice Gauge Theory: Renormalization to All Orders in the Loop Expansion, Nucl. Phys. B 318 (1989) 417–463. doi:10.1016/0550-3213(89)90613-5.

[57] C. Christou, A. Feo, H. Panagopoulos, E. Vicari, The three loop β-function of $SU(N)$ lattice gauge theories with Wilson fermions, Nucl. Phys. B525 (1998) 387–400, [Erratum: Nucl. Phys.B608,479(2001)]. arXiv:[hep-lat/9801007], doi:10.1016/S0550-3213(01)00268-1,10.1016/S0550-3213(98)00248-X.

[58] M. Luscher, P. Weisz, Computation of the relation between the bare lattice coupling and the MS coupling in SU(N) gauge theories to two loops, Nucl. Phys. B 452 (1995) 234–260. arXiv:hep-lat/9505011, doi:10.1016/0550-3213(95)00338-S.

[59] B. Alles, A. Feo, H. Panagopoulos, The Three loop Beta function in SU(N) lattice gauge theories, Nucl. Phys. B491 (1997) 498–512. arXiv:[hep-lat/9609025], doi:10.1016/S0550-3213(97)00092-8.

[60] A. Skouroupathis, H. Panagopoulos, Lambda-parameter of lattice QCD with Symanzik improved gluon actions, Phys. Rev. D76 (2007) 114514. arXiv:[arXiv:0709.3239], doi:10.1103/PhysRevD.76.114514.

[61] A. Bode, H. Panagopoulos, The Three loop beta function of QCD with the clover action, Nucl. Phys. B625 (2002) 198–210. arXiv:[hep-lat/0110211], doi:10.1016/S0550-3213(02)00012-3.

[62] M. Constantinou, H. Panagopoulos, QCD with overlap fermions: Running coupling and the 3-loop beta-function, Phys. Rev. D76 (2007) 114504. arXiv:[arXiv:0709.4368], doi:10.1103/PhysRevD.76.114504.

[63] M. Luscher, S. Sint, R. Sommer, P. Weisz, Chiral symmetry and O(a) improvement in lattice QCD, Nucl. Phys. B 478 (1996) 365–400. arXiv:hep-lat/9605038, doi:10.1016/0550-3213(96)00378-1.

[64] M. Dalla Brida, R. Höllwieser, F. Knechtli, T. Korzec, S. Sint, R. Sommer, Heavy Wilson quarks and O(a) improvement: nonperturbative results for b_g, JHEP 2024 (01) (2024) 188. arXiv:2401.00216, doi:10.1007/JHEP01(2024)188.

[65] B. Sheikholeslami, R. Wohlert, Improved continuum limit lattice action for qcd with wilson fermions, Nuclear Physics B 259 (4) (1985) 572–596. doi:https://doi.org/10.1016/0550-3213(85)90002-1.
URL https://www.sciencedirect.com/science/article/pii/0550321385900021

[66] R. Horsley, H. Perlt, P. E. L. Rakow, G. Schierholz, A. Schiller, One-loop renormalisation of quark bilinears for overlap fermions with improved gauge actions, Nucl. Phys. B 693 (2004) 3–35, [Erratum: Nucl.Phys.B 713, 601–606 (2005)]. arXiv:hep-lat/0404007, doi:10.1016/j.nuclphysb.2005.01.044.

[67] L. F. Abbott, The Background Field Method Beyond One Loop, Nucl. Phys. B 185 (1981) 189–203. doi:10.1016/0550-3213(81)90371-0.

[68] M. Constantinou, H. Panagopoulos, Improved renormalization scheme for nonlocal operators, Phys. Rev. D 107 (1) (2023) 014503. arXiv:2207.09977, doi:10.1103/PhysRevD.107.014503.

[69] S. Sint, R. Sommer, The running coupling from the qcd schrödinger functional: a one-loop analysis, Nuclear Physics B 465 (1) (1996) 71–98. doi:https://doi.org/10.1016/0550-3213(96)00020-X.
URL https://www.sciencedirect.com/science/article/pii/055032139600020X

[70] R. P. Feynman, Very high-energy collisions of hadrons, Phys. Rev. Lett. 23 (1969) 1415–1417. doi:10.1103/PhysRevLett.23.1415.

[71] R. P. Feynman, The behavior of hadron collisions at extreme energies, Conf. Proc. C 690905 (1969) 237–258.

[72] H.-W. Lin, et al., Parton distributions and lattice QCD calculations: a community white paper, Prog. Part. Nucl. Phys. 100 (2018) 107–160. arXiv:1711.07916, doi:10.1016/j.ppnp.2018.01.007.

[73] J. C. Collins, D. E. Soper, G. F. Sterman, Factorization of Hard Processes in QCD, Adv. Ser. Direct. High Energy Phys. 5 (1989) 1–91. arXiv:hep-ph/0409313, doi:10.1142/9789814503266_0001.

[74] V. N. Gribov, L. N. Lipatov, Deep inelastic e p scattering in perturbation theory, Sov. J. Nucl. Phys. 15 (1972) 438–450.

[75] L. N. Lipatov, The parton model and perturbation theory, Yad. Fiz. 20 (1974) 181–198.

[76] G. Altarelli, G. Parisi, Asymptotic Freedom in Parton Language, Nucl. Phys. B 126 (1977) 298–318. doi:10.1016/0550-3213(77)90384-4.

[77] H.-W. Lin, W. Melnitchouk, A. Prokudin, N. Sato, H. Shows, First Monte Carlo Global Analysis of Nucleon Transversity with Lattice QCD Constraints, Phys. Rev. Lett. 120 (15) (2018) 152502. arXiv:1710.09858, doi:10.1103/PhysRevLett.120.152502.

[78] J. J. Ethier, N. Sato, W. Melnitchouk, First simultaneous extraction of spin-dependent parton distributions and fragmentation functions from a global QCD analysis, Phys. Rev. Lett. 119 (13) (2017) 132001. arXiv:1705.05889, doi:10.1103/PhysRevLett.119.132001.

[79] E. R. Nocera, R. D. Ball, S. Forte, G. Ridolfi, J. Rojo, A first unbiased global determination of polarized PDFs and their uncertainties, Nucl. Phys. B 887 (2014) 276–308. arXiv:1406.5539, doi:10.1016/j.nuclphysb.2014.08.008.

[80] D. de Florian, R. Sassot, M. Stratmann, W. Vogelsang, Extraction of Spin-Dependent Parton Densities and Their Uncertainties, Phys. Rev. D 80 (2009) 034030. arXiv:0904.3821, doi:10.1103/PhysRevD.80.034030.

[81] A. Accardi, L. T. Brady, W. Melnitchouk, J. F. Owens, N. Sato, Constraints on large-x parton distributions from new weak boson production and deep-inelastic scattering data, Phys. Rev. D 93 (11) (2016) 114017. arXiv:1602.03154, doi:10.1103/PhysRevD.93.114017.

[82] R. D. Ball, et al., Parton distributions from high-precision collider data, Eur. Phys. J. C 77 (10) (2017) 663. arXiv:1706.00428, doi:10.1140/epjc/s10052-017-5199-5.

[83] S. Alekhin, J. Blümlein, S. Moch, R. Placakyte, Parton distribution functions, α_s, and heavy-quark masses for LHC Run II, Phys. Rev. D 96 (1) (2017) 014011. arXiv:1701.05838, doi:10.1103/PhysRevD.96.014011.

[84] L. V. Gribov, E. M. Levin, M. G. Ryskin, Semihard Processes in QCD, Phys. Rept. 100 (1983) 1–150. doi:10.1016/0370-1573(83)90022-4.

[85] L. D. McLerran, R. Venugopalan, Computing quark and gluon distribution functions for very large nuclei, Phys. Rev. D 49 (1994) 2233–2241. arXiv:hep-ph/9309289, doi:10.1103/PhysRevD.49.2233.

[86] A. H. Mueller, J.-w. Qiu, Gluon Recombination and Shadowing at Small Values of x, Nucl. Phys. B 268 (1986) 427–452. doi:10.1016/0550-3213(86)90164-1.

[87] D. Dolgov, et al., Moments of nucleon light cone quark distributions calculated in full lattice QCD, Phys. Rev. D 66 (2002) 034506. arXiv:hep-lat/0201021, doi:10.1103/PhysRevD.66.034506.

[88] D. Dolgov, et al., Moments of structure functions in full QCD, Nucl. Phys. B Proc. Suppl. 94 (2001) 303–306. arXiv:hep-lat/0011010, doi:10.1016/S0920-5632(01)00943-4.

[89] P. Dreher, et al., Continuum extrapolation of moments of nucleon quark distributions in full QCD, Nucl. Phys. B Proc. Suppl. 119 (2003) 392–394. arXiv:hep-lat/0211021, doi:10.1016/S0920-5632(03)01564-0.

[90] M. Gockeler, R. Horsley, D. Pleiter, P. E. L. Rakow, A. Schafer, G. Schierholz, Calculation of moments of structure functions, Nucl. Phys. B Proc. Suppl. 119 (2003) 32–40. arXiv:hep-lat/0209160, doi:10.1016/S0920-5632(03)01490-7.

[91] K. Cichy, M. Constantinou, A guide to light-cone PDFs from Lattice QCD: an overview of approaches, techniques and results, Adv. High Energy Phys. 2019 (2019) 3036904. arXiv:1811.07248, doi:10.1155/2019/3036904.

[92] X. Ji, Y.-S. Liu, Y. Liu, J.-H. Zhang, Y. Zhao, Large-momentum effective theory, Rev. Mod. Phys. 93 (3) (2021) 035005. arXiv:2004.03543, doi:10.1103/RevModPhys.93.035005.

[93] M. Constantinou, The x-dependence of hadronic parton distributions: A review on the progress of lattice QCD, Eur. Phys. J. A 57 (2) (2021) 77. arXiv:2010.02445, doi:10.1140/epja/s10050-021-00353-7.

[94] K. Cichy, Progress in x-dependent partonic distributions from lattice QCD, PoS LATTICE2021 (2022) 017. arXiv:2110.07440, doi:10.22323/1.396.0017.

[95] K. Cichy, Overview of lattice calculations of the x-dependence of PDFs, GPDs and TMDs, EPJ Web Conf. 258 (2022) 01005. arXiv:2111.04552, doi:10.1051/epjconf/202225801005.

[96] X. Ji, Parton Physics on a Euclidean Lattice, Phys. Rev. Lett. 110 (2013) 262002. arXiv:1305.1539, doi:10.1103/PhysRevLett.110.262002.

[97] X. Ji, Parton Physics from Large-Momentum Effective Field Theory, Sci. China Phys. Mech. Astron. 57 (2014) 1407–1412. arXiv:1404.6680, doi:10.1007/s11433-014-5492-3.

[98] Y.-Q. Ma, J.-W. Qiu, Extracting Parton Distribution Functions from Lattice QCD Calculations, Phys. Rev. D 98 (7) (2018) 074021. arXiv:1404.6860, doi:10.1103/PhysRevD.98.074021.

[99] W. Wang, J.-H. Zhang, S. Zhao, R. Zhu, Complete matching for quasidistribution functions in large momentum effective theory, Phys. Rev. D 100 (7) (2019) 074509. arXiv:1904.00978, doi:10.1103/PhysRevD.100.074509.

[100] W. Wang, S. Zhao, R. Zhu, Gluon quasidistribution function at one loop, Eur. Phys. J. C 78 (2) (2018) 147. arXiv:1708.02458, doi:10.1140/epjc/s10052-018-5617-3.

[101] L.-B. Chen, W. Wang, R. Zhu, Quasi parton distribution functions at NNLO: flavor non-diagonal quark contributions, Phys. Rev. D 102 (1) (2020) 011503. arXiv:2005.13757, doi:10.1103/PhysRevD.102.011503.

[102] Z.-Y. Li, Y.-Q. Ma, J.-W. Qiu, Extraction of Next-to-Next-to-Leading-Order Parton Distribution Functions from Lattice QCD Calculations, Phys. Rev. Lett. 126 (7) (2021) 072001. arXiv:2006.12370, doi:10.1103/PhysRevLett.126.072001.

[103] M. Constantinou, et al., Parton distributions and lattice-QCD calculations: Toward 3D structure, Prog. Part. Nucl. Phys. 121 (2021) 103908. arXiv:2006.08636, doi:10.1016/j.ppnp.2021.103908.

[104] X.-D. Ji, Gauge-Invariant Decomposition of Nucleon Spin, Phys. Rev. Lett. 78 (1997) 610–613. arXiv:hep-ph/9603249, doi:10.1103/PhysRevLett.78.610.

[105] X. Ji, Generalized parton distributions, Ann. Rev. Nucl. Part. Sci. 54 (2004) 413–450. doi:10.1146/annurev.nucl.54.070103.181302.

[106] A. V. Radyushkin, Scaling limit of deeply virtual Compton scattering, Phys. Lett. B 380 (1996) 417–425. arXiv:hep-ph/9604317, doi:10.1016/0370-2693(96)00528-X.

[107] A. V. Belitsky, A. V. Radyushkin, Unraveling hadron structure with generalized parton distributions, Phys. Rept. 418 (2005) 1–387. arXiv:hep-ph/0504030, doi:10.1016/j.physrep.2005.06.002.

[108] M. Diehl, Generalized parton distributions, Phys. Rept. 388 (2003) 41–277. arXiv:hep-ph/0307382, doi:10.1016/j.physrep.2003.08.002.

[109] J. C. Collins, D. E. Soper, Back-To-Back Jets in QCD, Nucl. Phys. B 193 (1981) 381, [Erratum: Nucl.Phys.B 213, 545 (1983)]. doi:10.1016/0550-3213(81)90339-4.

[110] D. Boer, et al., Gluons and the quark sea at high energies: Distributions, polarization, tomography, arXiv e-prints (8 2011). arXiv:1108.1713.

[111] A. Accardi, et al., Electron Ion Collider: The Next QCD Frontier: Understanding the glue that binds us all, Eur. Phys. J. A 52 (9) (2016) 268. arXiv:1212.1701, doi:10.1140/epja/i2016-16268-9.

[112] R. Angeles-Martinez, et al., Transverse Momentum Dependent (TMD) parton distribution functions: status and prospects, Acta Phys. Polon. B 46 (12) (2015) 2501–2534. arXiv:1507.05267, doi:10.5506/APhysPolB.46.2501.

[113] J. Collins, T. C. Rogers, Connecting Different TMD Factorization Formalisms in QCD, Phys. Rev. D 96 (5) (2017) 054011. arXiv:1705.07167, doi:10.1103/PhysRevD.96.054011.

[114] M. Engelhardt, P. Hägler, B. Musch, J. Negele, A. Schäfer, Lattice QCD study of the Boer-Mulders effect in a pion, Phys. Rev. D 93 (5) (2016) 054501. arXiv:1506.07826, doi:10.1103/PhysRevD.93.054501.

[115] M. A. Ebert, S. T. Schindler, I. W. Stewart, Y. Zhao, One-loop Matching for Spin-Dependent Quasi-TMDs, JHEP 09 (2020) 099. arXiv:2004.14831, doi:10.1007/JHEP09(2020)099.

[116] X. Ji, Y. Liu, Y.-S. Liu, Transverse-momentum-dependent parton distribution functions from large-momentum effective theory, Phys. Lett. B 811 (2020) 135946. arXiv:1911.03840, doi:10.1016/j.physletb.2020.135946.

[117] A. A. Vladimirov, A. Schäfer, Transverse momentum dependent factorization for lattice observables, Phys. Rev. D 101 (7) (2020) 074517. arXiv:2002.07527, doi:10.1103/PhysRevD.101.074517.

[118] C. Alexandrou, M. Constantinou, K. Hadjiyiannakou, K. Jansen, C. Kallidonis, G. Koutsou, A. Vaquero Avilés-Casco, C. Wiese, Nucleon Spin and Momentum Decomposition Using Lattice QCD Simulations, Phys. Rev. Lett. 119 (14) (2017) 142002. arXiv:1706.02973, doi:10.1103/PhysRevLett.119.142002.

[119] C. Alexandrou, S. Bacchio, M. Constantinou, J. Finkenrath, K. Hadjiyiannakou, K. Jansen, G. Koutsou, H. Panagopoulos, G. Spanoudes, Complete flavor decomposition of the spin and momentum fraction of the proton using lattice QCD simulations at physical pion mass, Phys. Rev. D 101 (9) (2020) 094513. arXiv:2003.08486, doi:10.1103/PhysRevD.101.094513.

[120] Y.-B. Yang, M. Gong, J. Liang, H.-W. Lin, K.-F. Liu, D. Pefkou, P. Shanahan, Nonperturbatively renormalized glue momentum fraction at the physical pion mass from lattice QCD, Phys. Rev. D 98 (7) (2018) 074506. arXiv:1805.00531, doi:10.1103/PhysRevD.98.074506.

[121] S. Alekhin, J. Blümlein, S. Moch, The abm parton distributions tuned to lhc data, Phys. Rev. D 89 (2014) 054028. doi:10.1103/PhysRevD.89.054028.
URL https://link.aps.org/doi/10.1103/PhysRevD.89.054028

[122] J. Butterworth, et al., PDF4LHC recommendations for LHC Run II, J. Phys. G 43 (2016) 023001. arXiv:1510.03865, doi:10.1088/0954-3899/43/2/023001.

[123] N. Sato, C. Andres, J. J. Ethier, W. Melnitchouk, Strange quark suppression from a simultaneous Monte Carlo analysis of parton distributions and fragmentation functions, Phys. Rev. D 101 (7) (2020) 074020. arXiv:1905.03788, doi:10.1103/PhysRevD.101.074020.

[124] T.-J. Hou, S. Dulat, J. Gao, M. Guzzi, J. Huston, P. Nadolsky, J. Pumplin, C. Schmidt, D. Stump, C. P. Yuan, CTEQ-TEA parton distribution functions and HERA Run I and II combined data, Phys. Rev. D 95 (3) (2017) 034003. arXiv:1609.07968, doi:10.1103/PhysRevD.95.034003.

[125] L. A. Harland-Lang, A. D. Martin, P. Motylinski, R. S. Thorne, Parton distributions in the LHC era: MMHT 2014 PDFs, Eur. Phys. J. C 75 (5) (2015) 204. arXiv:1412.3989, doi:10.1140/epjc/s10052-015-3397-6.

[126] E. Moffat, W. Melnitchouk, T. C. Rogers, N. Sato, Simultaneous monte carlo analysis of parton densities and fragmentation functions, Phys. Rev. D 104 (2021) 016015. doi:10.1103/PhysRevD.104.016015.
URL https://link.aps.org/doi/10.1103/PhysRevD.104.016015

[127] J. C. Collins, Renormalization, Vol. 26 of Cambridge Monographs on Mathematical Physics, Cambridge University Press, Cambridge, 2023. doi:10.1017/9781009401807.

[128] W. Wang, J.-H. Zhang, S. Zhao, R. Zhu, Complete matching for quasidistribution functions in large momentum effective theory, Phys. Rev. D 100 (7) (2019) 074509. arXiv:1904.00978, doi:10.1103/PhysRevD.100.074509.

[129] J.-H. Zhang, X. Ji, A. Schäfer, W. Wang, S. Zhao, Accessing Gluon Parton Distributions in Large Momentum Effective Theory, Phys. Rev. Lett. 122 (14) (2019) 142001. arXiv:1808.10824, doi:10.1103/PhysRevLett.122.142001.

[130] Z.-Y. Fan, Y.-B. Yang, A. Anthony, H.-W. Lin, K.-F. Liu, Gluon Quasi-Parton-Distribution Functions from Lattice QCD, Phys. Rev. Lett. 121 (24) (2018) 242001. arXiv:1808.02077, doi:10.1103/PhysRevLett.121.242001.

[131] I. Balitsky, W. Morris, A. Radyushkin, Gluon Pseudo-Distributions at Short Distances: Forward Case, Phys. Lett. B 808 (2020) 135621. arXiv:1910.13963, doi:10.1016/j.physletb.2020.135621.

[132] Z. Fan, R. Zhang, H.-W. Lin, Nucleon gluon distribution function from 2 + 1 + 1-flavor lattice QCD, Int. J. Mod. Phys. A 36 (13) (2021) 2150080. arXiv:2007.16113, doi:10.1142/S0217751X21500809.

[133] Z. Fan, H.-W. Lin, Gluon parton distribution of the pion from lattice QCD, Phys. Lett. B 823 (2021) 136778. arXiv:2104.06372, doi:10.1016/j.physletb.2021.136778.

[134] A. Salas-Chavira, Z. Fan, H.-W. Lin, First glimpse into the kaon gluon parton distribution using lattice QCD, Phys. Rev. D 106 (9) (2022) 094510. arXiv:2112.03124, doi:10.1103/PhysRevD.106.094510.

[135] T. Khan, et al., Unpolarized gluon distribution in the nucleon from lattice quantum chromodynamics, Phys. Rev. D 104 (9) (2021) 094516. arXiv:2107.08960, doi:10.1103/PhysRevD.104.094516.

[136] C. Egerer, et al., Toward the determination of the gluon helicity distribution in the nucleon from lattice quantum chromodynamics, Phys. Rev. D 106 (9) (2022) 094511. arXiv:2207.08733, doi:10.1103/PhysRevD.106.094511.

[137] T. Khan, T. Liu, R. S. Sufian, Gluon helicity in the nucleon from lattice QCD and machine learning, Phys. Rev. D 108 (7) (2023) 074502. arXiv:2211.15587, doi:10.1103/PhysRevD.108.074502.

[138] Z. Fan, W. Good, H.-W. Lin, Gluon parton distribution of the nucleon from (2+1+1)-flavor lattice QCD in the physical-continuum limit, Phys. Rev. D 108 (1) (2023) 014508. arXiv:2210.09985, doi:10.1103/PhysRevD.108.014508.

[139] J. Delmar, C. Alexandrou, K. Cichy, M. Constantinou, K. Hadjiyiannakou, Gluon PDF of the proton using twisted mass fermions, Phys. Rev. D 108 (9) (2023) 094515. arXiv:2310.01389, doi:10.1103/PhysRevD.108.094515.

[140] Y.-Q. Ma, J.-W. Qiu, Exploring Partonic Structure of Hadrons Using ab initio Lattice QCD Calculations, Phys. Rev. Lett. 120 (2) (2018) 022003. arXiv:1709.03018, doi:10.1103/PhysRevLett.120.022003.

[141] M. Constantinou, H. Panagopoulos, Perturbative renormalization of quasi-parton distribution functions, Phys. Rev. D 96 (5) (2017) 054506. arXiv:1705.11193, doi:10.1103/PhysRevD.96.054506.

[142] C. Alexandrou, K. Cichy, M. Constantinou, K. Hadjiyiannakou, K. Jansen, H. Panagopoulos, F. Steffens, A complete non-perturbative renormalization prescription for quasi-PDFs, Nucl. Phys. B 923 (2017) 394–415. arXiv:1706.00265, doi:10.1016/j.nuclphysb.2017.08.012.

[143] J.-H. Zhang, X. Ji, A. Schäfer, W. Wang, S. Zhao, Accessing Gluon Parton Distributions in Large Momentum Effective Theory, Phys. Rev. Lett. 122 (14) (2019) 142001. arXiv:1808.10824, doi:10.1103/PhysRevLett.122.142001.

[144] H. Dorn, D. Robaschik, E. Wieczorek, RENORMALIZATION AND SHORT DISTANCE PROPERTIES OF GAUGE INVARIANT GLUONIUM AND HADRON OPERATORS, Annalen Phys. 40 (1983) 166. doi:10.1002/andp.19834950208.

[145] W. Wang, S. Zhao, On the power divergence in quasi gluon distribution function, JHEP 05 (2018) 142. arXiv:1712.09247, doi:10.1007/JHEP05(2018)142.

[146] V. M. Braun, K. G. Chetyrkin, B. A. Kniehl, Renormalization of parton quasi-distributions beyond the leading order: spacelike vs. timelike, JHEP 07 (2020) 161. arXiv:2004.01043, doi:10.1007/JHEP07(2020)161.

[147] H. Dorn, Renormalization of Path Ordered Phase Factors and Related Hadron Operators in Gauge Field Theories, Fortsch. Phys. 34 (1986) 11–56. doi:10.1002/prop.19860340104.

[148] V. S. Dotsenko, S. N. Vergeles, Renormalizability of Phase Factors in the Nonabelian Gauge Theory, Nucl. Phys. B 169 (1980) 527–546. doi:10.1016/0550-3213(80)90103-0.

[149] R. A. Brandt, F. Neri, M.-a. Sato, Renormalization of Loop Functions for All Loops, Phys. Rev. D 24 (1981) 879. doi:10.1103/PhysRevD.24.879.

[150] S. D. Joglekar, B. W. Lee, General Theory of Renormalization of Gauge Invariant Operators, Annals Phys. 97 (1976) 160. doi:10.1016/0003-4916(76)90225-6.

[151] H. J. Rothe, Lattice Gauge Theories : An Introduction (Fourth Edition), Vol. 43, World Scientific Publishing Company, 2012. doi:10.1142/8229.

[152] C. Gattringer, C. B. Lang, Quantum chromodynamics on the lattice, Vol. 788, Springer, Berlin, 2010. doi:10.1007/978-3-642-01850-3.

[153] J. A. Gracey, Three loop anomalous dimension of nonsinglet quark currents in the RI-prime scheme, Nucl. Phys. B 662 (2003) 247–278. arXiv:hep-ph/0304113, doi:10.1016/S0550-3213(03)00335-3.

[154] G. Spanoudes, H. Panagopoulos, Renormalization of Wilson-line operators in the presence of nonzero quark masses, Phys. Rev. D 98 (1) (2018) 014509. arXiv:1805.01164, doi:10.1103/PhysRevD.98.014509.

[155] G. Spanoudes, M. Constantinou, H. Panagopoulos, Renormalization of asymmetric staple-shaped Wilson-line operators in lattice and continuum perturbation theory, arXiv e-prints (1 2024). arXiv:2401.01182.

[156] M. Costa, I. Karpasitis, T. Pafitis, G. Panagopoulos, H. Panagopoulos, A. Skouroupathis, G. Spanoudes, Gauge-invariant renormalization scheme in QCD: Application to fermion bilinears and the energy-momentum tensor, Phys. Rev. D 103 (9) (2021) 094509. arXiv:2102.00858, doi:10.1103/PhysRevD.103.094509.